2013

Spectroscopic Study Of The Use Of Lanthanide Metalloporphyrins As Sensors For Benzene And Acetonitrile Detection In Aqueous Studies

Jr Carlos Crawford
North Carolina Agricultural and Technical State University

Spectroscopic Study of the Use of Lanthanide Metalloporphyrins as Sensors for Benzene and Acetonitrile Detection in Aqueous Studies

Carlos Lemarr Crawford Jr

North Carolina A&T State University

A thesis submitted to the graduate faculty

in partial fulfillment of the requirements for the degree of

MASTER OF SCIENCE

Department: Chemistry

Major: Chemistry

Major Professor: Dr. Zerihun Assefa

Greensboro, North Carolina

2013

School of Graduate Studies
North Carolina Agricultural and Technical State University
This is to certify that the Master's Thesis of

Carlos Lemarr Crawford Jr

has met the thesis requirements of
North Carolina Agricultural and Technical State University

Greensboro, North Carolina
2013

Approved by:

Dr. Zerihun Assefa Major Professor	Dr. Alex Williamson Committee Member
Dr. Julius Harp Committee Member	Dr. Margaret Kanipes Department Chairperson

Dr. Sanjiv Sarin
Dean, The Graduate School

Biographical Sketch

Carlos Lemarr Crawford Jr., was born on March 26, 1989, in Winston-Salem, North Carolina. He obtained his high school education at Mount Tabor High School in 2007. He received the Bachelor of Science degree in Chemistry from North Carolina Agricultural & Technical State University in 2011. He is a candidate for the M.S. in Chemistry.

Dedication

This thesis is dedicated to Carlos Sr., Marilyn, and Zaria Crawford.

Acknowledgements

First and foremost, I would like to thank Jesus Christ for giving me the strength and endurance to finish this race that was set before me. Thank you Carlos L. Crawford Sr., my father, for all the times I would come home on the weekends and we would sit in the backyard and converse about school, life and being dedicated. Thank you Marilyn Crawford, my mother; I could always depend on you to give me the truth and guidance straight to the point. Thank you Zaria Crawford, my little sister and confidant; you always gave me the other perspective I needed. I would like to thank Dr. Zerihun Assefa for his mentorship and guidance throughout the years, whether it was about science or other life decisions. Thank you Dr. Harp and Dr. Williamson for the insight that both of you have given. Thank you, Ms. Carolyn Mayo for all of the help and kindness that you've shown me. Thank you, Mr. King for your instrumentation help and the "good" cuvettes. Thank you, Dr. Darkus Jenkins for all of your help and guidance; I could have never completed X-ray diffraction and Gaussian without you. Thank you, Dr. Matthew Mickens for your support and providing that example of a true role model. Thank you to my group members Kendra Whitehead, Shaka Gore, Derick Forcha, Jigar Prajapati, and Jennifer Stanley for all of your help and encouragement.

Table of Contents

List of Figures……..x

List of Tables…….xv

Abstract……2

CHAPTER 1 Introduction……4

1.1. Fundamentals and Properties of Luminescence……4

1.2. Lanthanides Role in Sensor Applications……6

1.2.1. Europium studies……9

1.2.2. Dysprosium applications……...10

1.2.3. Terbium usages……..……...……..10

1.2.4. Gadolinium studies……...11

1.2.5. Cerium applications...……...12

1.3. Silver Usage in Devices……....12

1.4. Sodium Applications...……13

1.5. Porphyrin Versatility and Functionality.…..……..14

1.6. Acetonitrile Awareness and Implications....…...……....16

1.7. Benzene Awareness and Implications……..……..18

CHAPTER 2 Experimental Methods……..…20

2.1 Chemical Reagents……...20

2.2. Material Synthesis……....20

2.2.1. Synthesis of Dy(TPP)……20

2.2.2. Synthesis of Dy(TPP) CH_3CN…….....20

2.2.3. Synthesis of Dy(TPP) C_6H_6…...……...20

2.2.4. Synthesis of Eu(TPP)……20

2.2.5. Synthesis of Eu(TPP) CH_3CN……..20

2.2.6. Synthesis of Eu(TPP) C_6H_6……..20

2.2.7. Synthesis of Eu(TPP) (Eu-a)……20

2.2.8. Synthesis of Eu(TPP) (Eu-b)……21

2.2.9. Synthesis of Eu(TPP) (Eu-c)……21

2.2.10. Synthesis of Eu(TPP) (Eu-d)……..22

2.2.11. Synthesis of Eu(TPP) (Eu-e)…….…..22

2.2.12. Synthesis of Eu(TPP) (Eu-f)……...22

2.2.13. Synthesis of Dy(TPP) (Dy-a)……...……...……....23

2.2.14. Synthesis of Dy(TPP) (Dy-b)……...……...23

2.2.15. Synthesis of Dy(TPP) (Dy-c)……..23

2.2.16. Synthesis of Eu(TBSP)……...24

2.2.17. Synthesis of Dy(TBSP)……..24

2.2.18. Synthesis of Tb(TBSP)……...24

2.2.19. Synthesis of Eu(TBSP) CH_3CN……..24

2.2.20. Synthesis of Dy(TBSP) CH_3CN…….…24

2.2.21. Synthesis of Tb(TBSP) CH_3CN……..24

2.2.22. Synthesis of Eu(TBSP) C_6H_6…….…….25

2.2.23. Synthesis of Dy(TBSP) C_6H_6……..…...25

2.2.24. Synthesis of Tb(TBSP) C_6H_6……..……25

2.2.25. Synthesis of Na(TPP)……..25

2.2.26. Synthesis of Na(TBSP)..……25

2.2.27. Synthesis of Ag(TBSP)…….…25

2.2.28. Synthesis of Ag(TPP)..……..25

2.2.29. Synthesis of Ce(TBSP)…….…25

2.2.30. Synthesis of Ce(TPP)…….....26

2.2.31. Synthesis of Gd(TBSP)…….…26

2.2.32. Synthesis of Gd(TPP)…….26

2.2.33. Synthesis of Ce(TPP) CH_3CN……26

2.2.34. Synthesis of Ce(TPP) C_6H_6……26

2.2.35. Synthesis of Gd(TPP) CH_3CN…….. 26

2.2.36. Synthesis of Gd(TPP) C_6H_6…….....26

2.2.37. Photoluminescence spectroscopy…….....……26

2.2.38. UV-Vis spectroscopy…….....……..27

2.2.39. X-ray diffraction crystallography…….……...……...27

CHAPTER 3 Results and Discussion……28

3.1. PL of (TPP)…..……28

3.2. PL of $EuCl_3 \bullet 6H_2O$……..…29

3.3. PL of Eu(TPP) Complexes…….31

3.4. PL of Dy(TPP) Complexes ……...……...……..48

3.5. PL of Ce(TPP) Complexes……..……...54

3.6. PL of Gd(TPP) Complexes……..…….....……58

3.7. PL of Ag(TPP) Complex……...……...…..61

3.8. PL of Lanthanide (TPP) Combined Complexes…….……...….62

3.9. PL of (TBSP).……70

3.10. PL of Lanthanide (TBSP) Combined Complexes…….……...72

3.11. UV-Vis Spectroscopy of Lanthanide (TPP) Combined Complexes……...…..…84

3.12. UV-Vis Spectroscopy of Lanthanide (TBSP) Combined Complexes…….....88

3.13. UV-Vis Spectroscopy of Metallo (TPP) and (TBSP) Complexes…..…….....93

3.14. X-ray Diffraction of (TPP)……..……95

CHAPTER 4 Conclusion……..……99

CHAPTER 5 Lanthanide Dual Donor Systems……..……..…...100

5.1. PL of $KLa[Pt(CN)_4]_2 \cdot 8.75H_2O$ Complex……..…..…..**.....**100

5.2. PL of $K_2[Dy(H_2O)_4(Pt(CN)_4)_2)](Au(CN)_2) \cdot 2H_2O$ Complex……...…..…103

References……...…..…108

Appendix…….....…...116

List of Figures

Figure 1.1 Jablonski diagram showing the absorption and emission mechanism...……5

Figure 1.2 Structure of terpyridine and tetracyanoplatinate. ……...…...8

Figure 1.3 Similarities of heme, chlorophyll a, and tetrapyrrole core……...14

Figure 3.1 PL of TPP excitaion spectra……...……..……28

Figure 3.2 PL of TPP emission spectra……...……...…….....29

Figure 3.3 PL of $EuCl_3$•$6H_2O$ excitation spectra……...……29

Figure 3.4 PL of $EuCl_3$•$6H_2O$ emission spectra……..……..30

Figure 3.5 PL of Eu(TPP)(Eu-a) green solution emission spectra……..……..…..…..... 31

Figure 3.6 PL of Eu(TPP)(Eu-a) green solution excitation spectra…….....….……32

Figure 3.7 PL of Eu(TPP)(Eu-a) yellow solution excitation spectra……..……..….....32

Figure 3.8 PL of Eu(TPP)(Eu-a) yellow solution emission spectra…….…...….….33

Figure 3.9 PL of Eu(TPP)(Eu-a) orange solution excitation spectra……...…...…….. 34

Figure 3.10 PL of Eu(TPP)(Eu-a) orange solution emission spectra……..……...…..... 34

Figure 3.11 PL of Eu(TPP)(C_6H_6)(Eu-b) green solution excitation spectra……..35

Figure 3.12 PL of Eu(TPP)(C_6H_6)(Eu-b) green solution emission spectra….……..35

Figure 3.13 PL of Eu(TPP)(C_6H_6)(Eu-b) yellow solution excitation spectra…….....…...36

Figure 3.14 PL of Eu(TPP)(C_6H_6)(Eu-b) yellow solution emission spectra……...…….37

Figure 3.15 PL of Eu(TPP)(C_6H_6)(Eu-b) orange solution excitation spectra…….……...38

Figure 3.16 PL of Eu(TPP)(C_6H_6)(Eu-b) orange solution emission spectra…….....…..38

Figure 3.17 PL of Eu(TPP)(CH_3CN)(Eu-c) green solution excitation spectra…..……...…….39

Figure 3.18 PL of Eu(TPP)(CH_3CN)(Eu-c) green solution emission spectra……...….....39

Figure 3.19 PL of Eu(TPP)(CH_3CN)(Eu-c) yellow solution excitation spectra……...…….....40

Figure 3.20 PL of Eu(TPP)(CH_3CN)(Eu-c) yellow solution excitation spectra…..……..……41

Figure 3.21 PL of Eu(TPP)(Eu-d) purple solution in NaOH excitation spectra……..…….41

Figure 3.22 PL of Eu(TPP)(Eu-d) purple solution in NaOH emission spectra…….....42

Figure 3.23 PL of Eu(TPP)(C_6H_6)(Eu-e) purple solution in NaOH excitation spectra…….....43

Figure 3.24 PL of Eu(TPP)(C_6H_6)(Eu-e) purple solution in NaOH emission spectra……..... 44

Figure 3.25 PL of Eu(TPP)(CH_3CN)(Eu-f) purple solution in NaOH excitation spectra...……..44

Figure 3.26 PL of Eu(TPP)(CH_3CN)(Eu-f) purple solution in NaOH emission spectra.....…… 45

Figure 3.27 PL of Eu(TPP)(CH_3CN)(Eu-f) yellow solution in NaOH excitation spectra...…….46

Figure 3.28 PL of Eu(TPP)(CH_3CN)(Eu-f) yellow solution in NaOH emission spectra...…….....47

Figure 3.29 PL of Dy(TPP)(Dy-a) purple solution excitation spectra……..…….... 48

Figure 3.30 PL of Dy(TPP)(Dy-a) purple solution emission spectra……..……..48

Figure 3.31 PL of Dy(TPP)(C_6H_6)(Dy-b) purple solution excitation spectra…….…..…….49

Figure 3.32 PL of Dy(TPP)(C_6H_6)(Dy-b) purple solution emission spectra…..…….…….....50

Figure 3.33 PL of Dy(TPP)(CH_3CN)(Dy-c) purple solution excitation spectra.....…...50

Figure 3.34 PL of Dy(TPP)(CH_3CN)(Dy-c) purple solution emission spectra.....……51

Figure 3.35 PL of Dy(TPP)(CH_3CN)(Dy-c) yellow solution excitation spectra……..…….....52

Figure 3.36 PL of Dy(TPP)(CH_3CN)(Dy-c) yellow solution emission spectra…….…….....53

Figure 3.37 PL of Ce(TPP) excitation spectra……...…..54

Figure 3.38 PL of Ce(TPP) emission spectra……..……..…...55

Figure 3.39 PL of Ce(TPP)(CH_3CN) excitation spectra…….……...…..55

Figure 3.40 PL of Ce(TPP)(CH_3CN) emission spectra……...…..……..…….56

Figure 3.41 PL of Ce(TPP)(C_6H_6) excitation spectra…….……...……...…...57

Figure 3.42 PL of Ce(TPP)(C_6H_6) emission spectra…….……..…….57

Figure 3.43 PL of Gd(TPP) excitation spectra……..……..…..58

Figure 3.44 PL of Gd(TPP) emission spectra…….……...……58

Figure 3.45 PL of Gd(TPP)(CH_3CN) excitation spectra…….……...…...59

Figure 3.46 PL of Gd(TPP)(CH_3CN) emission spectra…….……...…....59

Figure 3.47 PL of Gd(TPP)(C_6H_6) excitation spectra…….……...……60

Figure 3.48 PL of Gd(TPP)(C_6H_6) emission spectra……...…….……...……..60

Figure 3.49 PL of Ag(TPP) excitation spectra……..……...……..61

Figure 3.50 PL of Ag(TPP) emission spectra…….……...……61

Figure 3.51 PL of Ln(TPP) combined excitation spectra…….……...……..62

Figure 3.52 PL of Ln(TPP) combined emission spectra……..……..63

Figure 3.53 PL of Ln(TPP)(CH_3CN) combined excitation spectra…….……...……...64

Figure 3.54 PL of Ln(TPP)(CH_3CN) combined emission spectra…….…..……..…....66

Figure 3.55 PL of Ln(TPP)(C_6H_6) combined excitation spectra…….……...……...….....67

Figure 3.56 PL of Ln(TPP)(C_6H_6) combined emission spectra…….……....69

Figure 3.57 PL of TBSP excitation spectra……..…….....70

Figure 3.58 PL of TBSP emission spectra……..……...71

Figure 3.59 PL of Ln(TBSP) excitation spectra…….……..…….72

Figure 3.60 PL of Ln(TBSP) emission spectra monitored at 482nm……...…….74

Figure 3.61 PL of Ln(TBSP) emission spectra monitored at 459nm……...…….75

Figure 3.62 PL of Ln(TBSP)(CH_3CN) excitation spectra…….……..……..76

Figure 3.63 PL of Ln(TBSP)(CH_3CN) emission spectra…….……...…….....78

Figure 3.64 PL of Ln(TBSP)(C_6H_6) excitation spectra……...……..79

Figure 3.65 PL of Ln(TBSP)(C_6H_6) emission spectra…….……..……81

Figure 3.66 PL of Ln(TBSP)(C_6H_6) emission spectra monitored at 365nm……..…..82

Figure 3.67 PL of Ln(TBSP)(C_6H_6) emission spectra monitored at 334nm……..83

Figure 3.68 UV-Vis spectroscopy of Ln(TPP) complexes…….……...84

Figure 3.69 UV-Vis spectroscopy of Ln(TPP)(CH_3CN) complexes…….……85

Figure 3.70 UV-Vis spectroscopy of Ln(TPP)(C_6H_6) complexes…….87

Figure 3.71 UV-Vis spectroscopy of Ln(TBSP) complexes…….……88

Figure 3.72 UV-Vis spectroscopy of Ln(TBSP)(CH_3CN) complexes……..…….90

Figure 3.73 UV-Vis spectroscopy of Ln(TBSP)(C_6H_6) complexes…….…..91

Figure 3.74 UV-Vis spectroscopy of metallo(TPP) complexes…….…….....93

Figure 3.75 UV-Vis spectroscopy of metallo(TBSP) complexes…….….94

Figure 3.76 X-ray crystallography of TPP……...….….95

Figure 3.77 X-ray crystallography of TPP stacking……...….....97

Figure 5.1 PL of $KLa[Pt(CN)_4]_2•8H_2O$ complex excitation spectra……...….…100

Figure 5.2 PL of $KLa[Pt(CN)_4]_2•8H_2O$ complex emission spectra……..….…..101

Figure 5.3 PL of $KLa[Pt(CN)_4]_2•8H_2O$ complex excitation spectra liquid nitrogen temperature……..101

Figure 5.4 PL of $KLa[Pt(CN)_4]_2•8H_2O$ complex emission spectra liquid nitrogen temperature……..102

Figure 5.5 PL of $K_2[Dy(H_2O)_4(Pt(CN)_4)_2](Au(CN)_2)•2H_2O$ complex excitation spectra……..…103

Figure 5.6 PL of $K_2[Dy(H_2O)_4(Pt(CN)_4)_2](Au(CN)_2)•2H_2O$ complex emission spectra…….….104

Figure 5.7 PL of $K_2[Dy(H_2O)_4(Pt(CN)_4)_2](Au(CN)_2)•2H_2O$ complex excitation spectra liquid nitrogen temperature……...….105

Figure 5.8 PL of $K_2[Dy(H_2O)_4(Pt(CN)_4)_2](Au(CN)_2)•2H_2O$ complex emission spectra liquid nitrogen temperature……...….106

List of Tables

Table 1 Luminescent lanthanides..... 7

Table 2 X-ray crystallography data of TPP 96

Table 3 X-ray crystallography data of TPP stacking..... 98

Abstract

This work entails the research on lanthanide metalloporphyrins for their potential use as chemical sensors for benzene and acetonitrile. This research is of importance due to the health implications that benzene and acetonitrile cause; benzene is a known carcinogen and acetonitrile is a known lung irritant. The use of UV-Vis spectroscopy, Fluorescence spectroscopy, Gaussian DFT, and X-ray diffraction crystallography were used in the characterization and analysis of the lanthanide porphyrin complexes. Europium, terbium, dysprosium, cerium, and gadolinium were the lanthanides used in conjunction with 5,10,15,20-tetraphenylporphyrin, TPP and 5,10,15,20-tetrakissulfonato porphyrin, TBSP. Based on the luminescence spectroscopy and UV-Vis spectroscopy data, an aqueous sensor for acetonitrile and benzene was shown to be promising. Among the compounds studied, EuTPP and DyTPP complexes exposed to sodium hydroxide showed promising results for sensing acetonitrile due to significant narrowing of the soret band and the decrease of Q bands in the UV-Vis spectra, along with the blue shifting of luminescence emission spectra. On the other hand, the CeTPP and EuTPP solutions show promise as benzene sensors due to the blue shifting of emission luminescence and variation in intensity. Based on the lanthanide TBSP complexes, TbTBSP was shown to be a promising sensor for acetonitrile due to the narrow soret band, decreased Q bands, and blue shifted emission spectra. EuTBSP, DyTBSP, and TbTBSP were shown to be promising for benzene sensors. Benzene stabilized the TBSP at a higher energy state, S_2, to facilitate the energy transfer to the lanthanide ions.

List of Symbols

TPP	5,10,15,20-tetraphenylporphyrin, $C_{44}N_4H_{26}$
TBSP	5,10,15,20-tetrakissulfonato porphyrin, $C_{44}N_4H_{26}Na_4O_{12}S_4$
mL	Milliliter
g	Gram
MeOH	Methanol
EtOH	Ethanol
CH_3CN	Acetonitrile
Et_2O	Diethyl Ether
nm	Nanometers
µL	Microliters
DMF	N,N-dimethyl formamide
PL	Photoluminescence
VOC	Volatile Organic Compound

CHAPTER 1

Introduction

1.1. Fundamentals and Properties of Luminescence

Luminescence is defined as the emission of light from a substance that has been excited and is relaxing down to the ground state from an excited state with the emission of photons (Wiedemann, 1888). The term luminescence was coined by Eilhardt Wiedemann in 1888, although it had been observed for centuries among every nation. The earliest records of observation date back to Chinese literature between 1500-1000 B.C (Harvey, 1957). Luminescence encompasses a broad range of subcategories due to the different means of exciting electrons. Eilhardt Wiedemann specifically categorized luminescence into ten types: fluorescence, phosphorescence, thermoluminescence, electroluminescence, galvanoluminescence, sonoluminescence, triboluminescene, crystalloluminescence, chemiluminescence, and bioluminescence (Goldberg Marvin & Weiner Eugene, 1989).

The two main modes of luminescence are fluorescence and phosphorescence. Fluorescence is the emission of light, due to an allowed electronic transition from a ground state to an excited state. Both states will have the same singlet spin multiplicity. Fluorescence has a short lifetime in the 10^{-9} second range. Phosphorescence is a process where the initial excitation from a ground state to an excited state with the same spin multiplicity, undergoes intersystem crossing to the triplet state and relaxes down to the ground state. The lifetime for phosphorescence is longer than that of fluorescence and lasts from microseconds to milliseconds to minutes (Goldberg Marvin & Weiner Eugene, 1989). In 1935, Jablonski developed a visual diagram to explain the theory behind luminescence. His diagram briefly and efficiently describes how an electron is excited from a ground state to an excited state, resulting in fluorescence

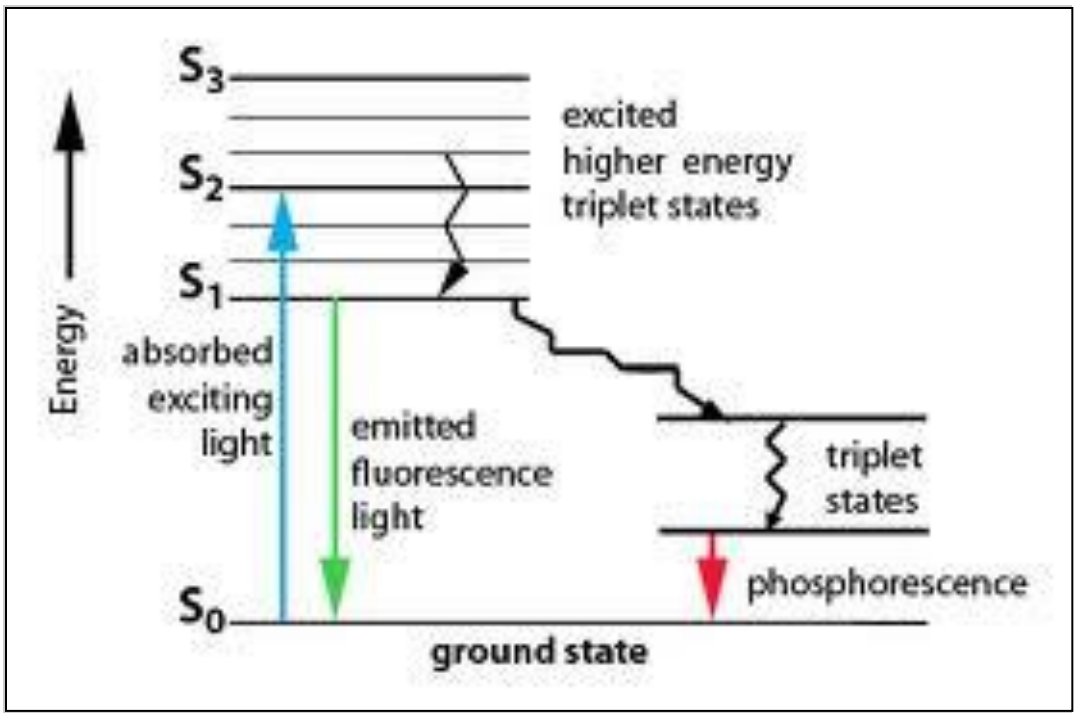

Figure 1.1. The Jablonski diagram showing the absorption and emission mechanism.

In the case of fluorescence, an electron at the ground state, S_0, absorbs energy and is excited to an excited state of the same multiplicity, S_1. As the state loses energy it will relax non-radiatively down to the ground state, causing the emission of photons; the photons are perceived as emitted light. If this process doesn't emit photons as it relaxes from the excited state, then it has undergone a process called non-radiative decay. In the non-radiative decay process, the energy that was supposed to be emitted as photons is instead emitted as phonons, lattice vibrations or heat (Vij, 1998). A phonon is defined as a unit of vibrational energy that exists from oscillating atoms within a crystal lattice (Grimvall, 1981).

In the case of phosphorescence, the intersystem crossing from an excited singlet state to a excited triplet state is the reason for the "forbidden" transition term. Through vibrational relaxation, the electron relaxes from the excited triplet state to various meta-stable triplet states before it finally reaches the S_0, ground state. The relaxation can occur radiatively or non-radiatively, releasing light and heat, respectively (Wiedemann, 1888).

Luminescence is a vital tool that can be used to conduct at least five important physical measurements: the emission wavelength, the excitation wavelength, the excited state lifetime, emission polarization, and the quantum yield (Bequerel, 1907). Luminescence techniques have a wide array of applications in sensors for volatile organic compounds, nerve gases, and photodynamic cancer research (Vij, 1998).

1.2. Role of Lanthanides in Sensor Applications

The Lanthanides are a family of elements that were first discovered in Scandinavia in 1794 by Johan Gadolin. Since then, the majority of lanthanide ores are found in the minerals, Monazite, Bastnasite, and Xenotime (Cotton, 2006). Lanthanides are known for their optical properties due to their f-f orbital characteristics. They have a wide range of coordination numbers, coordination geometries that are determined by steric hindrance, small crystal field splitting and preferably bond to hard base ligands (Wulfsberg, 2000).

The electronic transition properties of lanthanides are responsible for them exhibiting fluorescence or phosphorescence. For example europium exhibits phosphorescence from its main emission band at 615 nm due to the transition from the $^5D_0$ excited state to the ^7F_J ground state-manifold. Holmium on the contrary, exhibits fluorescence type luminescence from its main emission band at 540 nm. The emission band at 540 nm is due to the transition from $^5S_2$ excited state to the $^5I_8$ ground state manifold (J.-C. G. Bunzli & Piguet, 2005).

The optical properties of lanthanide systems are interesting due to their emission of color in the visible region of the electromagnetic spectrum as a result of f-f electronic transition from the shielded 4f. Since the 4f shell is shielded, it is disturbed minimally by the outside ligand, allowing the lanthanide retains its characteristic luminescent color (Binnemans, 2009). The characteristic colors of lanthanides are shown in table 1.

Table 1

Luminescent Lanthanides[9]

Lanthanide	Electronic Transition	Color	Luminescence Type
Dysprosium	$^4F_{9/2} \rightarrow {}^6H_J$	Yellow (570 nm)	Phosphorescence
Europium	$^5D_0 \rightarrow {}^7F_J$	Red (620 nm)	Phosphorescence
Samarium	$^4G_{5/2} \rightarrow {}^6H_J$	Orange (590 nm)	Phosphorescence
Terbium	$^5D_4 \rightarrow {}^7F_J$	Green (550 nm)	Phosphorescence

Lanza, et al. (Lanza, Varga, Kolonits, & Hargittai, 2008) expounds on the validity of the non reactivity of the 4f shell electrons in bonding. Their experiment sought further correlation between 4f shell electrons on the structural characteristics using dysprosium trichloride in particular. It was found that the electron configurations of the 4f shell electrons don't alter the geometry of dysprosium trichloride monomer. Their reasoning being that the 4f shell electrons are down deep below the $5s^2$ and $5p^6$ shells, thus deep away from valence region that's responsible for bonding and geometric configurations (RusCic, Goodman, & Berkowitz, 1983). They conducted other experiments only varying the lanthanide used, and came upon the same conclusion, thus validating that 4f shell electrons are minimally affected (Dolg, 1998).

Although lanthanides are known for their color characteristics, they are also known for providing a low intense luminescence. The inherently unaffected f-f transitions in lanthanides ions can be enhanced through indirect excitation (Hebbink, 2002). The case of direct excitation is when energy is directly added to the lanthanide ion in order to excite the electrons to an excited state. The case for indirect excitation is through the use of sensitizers; these are molecules, compounds, or complexes that are able to absorb energy and transfer it to the lanthanide ion to

compensate for the poor luminescence intensity of the ion (Bequerel, 1908). In order for the sensitizer to be effective, then it has to be in close proximity to the lanthanide ion to bond directly or allow for resonant electron energy transfer (A.S., 1995). The definition of resonant electron energy transfer is the non-radiative transfer of an electronic excitation from a donor molecule to an acceptor molecule in close proximity, 50-100 nm wavelength distances (Tokmakoff, 2011).

Sensitized fluorescence was first discovered by Cairo and Franck in 1922 (Cario, 1922). In an experiment consisting of a mixture of thallium and mercury vapors in a tube, selective excitation of the mercury atoms produced only the thallium emission suggesting the energy transfer from the donor mercury atoms to the acceptor thallium atoms (Maynard et al., 2009). Maynard, et al. (J. C. K. Bunzli, N.; Gunnlaugsson, T.; Stomeo, F. , 2008) also expounded on the effects of dual donor sensitization on the europium ion. The dual donors used were the tetracyanoplatinate complex and the organic terpyridine organic anion as shown in Figure 1.2. The terpyridine absorbed in the UV region and was able to transfer energy to the Eu^{3+} ion through a sensitization process (J. C. K. Bunzli, N.; Gunnlaugsson, T.; Stomeo, F. , 2008).

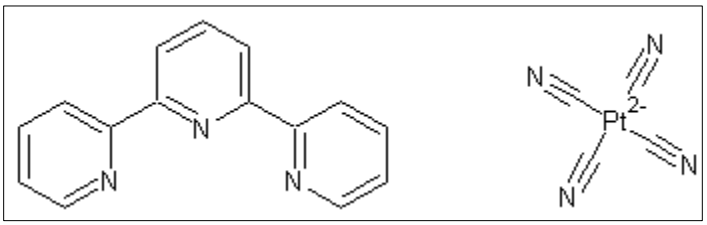

Figure 1.2. Structure of terpyridine and tetracyanoplatinate.

The coordination is through the nitrogen atoms to the lanthanide, Ln^{3+} ion by the tetracyanoplatinate functions as a sensitizer by donating energy, and it also functions as a bridging ligand by expanding the lattice network connecting multiple Eu^{3+} cores. The Eu^{3+} is coordinated to the terpyridine and tetracyanoplatinate; the intensity is higher and the $^5D_0 \rightarrow {}^7F_J$ emission band is more narrow and intense (J. C. K. Bunzli, N.; Gunnlaugsson, T.; Stomeo, F. , 2008).

1.2.1. Europium studies. Europium was first isolated and named in 1901. It is one of the most reactive lanthanides, in that it oxidizes in air leading to an explosion hazard if temperatures exceed 150°C. Europium can form stable complexes in its divalent state, Eu^{2+}, or in its trivalent state, Eu^{3+}. Although it isn't found free in nature, it can be extracted from mineral ore's, such as monazite, bastnasite, and xenotime through various chemical and physical processes (Szabadvary, 1998).

Europium has been studied extensively since its discovery due to its optical properties; it has been used in luminescence research, sensor applications, and biomedical assays. Europium is currently being investigated for its use in white light emitting diodes (Liu et al., 2012). Europium producing red light, a primary color, can be used in conjunction with other lanthanides in white light production (Luo, 2007).

Organic chromophores, organic compounds that are able to absorb light energy and transfer energy, are extensively used in Europium luminescent research to transfer energy. Cryptates have been shown to sensitize europium luminescence by absorbing UV light, transferring energy through LMCT, and exhibits low back transfer rates, which can decrease luminescence efficiency (J. G. Santos, Dutra, Junior, Freire, & da Costa Junior, 2012).

Terrestrial and marine toxins pose a threat to humans and animals alike. Saxitoxin is a paralytic shellfish toxin that has caused increasing concern in Southeast Asian and Pacific waters. Chromophores with europium incorporated into the structure have been used as sensors for saxitoxin. The chromophore has a moiety that hydrogen bonds with saxitoxin increases the luminescence emission intensity and increasing the quantum yield by more than 50 percent (He et al., 2011). Other lanthanides can be investigated in whether or not they also have an affinity for the chromophore that was used in the europium metal study.

1.2.2. Dysprosium applications. Dysprosium was first purely isolated in 1950 (Szabadvary, 1998). Dysprosium exists in its trivalent state and is commonly used in nuclear reactors, sonar systems and as neutron absorbers (Szabadvary, 1998). Dysprosium like any other trivalent lanthanides is paramagnetic. Its uses aren't as numerous as europium, yet it is used consistently and reliably in few roles that it is employed.

Dysprosium is being studied in thermal reactors and cancer imaging due to it serving as an electron trap for in vivo imaging (Risovany, Zakharov, Muraleva, Kosenkov, & Latypov, 2006). It was proven to enhance luminescence imaging when excited through x-ray irradiation, providing a persistent red codopant luminescence (Bessiere et al., 2013; Maldiney et al., 2011). Dysprosium is also used in studies with phthalocyanine films due to the physicochemical properties and electrochromic behavior. They are susceptible to environment and used for sensor materials (de Saja & Rodríguez-Méndez, 2005). Although they were great photosensitizers, their luminescence profile was temperature dependent, being red shifted after heating and blue shifted when heated to 350 K(Basova, Gürek, Ahsen, & Ray, 2007).

1.2.3. Terbium usages. Terbium was isolated from the mineral ore, bastnasite. It is commonly used in sensor devices, assays, LED lighting, and other biomedical uses. Terbium is often used due to its excitation wavelength in the UV region and emission wavelength in the visible part of the electromagnetic spectrum, 545 nm (Szabadvary, 1998).

Terbium has recently been used with an organic macrocycle as a chelating agent for Zn^{2+} ions in the extracellular matrix. Terbium along with the organic ligand N,N,N',N'-{2,6-bis(3'aminomethyl-1'-pyrazolyl)-4-[N,N-bis(2-picolyl)aminomethylenepyridine]} tetrakis (acetic acid), BBATA as a chelating agent for Zn^{2+}. In the absence of Zn^{2+}, the lanthanide-organic agent luminescence profile is quenched (Ye et al., 2010).

Terbium has also recently been used in the biomedical industry for the detection of neurotransmitters. Kamruzzaman, et al. (Kamruzzaman, Alam, Lee, Kim, & Kim, 2012) devised a method in which terbium could be used to chelate to epinephrine, norepinephrine, and dopamine in order to act as sensor for detection of quantitative amounts of catecholamines in blood serum. The data was successful resulting in enhanced terbium luminescence directly proportional to the concentration of the catecholamine (Kamruzzaman et al., 2012).

Zu-Jin, et al. (Lin, Yang, Liu, Huang, & Cao, 2012) investigated the use of terbium in metal organic frameworks for the use of gas absorption studies. Microwave synthesis reduced the energy and time consumption while providing metal organic framework crystals comparable to regular solvothermal synthesis techniques. The microwave assisted synthesized techniques. The microwave assisted synthesized crystals offered structures that retained CO_2, H_2, and CH_4 gases (Lin et al., 2012).

1.2.4. Gadolinium studies. Gadolinium was first isolated in 1901 from xenotime ore. Gadolinium has many uses, but primarily used in the biomedical industry as a MRI contrast agent.

Jongdoo, et al. (Lim et al., 2012) devised a practical use for gadolinium to be combined with dendrimers. The combination of the two will cause a slower pharmokinetic reaction of gadolinium in the organism, thus less Gd^{3+} used, reduced chance of kidney toxicity, and easier mode of excretion (Lim et al., 2012).

Que, et al. (Que & Chang, 2006) synthesized a gadolinium complex for chelating copper ions. A chelating agent has an affinity for a metal and withdraws it from a solution. It is one of the first successful copper selective gadolinium magnetic resonance sensors. The lanthanide organic ligand shows a constricted conformation in the absence of Cu^{2+}, but upon the coordination of Cu^{2+} the complex relaxes and extends (Que & Chang, 2006).

1.2.5. Cerium applications. Cerium was first isolated in 1803. It is commonly used in arc lighting, catalytic converters, and flint in cigarettes. Cerium is the most abundant lanthanide found free in nature and in allanite, bastnasite, and monazite (Szabadvary, 1998).

Ornatska, et al. (Ornatska, Sharpe, Andreescu, & Andreescu, 2011) had used cerium nanoparticles as chromogenic indicators for the detection of glucose. They were able to successfully produce results by immobilizing the cerium and enzyme into paper bioassay; the analyte was then added and color change occurred based on oxidation of Ce^{3+} to Ce^{4+}. The color changes from a white color to an orange color for the oxidized form (Ornatska et al., 2011).

Tanaka, et al. (Sreeremya, Thulasi, Krishnan, & Ghosh, 2011) used cerium to produce nanocrystals by using ammonium hydroxide. These nanocrystals show a red shift compared to nanocrystals produced by other methods. This is a cost effective and time effective method that has many applications (Sreeremya et al., 2011).

1.3. Silver Usage in Devices

Silver, a transition metal has been used in many instances; it is usually used as an oxidant, antibacterial, electric devices, and electrochemical sensors (Wohrle, 2008). Its uses have increased with the knowledge of nonmaterial. This is due to it being very versatile in that it is also stable; this allows for it to be used in the production of coins.

Kong, et al. (Kong & Jang, 2008) have devised a method of incorporating silver nanofibers with rhodanine nanofibers in order to create a highly efficient antimicrobial material. The nanofiber is effective against gram negative and gram positive bacteria and yeast. Silver has also been used in several studies to attach to nitrogen heterocycles. Many nitroaromatics are hazardous to health and are produced from cigarette smoke, and industrial sources (Rosenkranz, 1980). Maduraiveeran, et al. (Maduraiveeran & Ramaraj, 2009) successfully used silver

nanoparticles to bind to nitrobenzene and characterized the results using cyclic voltametric curves, UV-Vis, X-ray diffraction and fluorescence spectroscopy. Silver has also been used as a sensor for heavy metals in the body. Research indicates that an excess of Cu^{2+} in the human body can cause kidney damage and neurodegenerative problems. Kirubaharan, et al. (Kirubaharan et al., 2012) devised a procedure in which silver nanoparticles are used for the extraction of Cu^{2+} ions; a dye, Rh6G is used to track the progress of the reaction in which Cu^{2+} displaces the dye from its Ag^{+} attachment. Successful results were characterized by fluorescence spectroscopy, X-ray diffraction and UV-Vis spectroscopy (Kirubaharan et al., 2012).

1.4. Sodium Applications

Sodium, an alkali metal has many biological and industrial uses. Sodium cations are essential for electrical signal conduction in nerve cells. It is also used in heat transfer agents (Szabadvary, 1998).

Sodium has been shown to increase the luminescence efficacy of single-walled carbon nanotubes. These nanotubes have the potential uses for photonics and sensor applications. Duque, et al. (Duque, Pasquali, Cognet, & Lounis, 2009) noticed that when carbon nanotubes were dispersed in liquid suspensions containing sodium anions such as sodium dodecylbenzene sulfonate or sodium deoxycholate, there was an enhancement of luminescence, decrease of decay time and narrow emission bands. This proved that sodium salts beneficially alter the environment of carbon nanotubes (Duque et al., 2009).

Sodium has also been used in everyday applications such as hand warmers. By taking advantage of the chemical properties of sodium acetate trihydrate it has been shown that when it reacts with water it behaves exothermically. This process also causes rapid crystallization to occur (Jackson & Dicks, 2012).

Sodium salts have also been used to affect crystal morphology and kinetics. Burrows, et al., devised an experiment that showed that with increasing sodium nitrate concentration, the growth rate of crystals increased and influenced ordered aggregation (Burrows, Hale, & Penn, 2012). It continues to be investigated in its affect as a solvent system for other crystal systems.

1.5. Porphyrin Versatility and Functionality

Porphyrins are some of the most versatile molecules and their derivatives are found in the heme group of hemoglobin, petroleum, chlorophyll α, and chlorophyll β. Figure 1.8 shows the similarities in the tetrapyrrole derivatives. The main structure of the porphyrin molecule is classified as a tetrapyrrole (Baker, 1978). In order to explore on how porphyrin is found in those three places, a common source has to be found. The crude oil that is trapped in the Earth's crust first derived from decayed plant and animal remains.

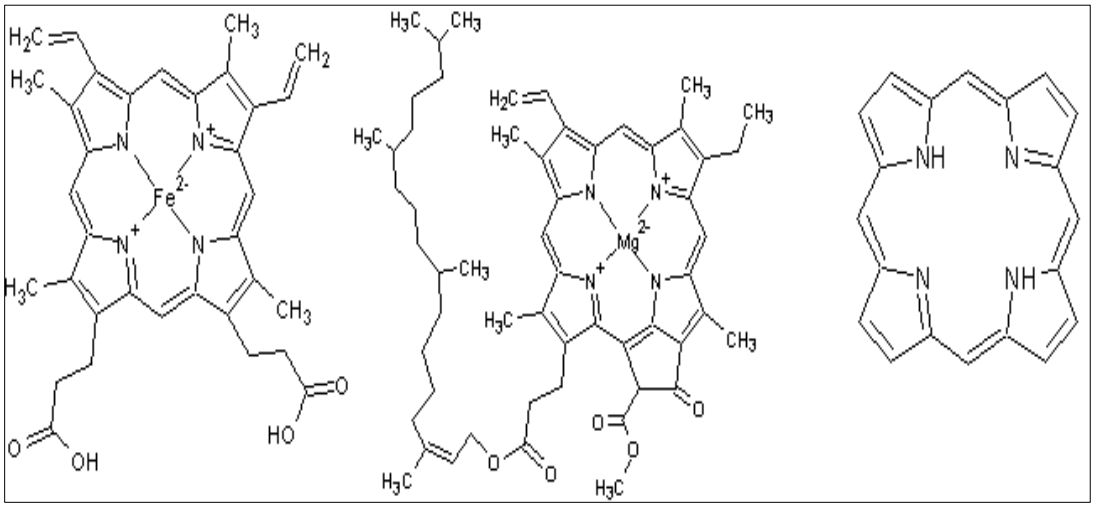

Figure 1.3. Similarities of the heme, chlorophyll α, and tetrapyrrole core.

Muniyappan, et al., published an article in which two types of porphyrin are found in petroleum. There are etio-porphyrin and phyllo porphyrin; etio-porphyrin is the porphyrin that is derived from hemoglobin in animals. It is a necessity in animals because the tetrapyrrole binds to iron (Muniyappan, 1955). With iron bound to the tetrapyrrole, it is able to bind four oxygen atoms

to it and transport oxygen to tissues in animal/human body (Voet, Pratt, & Voet, 2008). Pyllo-porphyrin is derived from the chlorophyll in plants; it is a vital component in the life process of plants. The porphyrin component of chlorophyll is responsible for harvesting light from the sun and electron transport. This is due to porphyrin having large absorption coefficients in the visible-near infrared region (T. D. Santos et al., 2010).

The absorption coefficient is defined as the change in energy of the wave of light that is proportional to the thickness of the layer of material (Harris, 2007). Due to the high absorption coefficient, Santos, et al., used porphyrins in combination with titanium oxide films in solar cells. Their research found that zinc porphyrins were better suited for solar cells rather than titanium oxide porphyrin due to the higher, faster injection dynamics, and higher singlet excited state energies (T. D. Santos et al., 2010).

Tin-porphyrin complexes were used in metal organic frameworks to degrade sulfides and phenols (Xie, Yang, Zou, & Wu, 2011). Herbicides, pesticides, and insecticides contain large amounts of phenols and sulfides which aid in pollution, thus the need for a material to degrade the toxic substances into a less harmful derivative (Lente, 2004). This was achieved by immobilizing the porphyrin complex in the following purple crystal framework: $[Zn_2(H_2O)_4Sn^{IV}(TPYP)(HCOO)_2]\bullet 4NO_3\bullet DMF\bullet 4H_2O$. The $Zn_2(H_2O)_4$ was used as a bridging ligand to create the framework with the $Sn^{IV}(TPYP)$ and acted as reaction centers. The nitrate group, NO_3 acted as counter ions to balance the charge of the porous crystal; the DMF is solvent that was trapped in the crystal lattice. The crystal successfully photo oxidized 1,5-dihydroxynapthalene in the presence of oxygen and xenon light source into a less harmful 5-hydroxynaphthalene-1,4-dione. Their compound was also successful in photo oxidizing sulfide into 94 percent sulfoxide and 6 percent sulphone (Xie et al., 2011).

Porphyrins' versatility aids in it being perfect for sensor applications. Wang, et al., investigated the effect that free base porphyrins and metalloporphyrins had on the removal of Benzo[a]pyrene (B[a]P), and N-Nitrosamines (TSNAs) from mainstream cigarette smoke (Wang et al., 2011). In their research there were several types of free base porphyrins added to filters. Metalloporphyrins were used to attract gases that consisted of hard bases. The free core of the free base porphyrin allows the nitrogen atoms to attract the hard acids from the gases. The increased concentration of porphyrin added to the filter, increased the amount of TSNAs and B[a]Ps that were filtered out of the cigarette smoke (Zhang, 2002).

Porphyrins are also used for sensing and intervention purposes non-directly related to volatile organic compounds. Ozawa, et al., published work on the use of boronated porphyrin TABP-1 in U-87 MG intracerebral human glioblastoma xenografts. The boronated porphyrin complexes were successfully shown to reduce the concentration of tumor cells due to direct injection without having to concede to intravenous injections. Direct injections are more beneficial due to the lack of harmful side effects that are brought on by intravenous injections such as degradation into toxic simpler substances and difficult passage through the blood brain barrier (Ozawa et al., 2004).

1.6. Acetonitrile Awareness and Implications

Acetonitrile is a gas that is emitted through biogenic and anthropogenic means. The vast majority of volatile organic compounds that are emitted into the atmosphere are biogenic in nature, being that nature itself is the cause. The small amounts of emitted volatile organic compounds that are left are those of anthropogenic nature, being that human beings cause its emission into the atmosphere (Girard, 1994). Examples of anthropogenic v.o.c.s are those emitted from vehicle exhaust, coal burning, smoke stacks, and other industrial emissions.

Acetonitrile and benzene are two of the many volatile organic compounds that need sensing apparatuses due to their harmful nature to living organisms. Many studies have been done on the toxicity of acetonitrile and benzene on living organisms. Jones, et al. published a scientific journal on the effects of acetonitrile on the bone marrow and peripheral blood tissue of laboratory mice (Jones, Fox, Elliott, & Moore, 2001). Their studies showed that acetonitrile was toxic because it is metabolized into cyanide (Greenberg, 1999). The indirect effect of cyanide production causes ataxia, convulsions, urine stains, and increases breathing rate. They also found that it increases the incidence of micronucleated cells due to cyanide-mediated stimulation of erythropoiesis (Jones et al., 2001).

Another study, that investigated V.O.C. effects, by Wang, et al., examined the correlation between acetonitrile concentration and the dehydration of phospholipid membranes of surface tissue; surface tissue was examined due to the modes of contact with acetonitrile by living systems are inhalation, ingestion, and skin absorption (Wu, Wang, Tao, & Yu, 2010). Their studies found that at 4 weight percent acetonitrile, there was a tighter packing of the phospholipid bilayer; the packing mode and the hydration properties of the lipid polar groups didn't change. When 12 weight percent acetonitrile was added then it does dehydrate the carbonyl group of phospholipids (Wu et al., 2010). The affects of acetonitrile were tested on various other animals and insects for evidence of the harmful effects that are produced.

Petersen, et al., published a scientific article on the effect of acetonitrile on spider mites. The spider mites, Tetranychus urticae Koch, in their study were natural pests that fed on and damaged the African spider plant, Gynandropsis gynandra L (Nyalala, Petersen, & Grout, 2011). Their studies found that acetonitrile was the major volatile organic compound that was emitted from each part of the plant. Spider mites upon exposure to 2.5 µL concentration acetonitrile were

rendered immobile. When the affected spider mites were then introduced to pure air without acetonitrile concentration, only 10 percent regained their mobility. Thus acetonitrile was proved an effective repellant against spider mites based on how its prescence, it can render the spider mites disabled. (Nyalala et al., 2011).

1.7. Benzene Awareness and Implications

Benzene is a known carcinogen on the EPA toxic compounds list (Carletti & Romano, 2002). The BP oil spill created an environment in which there were large amounts of crude oil submerged below ocean water, in marshes, and on the coastlines of beaches (Kujawinski et al., 2011). Crude oil emits benzene, toluene, and xylene into the atmosphere. Kalf, et al., conducted studies on the effects of benzene on humans and concluded that benzene is a myelotoxin that causes blood dyscrasias and multiple other ailments (Kalf, 1987).

Benzene is a known bone marrow toxicant and carcinogen; its industrial uses range from gasoline additives to the use as a solvent for manufacturing rubber, drugs, and explosives ("Case Studies in Environmental Medicine: Benzene Toxicity," 2000). Chen, et al., expounded on the effects of benzene on the bone marrow of $B_6C_3F_1$ mice. When the mice metabolized the benzene, it caused the redox cycling of ring-hydroxylated benzene metabolites which yields peroxynitrite and other NO-derivatives. Nitric oxide is a contributor to benzene metabolism and can form nitrated derivatives that account for bone marrow toxicity (Chen et al., 2004).

Singh, et al., investigated the effects of benzene, toluene, and xylene on the genotoxicity and apoptosis in Drosophila melanogaster. Their studies showed that of the three volatile organic compounds, benzene caused the most damage to cells because it enhanced the activity of pro-apoptotic proteins in the Drosophila. The increased exposure time to all three of the volatile organic compounds yielded greater cell death (Singh et al., 2011).

This study will attempt to coordinate luminescent lanthanides, porphyrins, benzene and acetonitrile for the potential use as a sensor. The porphyrin's ability to sensitize and donate energy to the lanthanide makes it a better complex to sense the fluorescence change once the volatile organic compound alters the lanthanide properties. Sensing benzene and acetonitrile before they reach unhealthy levels is the main preventative measure to reduce the amount of people seriously affected.

CHAPTER 2

Experimental Methods

2.1. Chemical Reagents

The chemicals used, acetonitrile, ethanol, diethyl ether, benzene, $EuCl_3 \cdot 6H_2O$, $TbCl_3 \cdot 6H_2O$, $Dy(N0_3)_3 \cdot 5H_2O$, TPP 5,10,15,20-tetraphenylporphyrin, TBSP 5,10,15,20-tetrakisbenzylsulfonyl porphyrin, and NaCl were purchased from Sigma Aldrich without further purification.

2.2. Material Synthesis

2.2.1. Synthesis of Dy(TPP). A solution made by mixing 1.26 mg of $Dy(N0_3)_3 \cdot 5H_2O$ and 0.82 mg TPP in 10 mL DMF. The solution was sonicated for 3 minutes.

2.2.2. Synthesis of Dy(TPP) CH_3CN. A test tube containing 1.34 mg of $Dy(N0_3)_3 \cdot 5H_2O$ and 0.8 mg of TPP in 10 mL of DMF and 5 mL of CH_3CN was sonicated for 3 minutes.

2.2.3. Synthesis of Dy(TPP) C_6H_6. A 1.28 mg $Dy(N0_3)_3 \cdot 5H_2O$, 0.81 mg TPP, 10 mL DMF and 5 mL of benzene was sonicated in a test tube for 3 minutes.

2.2.4. Synthesis of Eu(TPP). A solution made by mixing 2.4 mg of $EuCl_3 \cdot 6H_2O$ and 0.83 mg of TPP in 10 mL of DMF. The solution was then sonicated for 3 minutes.

2.2.5. Synthesis of Eu(TPP) CH_3CN. A 2.4 mg $EuCl_3 \cdot 6H_2O$, 0.85 mg TPP, 10 mL DMF, and 5 mL of CH_3CN was mixed in a test tube and sonicated for 3 minutes.

2.2.6. Synthesis of Eu(TPP) C_6H_6. In a test tube 2.4 mg of $EuCl_3 \cdot 6H_2O$ was mixed with 0.9 mg TPP in 10 mL of DMF and 5 mL of benzene. The solution was then sonicated for 3 minutes.

2.2.7. Synthesis of Eu(TPP) (Eu-a). The synthesis of EuTPP complex **(Eu-a)** proceeded as follows: 2.66 mg of 5,10,15,20-tetraphenylporphyrin was dissolved in 9 mL of Et_2O in a 25

mL beaker which resulted in a purple solution. A second 25 mL beaker contained 12.15 mg of $EuCl_3 \bullet 6H_2O$ dissolved in 8 mL of EtOH, which resulted in a clear solution. The two were mixed together to form a green solution, which was transferred to a 25 mL round bottom flask and refluxed for 5 hours. Solution was then cooled to room temperature then transferred to a 50 mL beaker covered with parafilm and aluminum foil. After one week green solution turned to yellow solution; after another week yellow solution turned orange color. Luminescence studies collected on all three aliquots.

2.2.8. Synthesis of Eu(TPP) (Eu-b). The synthesis of EuTPP complex **(Eu-b)** proceeded as follows: 3.77 mg of 5,10,15,20-tetraphenylporphyrin was dissolved in 9 mL of Et_2O in a 25 mL beaker which resulted in a purple solution. A second 25 mL beaker contained 17.95 mg of $EuCl_3 \bullet 6H_2O$ dissolved in 9 mL of EtOH, which resulted in a clear solution. The two were mixed together to form a green solution, which was transferred to a 25 mL round bottom flask and refluxed for 5 hours. Solution was then cooled to room temperature then transferred to a 50 mL beaker, layered 10 mL of benzene, and covered with parafilm and aluminum foil.

2.2.9. Synthesis of Eu(TPP) (Eu-c). The synthesis of EuTPP complex **(Eu-c)** proceeded as follows: 2.39 mg of 5,10,15,20-tetraphenylporphyrin was dissolved in 10 mL of Et_2O in a 25 mL beaker which resulted in a purple solution. A second 25 mL beaker contained 11.3 mg of $EuCl_3 \bullet 6H_2O$ dissolved in 10 mL of EtOH, which resulted in a clear solution. The two were mixed together to form a green solution, which was transferred to a 25 mL round bottom flask and refluxed for 5 hours. Solution was then cooled to room temperature then transferred to a 50 mL beaker, layered 10 mL of acetonitrile, and covered with parafilm and aluminum foil. Endothermic reaction occurred resulting in condensation on outside of beaker.

2.2.10. Synthesis of Eu(TPP) (Eu-d). The synthesis of EuTPP complex **(Eu-d)** proceeded as follows: 2.25 mg of 5,10,15,20-tetraphenylporphyrin was dissolved in 10 mL of Et_2O, sonicated for 3 minutes in a 25 mL beaker, which resulted in a purple solution. Another 25 mL beaker contained 10 mL of 3.746 x 10^{-4}M NaOH solution. The two beakers were mixed into a 50 mL round bottom flask and solution stayed purple. The reaction was refluxed for 3 hours when 9.45 mg $EuCl_3 \bullet 6H_2O$ dissolved in 11 mL of EtOH was added to reaction vessel, then refluxed for 3 additional hours. The reaction was cooled to room temperature, transferred to 50 mL beaker, covered with parafilm and aluminum foil.

2.2.11. Synthesis of Eu(TPP) (Eu-e). The synthesis of EuTPP complex **(Eu-e)** proceeded as follows: 2.62 mg of 5,10,15,20-tetraphenylporphyrin was dissolved in 10 mL of Et_2O, sonicated for 3 minutes in a 25 mL beaker, which resulted in a purple solution. Another 25 mL beaker contained 10 mL of 3.746 x 10^{-4}M NaOH solution. The two beakers were mixed into a 50 mL round bottom flask and solution stayed purple. The reaction was refluxed for 3 hours when 10.54 mg $EuCl_3 \bullet 6H_2O$ dissolved in 10 mL of EtOH was added to reaction vessel, then refluxed for 3 additional hours. The reaction was cooled to room temperature, transferred to 50 mL beaker, layered with 10 mL benzene, covered with parafilm and aluminum foil. The layering resulted in an endothermic reaction.

2.2.12. Synthesis of Eu(TPP) (Eu-f). The synthesis of EuTPP complex **(Eu-f)** proceeded as follows: 2.10 mg of 5,10,15,20-tetraphenylporphyrin was dissolved in 10 mL of Et_2O, sonicated for 3 minutes in a 25 mL beaker, which resulted in a purple solution. Another 25 mL beaker contained 10 mL of 3.746 x 10^{-4}M NaOH solution. The two beakers were mixed into a 50 mL round bottom flask and solution stayed purple. The reaction was refluxed for 3 hours when 12.58 mg $EuCl_3 \bullet 6H_2O$ dissolved in 10 mL of EtOH was added to reaction vessel, then refluxed

for 3 additional hours. The reaction was cooled to room temperature, transferred to 50 mL beaker, layered with 10 mL acetonitrile, covered with parafilm and aluminum foil. The layering resulted in an endothermic reaction.

2.2.13. Synthesis of Dy(TPP) (Dy-a). The synthesis of DyTPP complex **(Dy-a)** proceeded as follows: 2.29 mg of 5,10,15,20-tetraphenylporphyrin was dissolved in 10 mL of Et_2O, sonicated for 3 minutes in a 25 mL beaker, which resulted in a purple solution. Another 25 mL beaker contained 9.18 mg $Dy(NO_3)_3 \bullet 5H_2O$ dissolved in 10 mL of EtOH, sonicated for 3 minutes and added to the first beaker then refluxed for 6 hours. The reaction was still purple in color. The reaction was cooled to room temperature, transferred to 50 mL beaker, covered with parafilm and aluminum foil.

2.2.14. Synthesis of Dy(TPP) (Dy-b). The synthesis of DyTPP complex **(Dy-b)** proceeded as follows: 2.18 mg of 5,10,15,20-tetraphenylporphyrin was dissolved in 10 mL of Et_2O, sonicated for 3 minutes in a 25 mL beaker, which resulted in a purple solution. Another 25 mL beaker contained 17.49 mg $Dy(NO_3)_3 \bullet 5H_2O$ dissolved in 10 mL of EtOH, sonicated for 3 minutes and added to the first beaker then refluxed for 6 hours. The reaction was still purple in color. The reaction was cooled to room temperature, transferred to 50 mL beaker, layered with 10 mL of benzene, covered with parafilm and aluminum foil. The layering resulted in an endothermic reaction.

2.2.15. Synthesis of Dy(TPP) (Dy-c). The synthesis of DyTPP complex **(Dy-c)** proceeded as follows: 2.96 mg of 5,10,15,20-tetraphenylporphyrin was dissolved in 10 mL of Et_2O, sonicated for 3 minutes in a 25 mL beaker, which resulted in a purple solution. Another 25 mL beaker contained 11.88 mg $Dy(NO_3)_3 \bullet 5H_2O$ dissolved in 10 mL of EtOH, sonicated for 3 minutes and added to the first beaker then refluxed for 6 hours. The reaction was still purple in

color. The reaction was cooled to room temperature, transferred to 50 mL beaker, layered with 10 mL of acetonitrile, covered with parafilm and aluminum foil. The layering resulted in an endothermic reaction.

2.2.16. Synthesis of Eu(TBSP). A 6.2 mg $EuCl_3 \bullet 6H_2O$, 0.9 mg TBSP were mixed in a 4 mL solution of a 3:1 H_2O:EtOH. The solution was then sonicated for 2 minutes.

2.2.17. Synthesis of Dy(TBSP). A test tube containing 9.62 mg of $Dy(NO_3)_3 \bullet 5H_2O$, 1.2 mg TBSP, 4 mL of a 3:1 H_2O:EtOH solution was sonicated for 2 minutes.

2.2.18. Synthesis of Tb(TBSP). A test tube containing 8.9 mg of $TbCl_3 \bullet 6H_2O$, 0.77 mg TBSP, 4 mL of 3:1 H_2O:EtOH solution was sonicated for 2 minutes.

2.2.19. Synthesis of Eu(TBSP) CH_3CN. The synthesis of EuTBSP CH_3CN proceeds as follows: 9.15 mg $EuCl_3 \bullet 6H_2O$, .90 mg 5,10,15,20-tetrakisbenzylsulfonyl porphyrin were dissolved in 4 mL of a 3:1 H_2O:EtOH solution in a test tube. A 2 mL of CH_3CN was added and solution was sonicated for 3 minutes.

2.2.20. Synthesis of Dy(TBSP) CH_3CN. The synthesis of DyTBSP CH_3CN proceeds as follows: 9.62 mg $Dy(NO_3)_3 \bullet 5H_2O$, 1.28 mg 5,10,15,20-tetrakisbenzylsulfonyl porphyrin were dissolved in 4 mL of a 3:1 H_2O:EtOH solution in a test tube. A 2 mL of CH_3CN was added and solution was sonicated for 3 minutes.

2.2.21. Synthesis of Tb(TBSP) CH_3CN. The synthesis of TbTBSP CH_3CN proceeds as follows: 8.93 mg $TbCl_3 \bullet 6H_2O$, 0.77 mg 5,10,15,20-tetrakisbenzylsulfonyl porphyrin were dissolved in 4 mL of a 3:1 H_2O:EtOH solution in a test tube. A 2 mL of CH_3CN was added and solution was sonicated for 3 minutes. This sample was prepared and collected using the same procedure as the other lanthanide, TBSP, and solvent experiments. Attention to the ambient conditions was noted as well.

2.2.22. Synthesis of Eu(TBSP) C_6H_6. The synthesis of EuTBSP benzene proceeds as follows: 9.24 mg $EuCl_3 \bullet 6H_2O$, 1.08 mg 5,10,15,20-tetrakisbenzylsulfonyl porphyrin were dissolved in 4 mL of a 3:1 H_2O:EtOH solution in a test tube. A 2 mL of benzene was added and solution was sonicated for 3 minutes.

2.2.23. Synthesis of Dy(TBSP) C_6H_6. The synthesis of DyTBSP benzene proceeds as follows: 11.37 mg $Dy(NO_3)_3 \bullet 5H_2O$, .87 mg 5,10,15,20-tetrakisbenzylsulfonyl porphyrin were dissolved in 4 mL of a 3:1 H_2O:EtOH solution in a test tube. A 2 mL of benzene was added and solution was sonicated for 3 minutes.

2.2.24. Synthesis of Tb(TBSP) C_6H_6. The synthesis of TbTBSP benzene proceeds as follows: 12.45 mg $TbCl_3 \bullet 6H_2O$, 1.15 mg 5,10,15,20-tetrakisbenzylsulfonyl porphyrin were dissolved in 4 mL of a 3:1 H_2O:EtOH solution in a test tube. A 2 mL of benzene was added and solution was sonicated for 3 minutes.

2.2.25. Synthesis of Na(TPP). A mixture of 0.5 mg TPP, 2.65 mg NaCl, and 3 mL of a 2:1 EtOH:H_2O solution was sonicated for 2 minutes.

2.2.26. Synthesis of Na(TBSP). A test tube containing 2.3 mg of NaCl, 0.4 mg TBSP, and 3 mL of a 2:1 EtOH:H_2O solution was sonicated for 2 minutes.

2.2.27. Synthesis of Ag(TBSP). A solution of 13.3 mg $AgNO_3$, 2.8 mg TBSP, 5 mL of a 3:2 EtOH:H_2O was sonicated for 2 minutes.

2.2.28. Synthesis of Ag(TPP). A solution of 3.49 mg of $AgNO_3$, 0.4 mg TPP, and 5 mL of Et_2O was sonicated for 2 minutes.

2.2.29. Synthesis of Ce(TBSP). A test tube containing 23.5 mg of $Ce(NO_3)_3 \bullet 6H_2O$, 2.2 mg of TBSP, and 10 mL of a 3:2 H_2O:EtOH solution was sonicated for 3 minutes.

2.2.30. Synthesis of Ce(TPP). A solution containing 7.2 mg $Ce(NO_3)_3•6H_2O$, 0.6 mg of TPP, and 10 mL of Et_2O was sonicated for 3 minutes in a test tube.

2.2.31. Synthesis of Gd(TBSP). A 32.5 mg $Gd(NO_3)_3•6H_2O$, 2.5 mg TBSP, and 10 mL of 3:2 H_2O:EtOH solution was sonicated for 3 minutes in a test tube.

2.2.32. Synthesis of Gd(TPP). A test tube containing 8.5 mg of $Gd(NO_3)_3•6H_2O$, 0.6 mg of TPP, and 10 mL of Et_2O was sonicated for 3 minutes.

2.2.33. Synthesis of Ce(TPP) CH_3CN. A test tube containing a mixture of 7.15 mg of Ce(NO3)36H2O, 0.5 mg of TPP, 3 ml of acetonitrile, and 10 ml of Et2O was sonicated for 2 minutes.

2.2.34. Synthesis of Ce(TPP) C_6H_6. A solution containing 9.62 mg of Ce(NO3)36H2O, 1.4 mg of TPP, 3 ml of benzene, and 10 ml of DMF was sonicated for 2 minutes in a test tube.

2.2.35. Synthesis of Gd(TPP) CH_3CN. A mixture of 8.53 mg of Gd(NO3)36H2O, 0.5 mg of TPP, 3 ml of acetonitrile, and 10 ml of Et2O was sonicated for 2 minutes in a test tube.

2.2.36. Synthesis of Gd(TPP) C_6H_6. A test tube containing 6.9 mg of Gd(NO3)36H2O, 5.6 mg of TPP, 3 ml of benzene, and 10 ml of DMF was sonicated for 2 minutes.

2.2.37. Photoluminescence spectroscopy. Photoluminescence measurements were obtained using a photon technology international (PTI) spectrometer. The instrument uses a Ushio -75Xe xenon arc lamp. It is also equipped with a Hamamatsu R928P photomultiplier tube. It uses a LPS-220B power supply unit, a Brytebox and a MD-5020 motor driver. The monochromator is a model 101M f/4 0.2-meter Czerny-Turner with a 4 nm/mm bandpass. The detector is a model 814 analog/photon-counting photomultiplier detector. FeliX32 software purchased from photon technology international was used to collect emission and excitation data.

For liquid samples, a quartz cuvette was used for the collection of emission and excitation data at room temperature. Solid samples were placed in borosilicate capillary tubes annealed by heating to exclude exposure to oxygen for air sensitive complexes and to ensure sample integrity. Photoluminescence spectra were collected both at room temperature and liquid nitrogen temperatures; the liquid nitrogen temperature data was collected using a cold-finger dewar for the samples encapsulated by borosilicate capillary tubes. The data that was collected from the spectrometer was transferred to Microsoft Excel spreadsheet for analysis.

2.2.38. UV-Vis spectroscopy. The UV-Vis spectroscopy data was collected on a Shimadzu spectrometer model UV-2401PC/2501PC. The instrument has a wave length range of 190 nm to 1100 nm and a resolution of 0.1 nm. The wavelength accuracy is ± 0.3 nm. An R-928 photomultiplier detector was used for detection. The instrument operates with a double beam summing feed-back photometric system. A 50 Watt halogen lamp and deuterium lamp is used as light sources. Spectra for liquid samples were collected using quartz cuvettes at a slow scan rate. Data was transferred from the spectrometer to Microsoft Excel spreadsheet.

2.2.39. X-ray diffraction crystallography. X-ray diffraction crystallography data was collected using a Bruker AXS Smart X2S system. The instrument uses a CCD 485 Breeze detector and a Ricor K535 power supply unit. It uses an Oxford Cryosystems desktop cooler, AD 51 dry air unit, and a Pfeifer vacuum model DUO 2.5. The images were collected by transferring data from the X-ray apparatus to the computer using Apex, Xshell, and Mercury software; they were then analyzed, refined, and interpreted based on the previous three software packages. Crystal samples were mounted on micromount needles purchased from the Bruker Corporation, using Paratone-N oil purchased from Hampton Research. Another batch of crystal data was collected when using UV light curable adhesive to mount the crystal to the micromount.

CHAPTER 3

Results and Discussion

3.1. PL of (TPP)

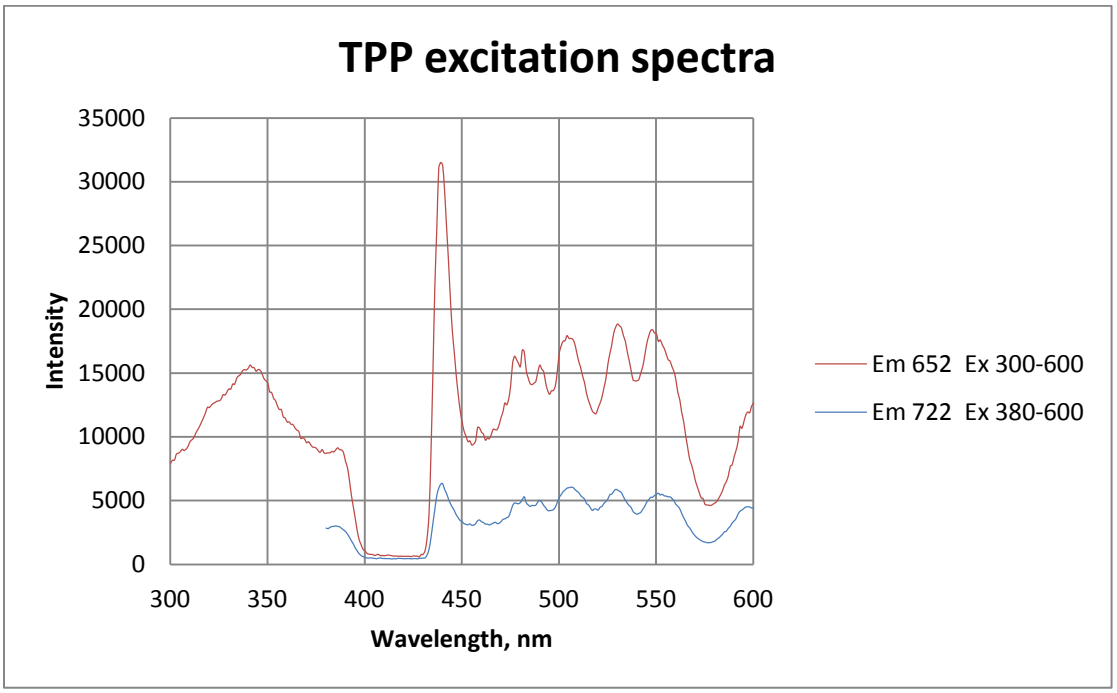

Figure 3.1. PL of TPP excitation spectra.

The above figure 3.1 contains the excitation spectra of TPP dissolved in Et_2O. The red spectrum was monitored at 652 nm, while the blue spectrum was at 722 nm. The two spectra show similar profile with only variation being the peak intensities. The major characteristic TPP excitation peaks are observed at 345 nm (broad), 440 nm (sharp), 504 nm (broad), 530 nm (broad), 549 nm (broad), and 600 nm (broad). There is a negative slope from the peak at 345 to the shoulder at 380 nm.

The peak shown at 440 nm is consistent with the wavelength required to promote the molecule from the ground state to the second excited state. The subsequent peaks at 504, 530, 547, 560, and 600 nm have an average spacing of ~1200 cm^{-1} indicating vibronic coupling between the electronic transition and the ring system.

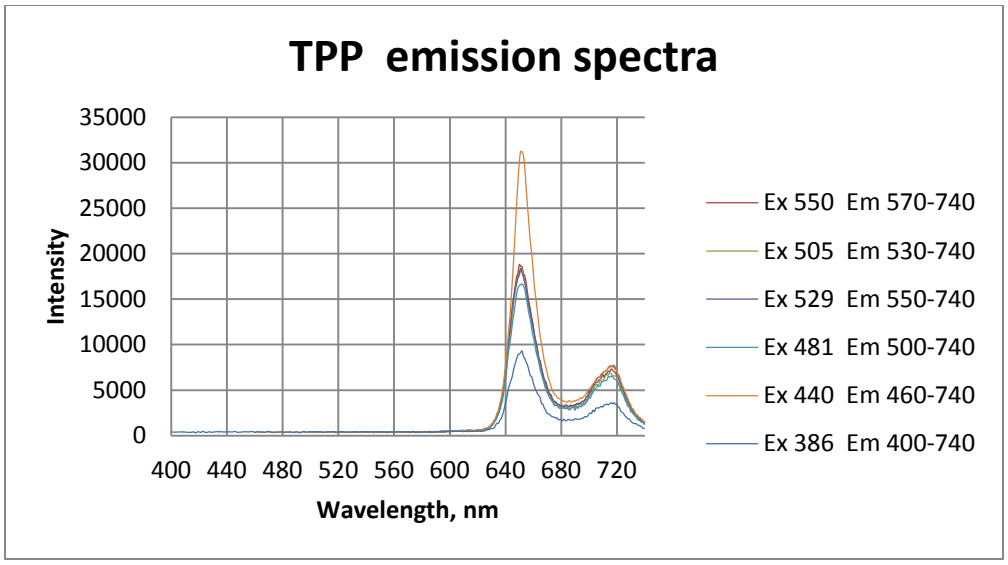

Figure 3.2. PL of TPP emission spectra.

Figure 3.2., shows the emission spectra for TPP dissolved in Et_2O. These spectra show the characteristic TPP emission bands at 652 nm (sharp), and 719 nm (broad). When excited at 440 nm the TPP shows the maximum intensity, whereas excitation at 386 nm provides the lowest intensity. The peak intensity of the low energy emission band at 719 nm is nearly independent of the wavelength, except when excited at 386 nm.

3.2. PL of $EuCl_3 \cdot 6H_2O$

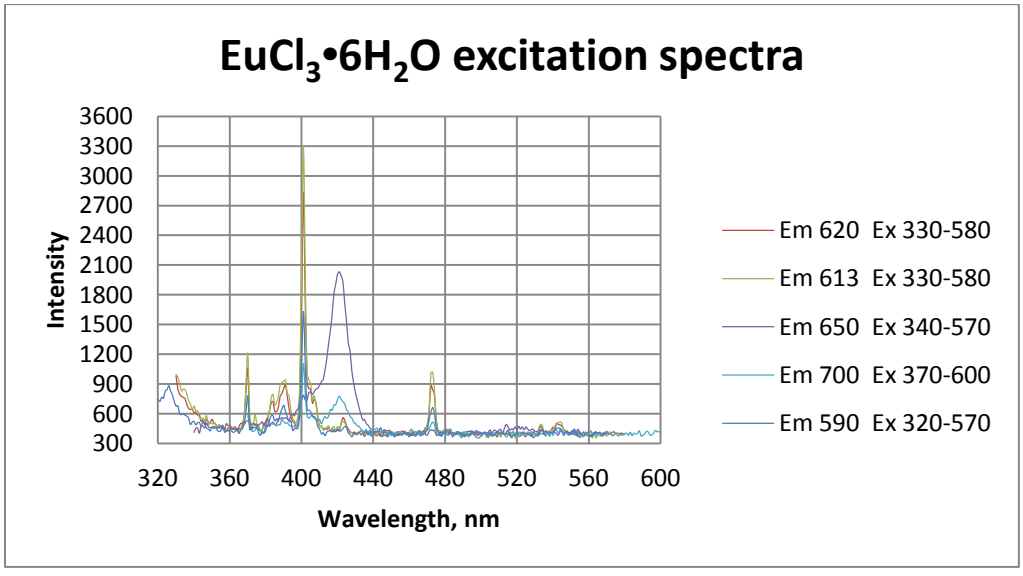

Figure 3.3. $EuCl_3 \cdot 6H_2O$ photoluminescence excitation spectra.

The figure 3.3., shows the excitation spectra of $EuCl_3 .6H_2O$ consisting of two different profiles based on the monitoring wavelength. When monitored at 650 nm, the spectrum shows broad band at 420 nm, whereas when monitored at other wavelengths the profiles show sharp bands at 370, 393, 401, and 473 nm characteristics of f-f transitions within Eu^{3+} ion.

The overall excitation bands and their respective assignments given in parenthesis: 327 nm ($^7F_1 \rightarrow {}^5H_3$), 370 nm ($^7F_1 \rightarrow {}^5L_8$), 381 nm ($^7F_1 \rightarrow {}^5L_7$), 401 nm ($^7F_1 \rightarrow {}^5L_6$), 420 nm ($^7F_1 \rightarrow {}^5D_3$), 473 nm ($^7F_1 \rightarrow {}^5D_2$). All of the peaks that are below 400 nm are located in the ultraviolet region of the electromagnetic spectrum. The peaks at 420 nm and 473 nm show in the violet and blue region of the electromagnetic spectrum.

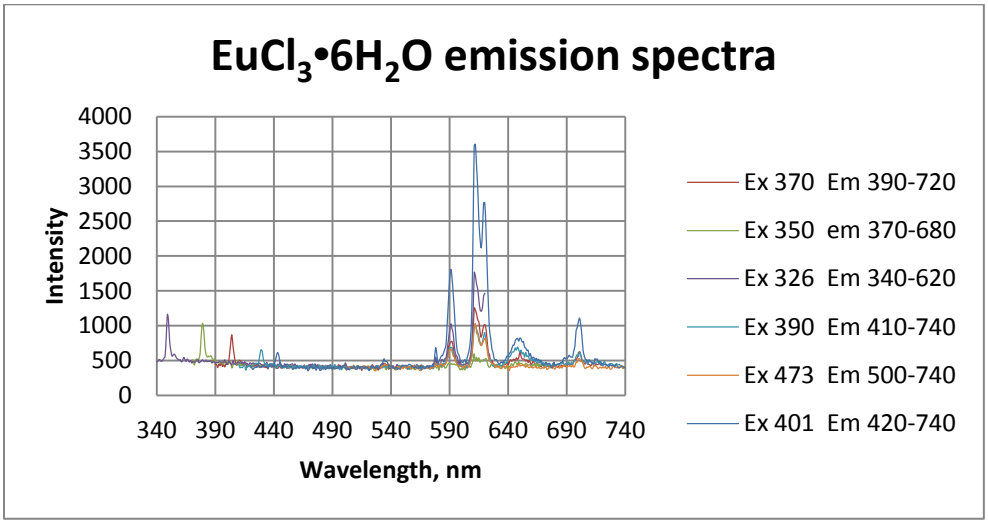

Figure 3.4. $EuCl_3•6H_2O$ photoluminescence emission spectra.

The figure 3.4., shows the emission profile of $EuCl_3•6H_2O$ with its prominent peaks at 593, 613, 620, 650, and 700 nm. The 593 and 700 nm peaks are sharp, whereas the 650 nm peak is broad. The most intense peak usually occurring at 615 nm is split to a doublet producing sharp peaks at 613 and 620 nm. The emission spectra are very low in intensity. The emission peaks, characteristic to europium salts, correspond to the transitions that arise from photons being emitted from an excited state to various electronic ground state manifolds. The wavelengths,

along with the transitions are listed as follows: 593 nm $^5D_0 \rightarrow {}^7F_2$, 613 nm $^5D_0 \rightarrow {}^7F_3$, 620 nm $^5D_0 \rightarrow {}^7F_3$, 650 nm $^5D_0 \rightarrow {}^7F_4$, and 700 nm $^5D_0 \rightarrow {}^7F_6$. These ground state to excited state transitions occur at different wavelengths although they emit in the red portion of the electromagnetic spectrum.

3.3. PL of Eu(TPP) Complexes

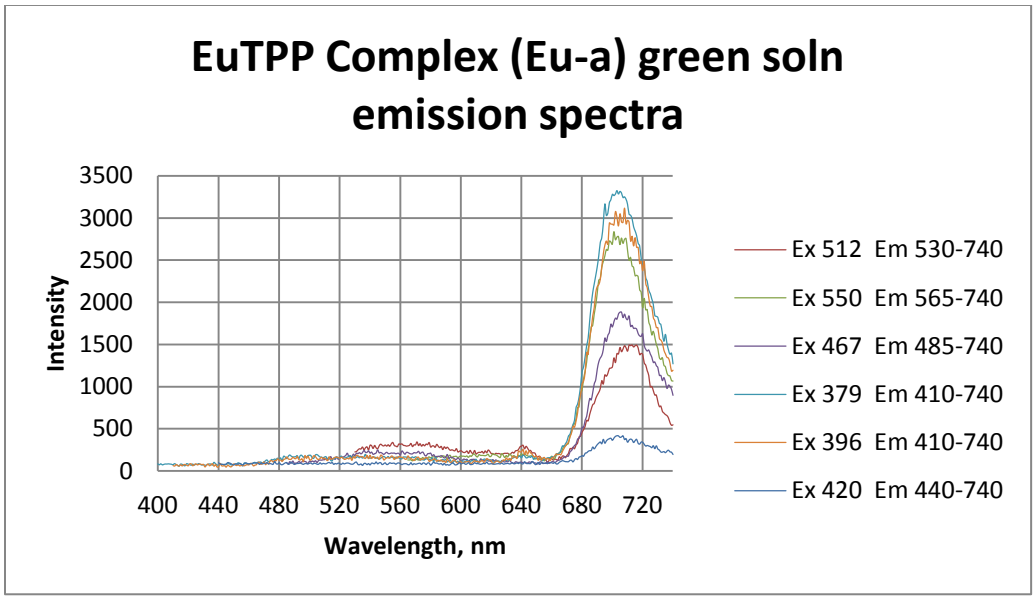

Figure 3.5. PL of Eu(TPP)(**Eu-a**) green solution emission spectra.

Figure 3.5., shows the alteration in spectra from the previous TPP dissolved in Et_2O alone. There is red shift from the 650 nm peak to a peak at 705 nm and disappearance of the peak observed at 719 nm. There is also a tenfold decrease in emission intensity along with the appearance of a small peak at 640 nm which corresponds to europium salt peak; there's a broad band spanning 530 nm to 607 nm.

The emission intensity at 705 nm increases with the excitation wavelength. When excited at 512 nm and 467 nm, the profiles show slight deviation from the other profiles. Rather than a non-luminescent beginning part of the spectrum, a very broad band, albeit very weak spanning the 520-600 nm range band is observed along with a sharper (but weak) band, small band at 640 nm.

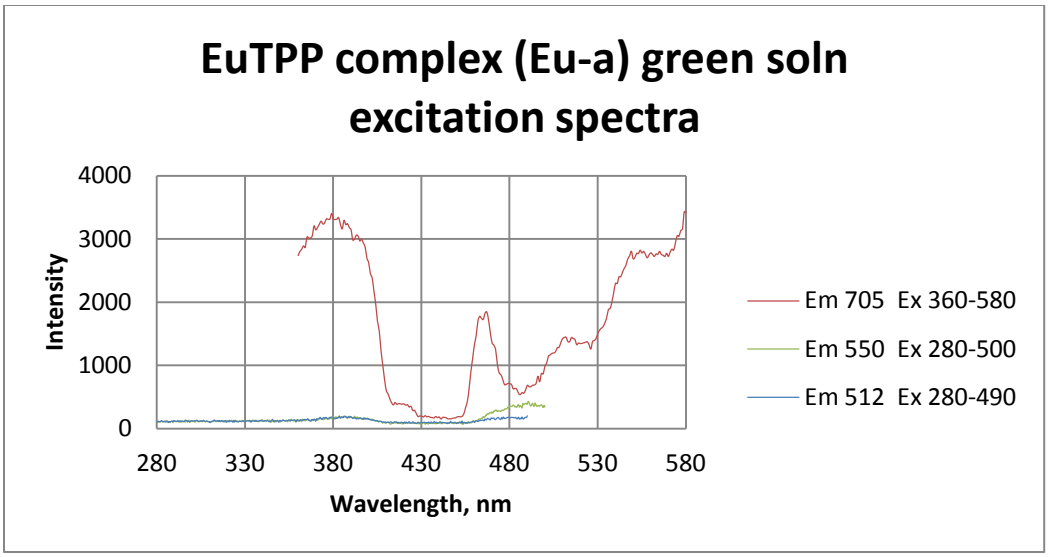

Figure 3.6. PL of Eu(TPP)**(Eu-a)** green solution excitation spectra.

Figure 3.6 shows the excitation spectra of EuTPP **(Eu-a)** green solution with a broad band at 380 nm, and sharper bands at 427, 467, 512, and 550 nm. The most prominent spectrum was collected when monitored at 705 nm which corresponds to the emission maximum. The least prominent spectra were monitored at 550 and 512 nm.

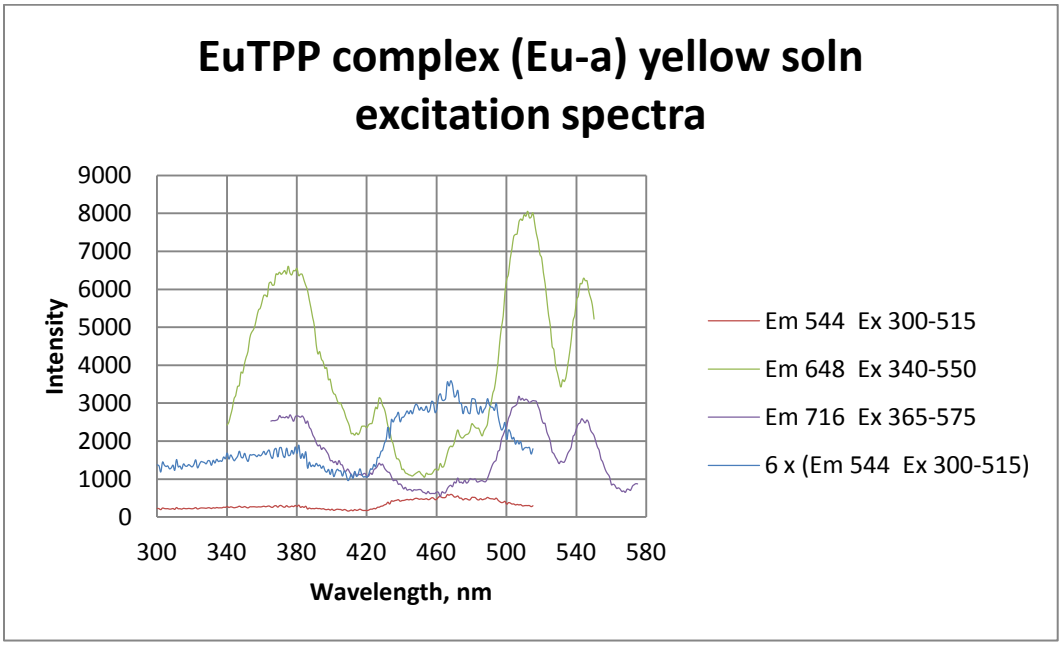

Figure 3.7. PL of Eu(TPP)**(Eu-a)** yellow solution excitation spectra.

In Figure 3.7 is shown the change in the excitation spectrum from the green solution. There are four major peaks shown at 375 (broad), 427, 514 (broad), and 544 nm. The yellow solution retains the prominent broad band peak at 380 nm. The small broad band that was at 427 on the green solution excitation spectrum has now become more prominent and sharper in the yellow solution.

The band at 514 nm becomes more pronounced and defined as it more than quadruples in intensity. The band at 544 nm becomes more pronounced as it doubles in intensity. The broad band maximizing at 467 nm is from monitoring at the broad emission peak at 540 of the emission spectrum. There are two different profiles in the excitation spectrum with three different spectra. When monitored at 648 nm and 716 nm the same profile exists although differing in intensity.

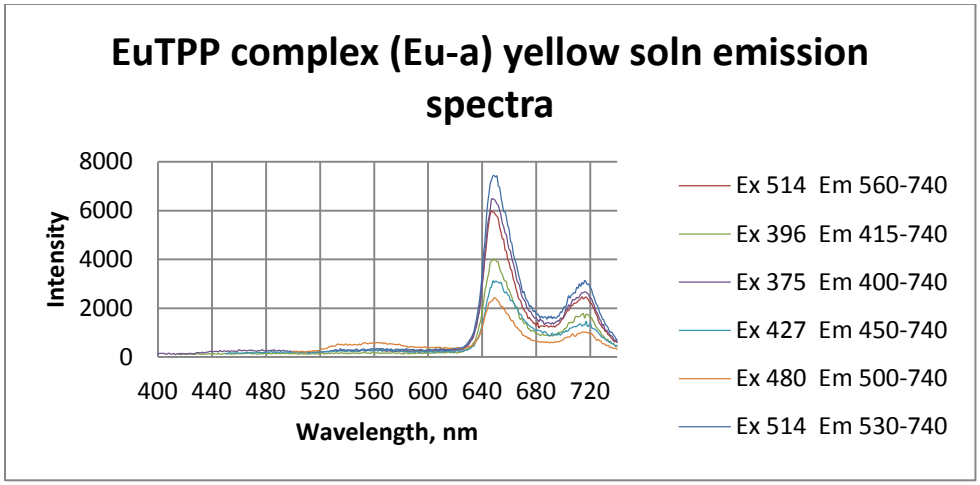

Figure 3.8. PL of Eu(TPP)**(Eu-a)** yellow solution emission spectra.

Figure 3.8 shows the emission spectra of EuTPP **(Eu-a)** yellow solution. The 650 and 715 nm peaks are characteristic of TPP. The spectra show maxima at 545 nm (broad), 647 nm and 715 nm. The maxima have blue-shifted from 652 nm to 647nm and from 719 nm to 715 nm in these spectra compared to the TPP spectrum. There is an even distribution of intensity that is wavelength dependent, although the intensity of the 647 nm maximum has decreased by a factor of 4. The smaller 715 nm peak decreased in intensity by a factor of 2.

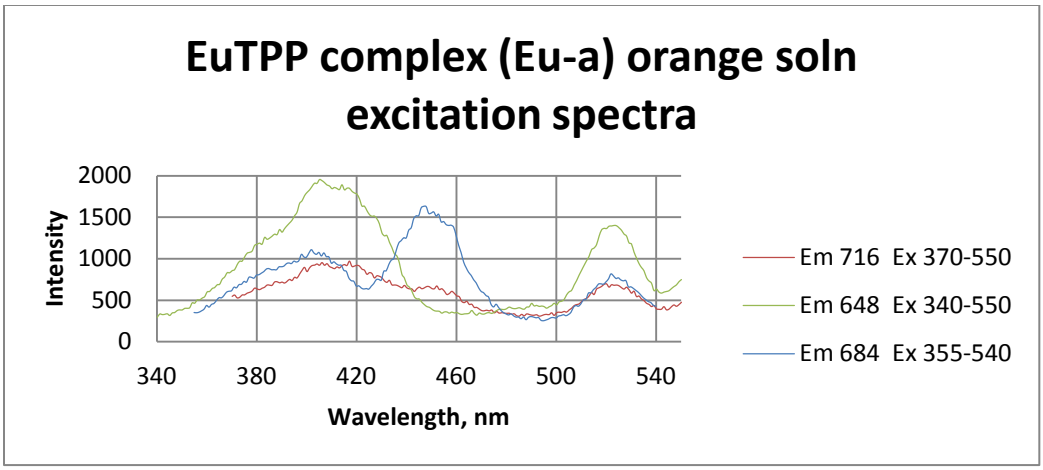

Figure 3.9. PL of Eu(TPP)**(Eu-a)** orange solution excitation spectra.

In Figure 3.9 is shown the excitation spectra of the orange solution of EuTPP **(Eu-a)**. There are three broad maxima in the spectra at 408 nm, 448 nm, and 526 nm. There is a small shoulder at 380 nm. The peaks have shifted and the intensity has vastly diminished showing the great affect europium has on altering excitation spectra.

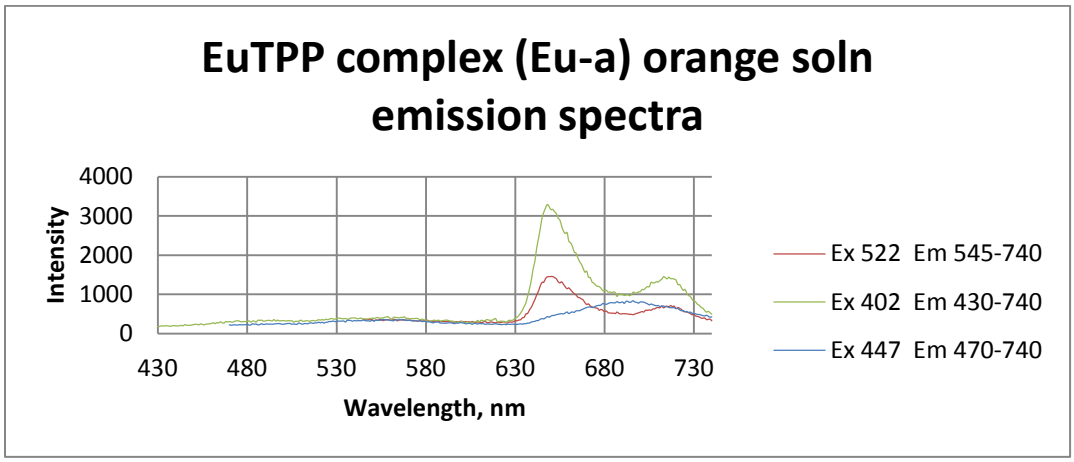

Figure 3.10. PL of Eu(TPP)**(Eu-a)** orange solution emission spectra.

Figure 3.10 shows the emission spectra of the orange EuTPP **(Eu-a)** solution with maxima at 650 nm and 712 nm. The broad band spanning 530 nm to 600 nm is still persistent in the orange solution. There is a broad peak at 698 nm when the sample was excited at 447 nm; consistent with the broad emission band that was seen in the green solution of EuTPP **(Eu-a)**.

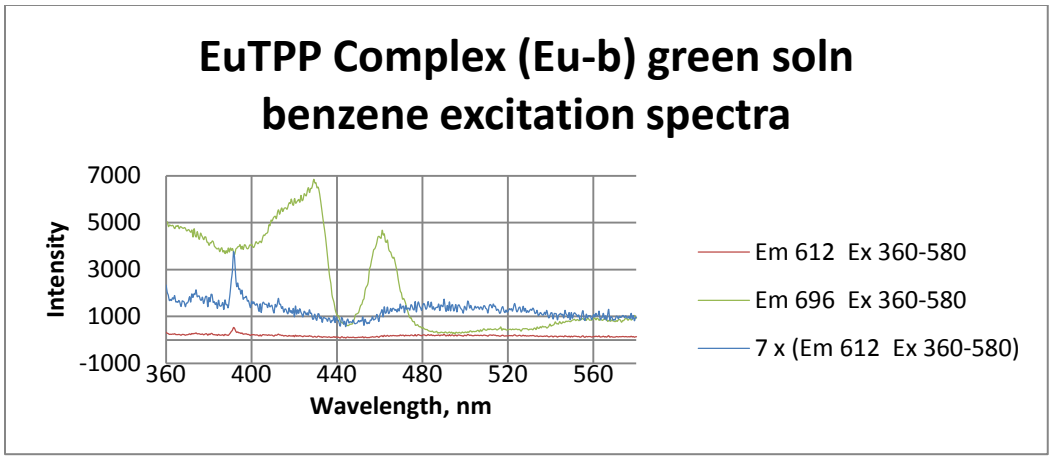

Figure 3.11. PL of Eu(TPP)(C_6H_6)**(Eu-b)** green solution excitation spectra.

The above figure, (Figure 3.11), shows the excitation spectra with maxima at 373 nm, 391 nm, 431 nm and 462 nm. Both the 373 and 431 bands are observed at a blue shifted position when compared with the original TPP excitation bands at 380 and 440 nm, respectively. The 462 nm peak, however, is consistent with the original although it has lower intensity for the entire spectrum. The subsequent bands after the 462 nm wavelength were silenced.

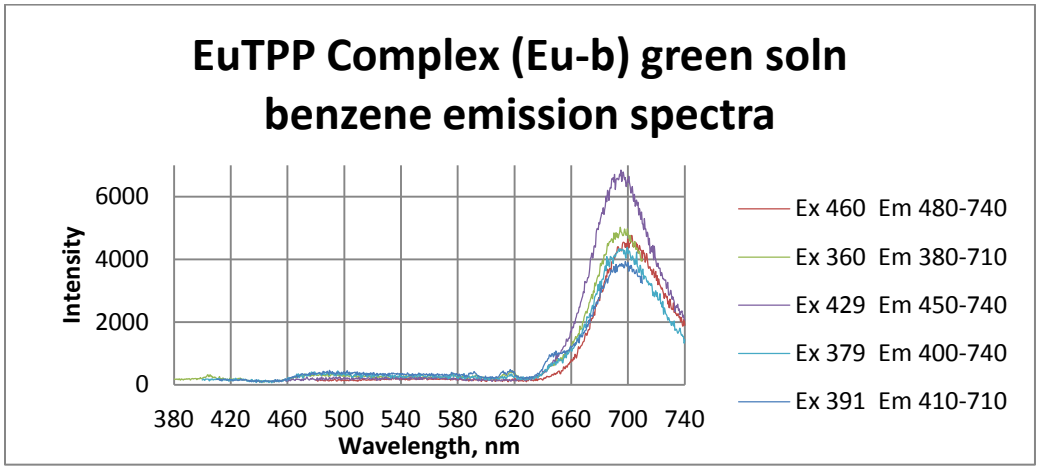

Figure 3.12. PL of Eu(TPP)(C_6H_6)**(Eu-b)** green solution emission spectra.

The above figure, (3.12), shows a broad peak maximizing at 698 nm, which is shifted compared with the peak at 705 nm when Eu(TPP) **(Eu-b)** wasn't layered with benzene. There are also smaller characteristic peaks at 590, 610, 615, and 647 nm. These smaller peaks are most

prominent when the spectrum is excited at 360 nm or 391 nm. The 590, 610, and 615 nm are characteristic bands for europium salt when it's dissolved in ethanol. The appearance of these smaller peaks shows that europium and benzene influence the natural emission characteristics of TPP and benzene is able to influence the expression of europium emission peaks.

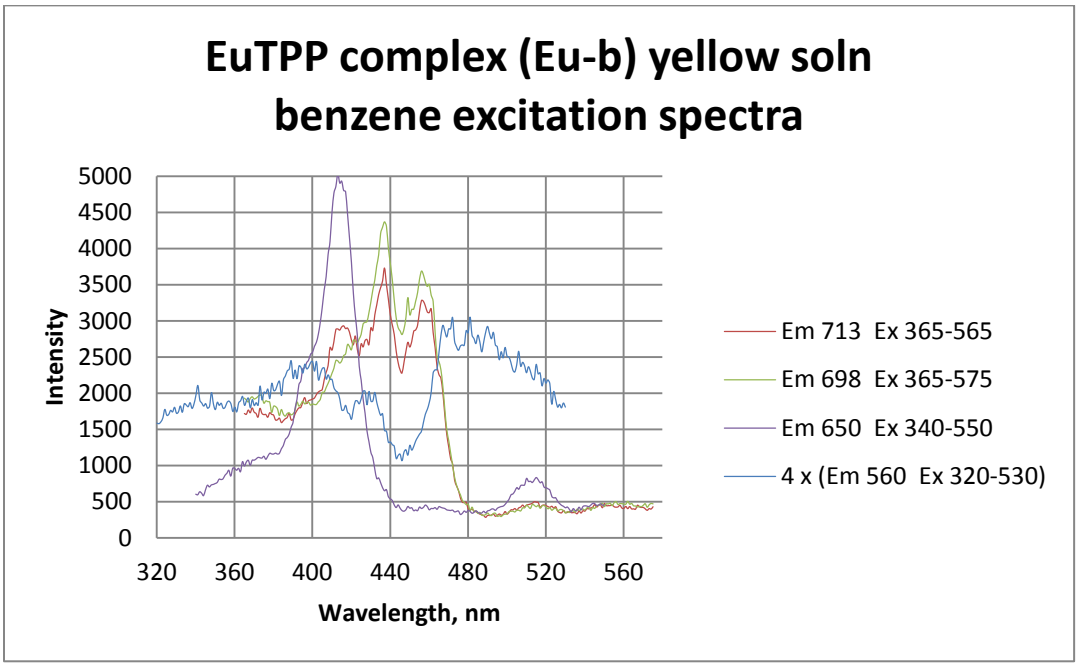

Figure 3.13. PL of Eu(TPP)(C_6H_6)**(Eu-b)** yellow solution excitation spectra.

The above Figure 3.13 shows the excitation spectra of Eu(TPP) **(Eu-b)** layered in benzene after it has changed from a green colored to a yellow solution. Three maxima are located at 416, 438, and 457 nm. There are three distinctly, different profiles existing in the excitation spectrum; two are similar when monitored at 713 nm and 698 nm, whereas when monitoring at 650 nm the profile is vastly different. The peaks at 438 nm and 457 nm are absent and a small broad peak at 513 nm appears. The spectral profile exhibited when monitored at 560 nm and magnified four times is completely different from the other two profiles. The excitation peaks arising at 438 nm and 457 nm are in the blue region of the electromagnetic spectrum, with the peak at 513 nm is located in the green portion of the spectrum.

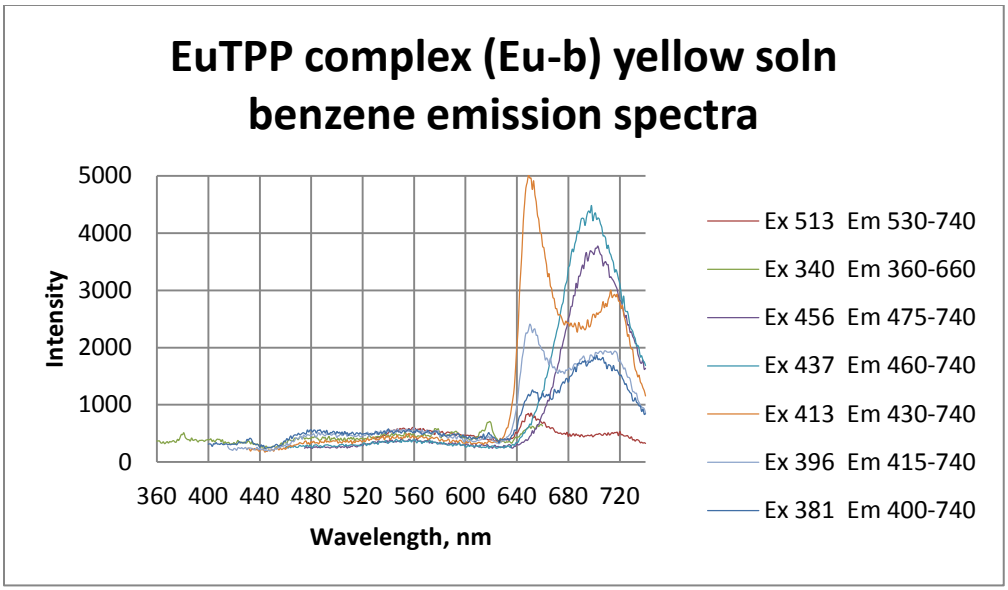

Figure 3.14. PL of Eu(TPP)(C_6H_6)**(Eu-b)** yellow solution emission spectra.

The spectra shown in Figure 3.14 correspond to the emission profile of the yellow solution of Eu(TPP) **(Eu-b)** that was layered in benzene. There are several maxima at 649, 697, and 715 nm. There is a small peak that appears at 617 nm, corresponding to Eu^{3+} f-f transition when the compound is excited at 340 nm. There are three behaviors coexisting in this emission profile.

When the solution is excited at 437 or 456 nm then the predominant peak maximum is observed at 697nm; this corresponds to the excitation spectra when it was monitored at 698 nm. When excited at 381, and 396 nm, two peaks are seen maximizing at 649 and 697 nm. When excited at 413 and 513 nm, the spectrum produces maxima at 649 and 715 nm; these correspond to the excitation profile when it was monitored at the 650 nm. Instead of no observed luminescence at the beginning of the emission spectra from 360 to 630 nm, there is luminescence activity when benzene was added, resulting in an europium maximum at 617 nm and broad band spanning 460 to 600 nm. The different profiles observed in this emission profile signify that there are two independent species in solution that show independent emissions when excited at their respective wavelengths.

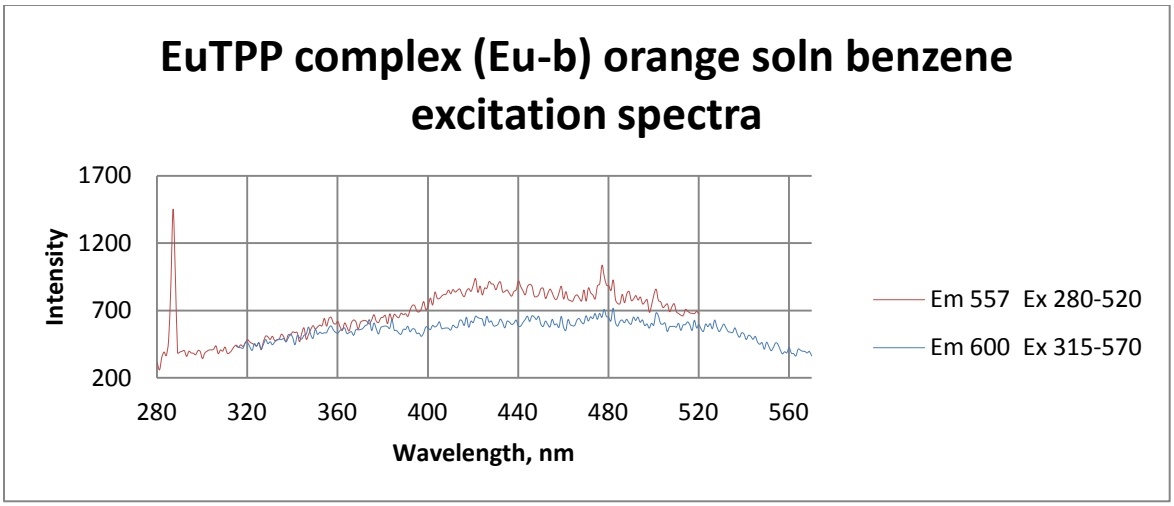

Figure 3.15. PL of Eu(TPP)(C_6H_6)**(Eu-b)** orange solution excitation spectra.

In Figure 3.15 are shown broad excitation bands with maxima at 421 nm and 477 nm. The lower profile in blue is the excitation spectrum when monitored at 600 nm. There is a sharp peak occurring at 287 nm due to instrumental artifact.

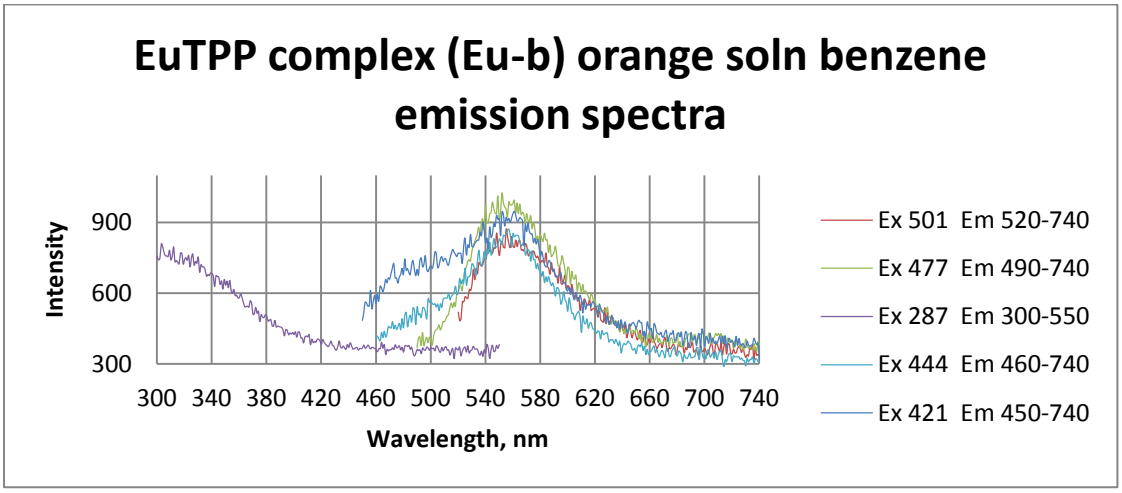

Figure 3.16. PL of Eu(TPP)(C_6H_6)**(Eu-b)** orange solution emission spectra.

The spectrum in figure 3.16., shows coherent profiles that maximize at 557 and 300 nm dependent on the excitation wavelength. There is a small shoulder appearing at 477 nm. The emission profile shows maxima in the ultraviolet and green region of the electromagnetic spectrum respectively.

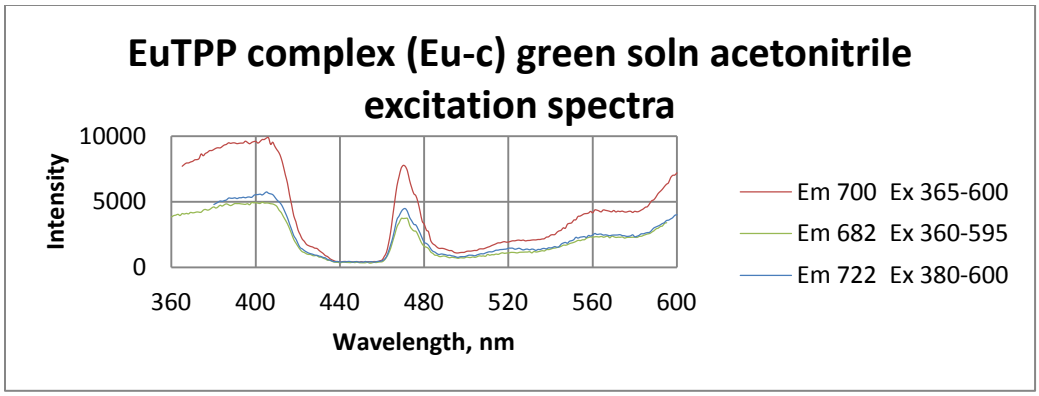

Figure 3.17. PL of Eu(TPP)(CH_3CN)**(Eu-c)** green solution excitation spectra.

Figure 3.17 shows the excitation profile of the green solution of Eu(TPP) **(Eu-c)** layered with acetonitrile. There are two maxima 404 and 472 nm, with small shoulders at 520 and 560 nm. All three monitoring wavelengths produce similar spectra with varying intensities. The broad band at 404 nm is shifted from 380 nm; the 472 nm peak is shifted from the 467 nm as in the Eu(TPP) **(Eu-c)** green solution with no layering. These spectra show a peak at 472 nm instead of the pronounced peak at 440 nm in the TPP excitation spectra; the peaks at 520 and 560 nm are absent in comparison to their distinct peaks in the TPP excitation spectra.

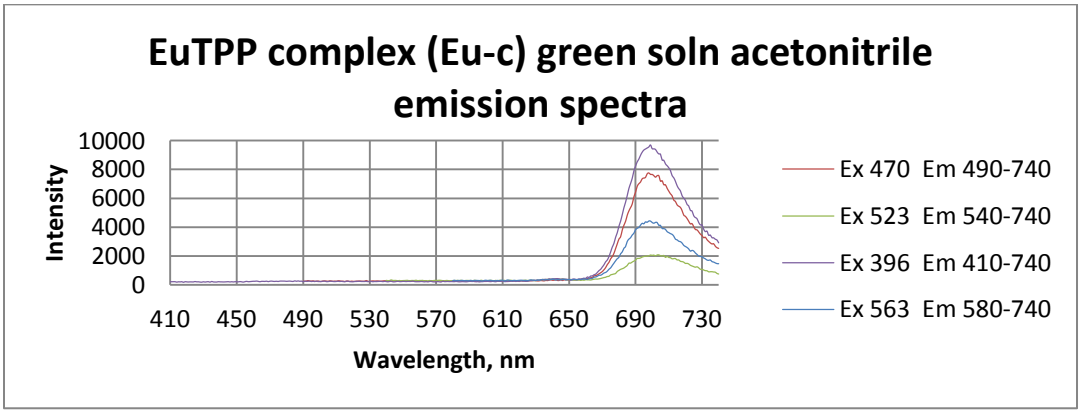

Figure 3.18. PL of Eu(TPP)(CH_3CN)**(Eu-c)** green solution emission spectra.

Figure 3.18 shows the emission profile of the Eu(TPP) **(Eu-c)** green solution when it was layered with acetonitrile. There is one maximum at 699 nm; its intensity is the highest, smoothest, and least peaks in the beginning of the spectra than the other EuTPP spectra. Its intensity is also

wavelength dependent. This is due to the addition of acetonitrile. There is a coherent distribution of the intensity due to the excitation wavelength. The most prominent peak is due to excitation at 396 nm. The least prominent peak is due to excitation at 523 nm. The alteration of the spectra due to europium is consistent.

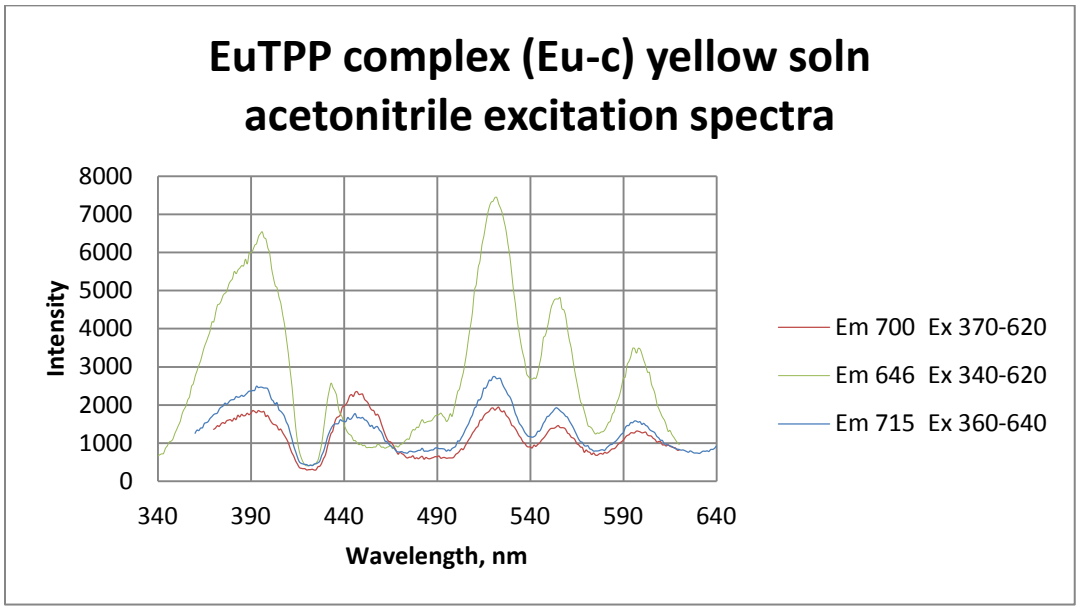

Figure 3.19. PL of Eu(TPP)(CH_3CN)**(Eu-c)** yellow solution excitation spectra.

Figure 3.19 shows the excitation profile of the yellow solution of Eu(TPP) **(Eu-c)** layered with acetonitrile. The maxima show broad peaks at 393, 433, 445, 524, 554, and 597 nm. The subsequent peaks are much smoother and more pronounced than previous Eu(TPP) spectra. The first and second broad peaks show up at 524 and 554 nm, compared to the peaks at 514 and 544 nm of the Eu(TPP) **(Eu-a)** yellow solution which wasn't layered with any other solvent.

The sharp peak at 433 nm is comparable in shape to the sharp peak seen in the TPP excitation profile; the height in comparison to the other peaks is lower than the TPP profile, suggesting the energy transfer from the porphyrin to the europium. The maximum at 400 nm corresponds to $^7F_0 \rightarrow {}^5L_6$ europium transition. This leads to the energy transfer and alteration of the porphyrin profile.

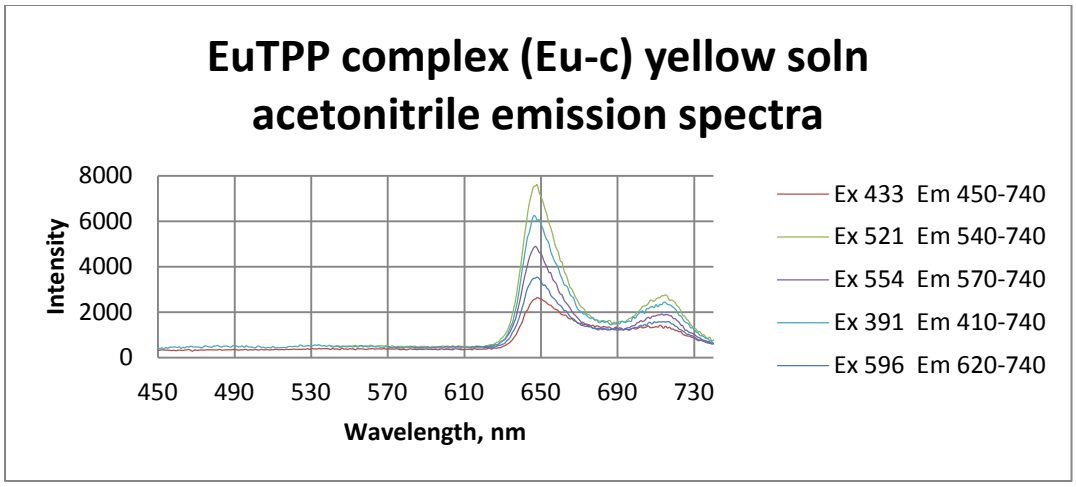

Figure 3.20. PL of Eu(TPP)(CH_3CN)**(Eu-c)** yellow solution emission spectra.

The spectra shown in figure 3.20 has no luminescence from 450 to 620 nm, but has two maxima at 648 nm and 716 nm; it continues to show a smoother spectra than the others and even distribution of wavelength dependent intensity. It shows similar spectra compared to the TPP, the only differences are a 3 nm blue shift of the entire spectra and decrease in luminescence intensity.

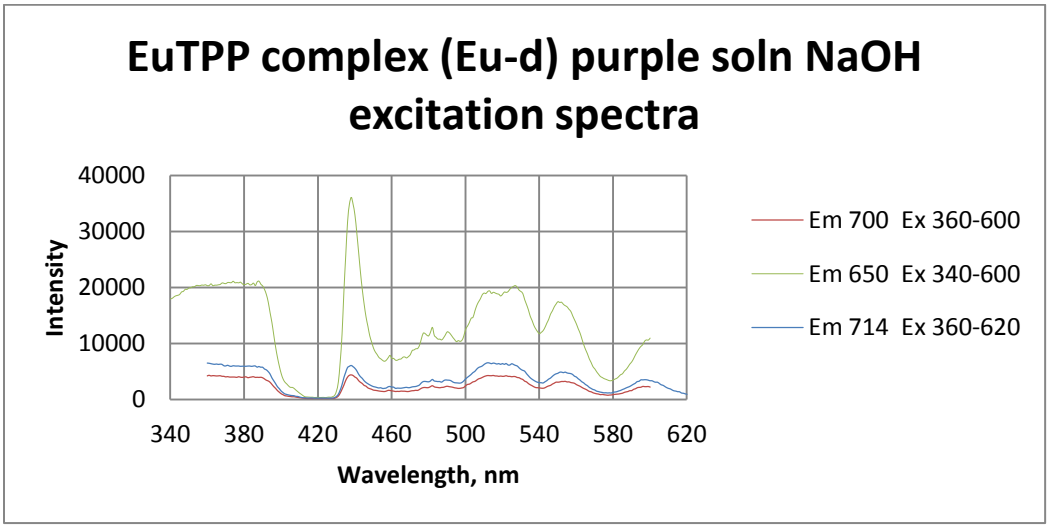

Figure 3.21. PL of Eu(TPP)**(Eu-d)** purple solution in NaOH excitation spectra.

The spectra shown in figure 3.21., depict the excitation spectra of Eu(TPP) **(Eu-d)** when a NaOH solution was added. There are maxima shown at 389, 438, 513, 530, 551 and 600 nm. The excitation profile is wavelength dependent with consistent spectra.

This excitation spectrum is most consistent with the original excitation spectra of TPP. The differences being a deviation from 383 nm peak in the original compared to the 389 nm, and the 504 peak to the 513 nm peak. There is an even plateau leading to the peak that appears at 389 nm before descending to a non luminescent area.

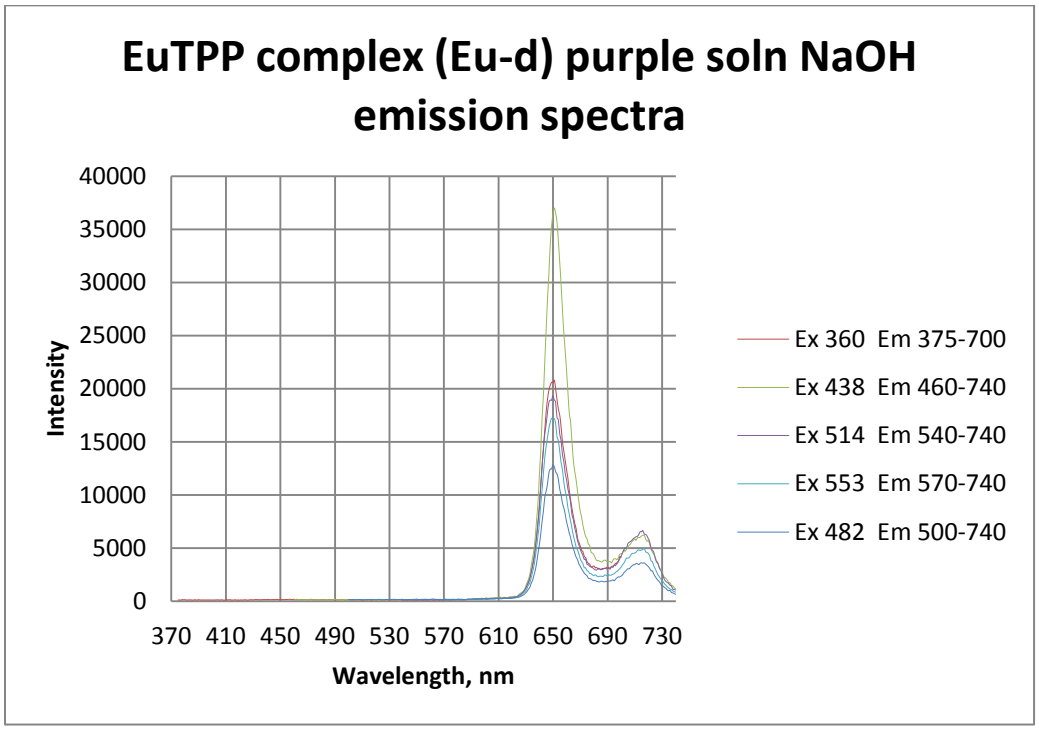

Figure 3.22. PL of Eu(TPP)**(Eu-d)** purple solution in NaOH emission spectra.

The emission spectra of figure 3.22 shows the luminescence behavior of Eu(TPP) **(Eu-d)** when NaOH was added. The maxima are shown at 652 and 716 nm. Compared to the original TPP emission spectra, the spectra are consistent in 652 nm wavelength, and slight deviation from 719 to 716 nm for the lower emission peak. The 652 nm peak of Eu(TPP) **(Eu-d)** has increased in intensity and the 716 nm peak decreased in intensity compared to the original TPP emission spectra. The beginning part of the emission spectra from 370 to 630 nm shows no luminescent activity as they approach the major peak. Excitation at 438 nm leads to the most intense peak at 652 nm, while the peaks at 716 nm are comparable in intensity.

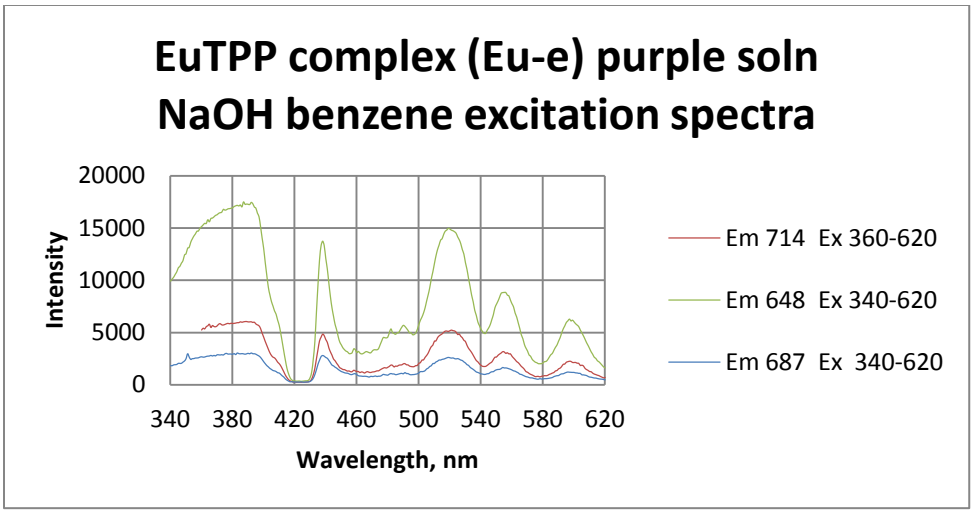

Figure 3.23. PL of Eu(TPP)(C_6H_6)**(Eu-e)** purple solution in NaOH excitation spectra.

The excitation spectra of Eu(TPP) **(Eu-e)** when NaOH and benzene were added is shown in figure 3.23. The maxima are shown at 393 nm (broad), a shoulder at 406, 438 (sharp), 519 (broad), 555 (broad), and 600 nm (broad). The intensity of the 393 nm and 519 nm peaks are greater than the 438 nm peak. In the TPP original spectra, the 440 nm was more intense than the 383 and 530 nm peaks. The positive slope to the maximum at 393 nm, a transition of europium corresponding to $^7F_0 \rightarrow {}^5L_6$ is prevalent in all three excitation profiles.

This spectrum also shows that the 519, 555, and 600 nm peaks are descending in intensity whereas in the TPP spectra they're of the same intensity. The 504 and 530 nm peaks have disappeared to form a new peak at 519 nm. With the addition of benzene the 438 nm peak decreased in intensity, thus benzene facilitates the transfer of energy from porphyrin to the europium.

The three profiles on the excitation profile show consistent spectra with differing intensity; monitoring at 648 nm exhibits the most intense excitation spectrum. Monitoring at 714 nm exhibits the second lowest excitation spectrum. When monitoring at 687 nm the least intense spectrum is produced with the similar profile.

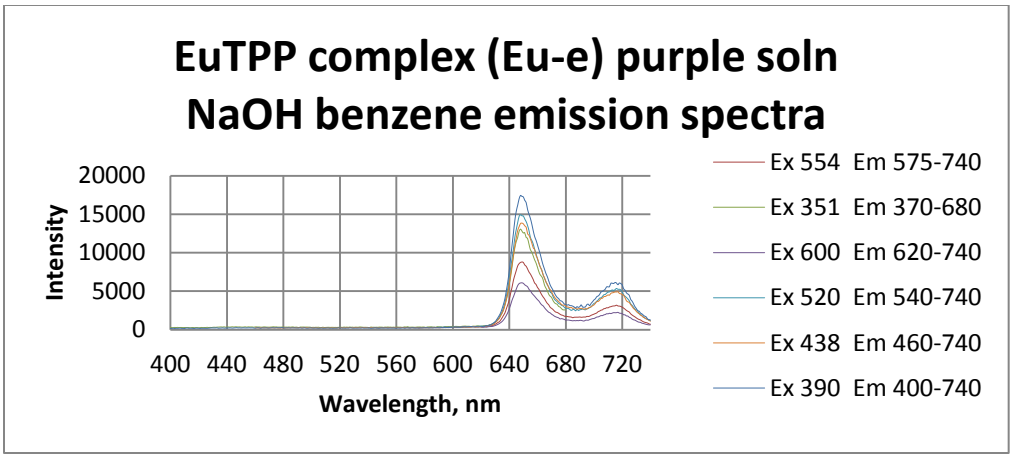

Figure 3.24. PL of Eu(TPP)(C_6H_6)**(Eu-e)** purple solution in NaOH emission spectra.

The emission spectra in figure 3.24., show the profiles when NaOH and benzene are added to Eu(TPP). The maxima are shown at 648 and 714 nm. There are no peaks at the beginning of the spectra and the intensity is decreased compared to the TPP emission spectra. There is a 4 nm blue shift of the major maximum and a 5 nm peak shift of the lower peak maximum compared to the TPP original spectra. The intensity continues to show wavelength dependence.

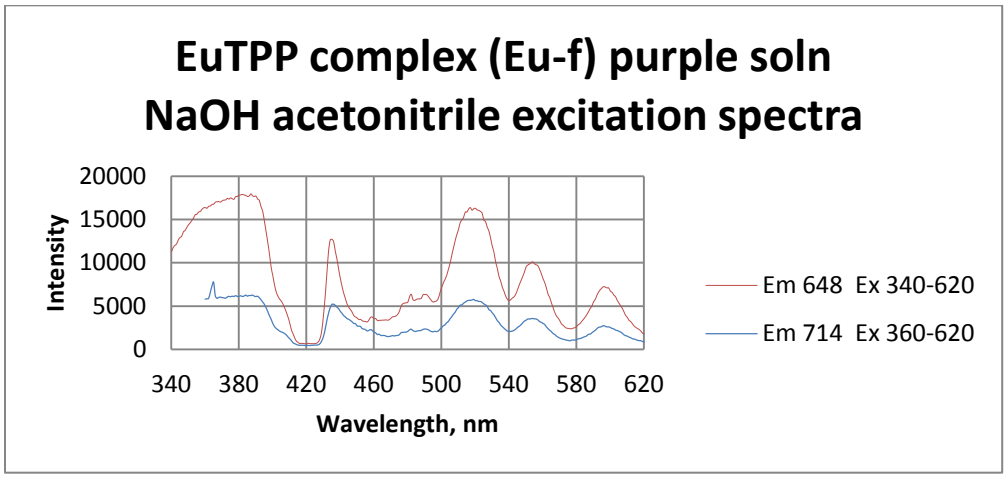

Figure 3.25. PL of Eu(TPP)(CH_3CN)**(Eu-f)** purple solution in NaOH excitation spectra.

The excitation profile of Eu(TPP) **(Eu-f)** when NaOH and acetonitrile was added is shown in figure 3.25. The spectra show maxima at 387, a shoulder at 405, 433, 515, 553, and 600 nm. The 387 and 515 nm peaks are more intense than the 433 nm peak. The reverse is opposite in the

original TPP spectrum. There is a 7 nm blue shift in the 440 nm peak to 433 nm. There are 3 broad peaks, starting with 515 nm that decrease in intensity in the same manner as Eu(TPP) **(Eu-e)**. The 504 and 530 nm peaks aren't evident in this spectrum, but there is the formation of a 515 nm peak. The intensity is shown to be wavelength dependent.

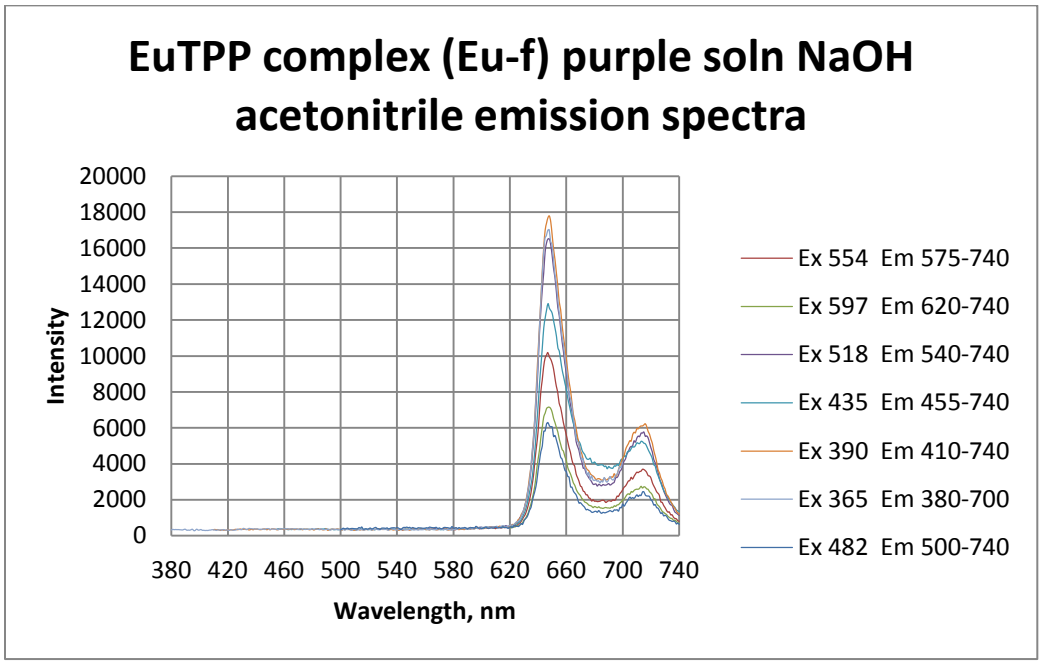

Figure 3.26. PL of Eu(TPP)(CH_3CN)**(Eu-f)** purple solution in NaOH emission spectra.

Figure 3.26., shows the emission profile of Eu(TPP) **(Eu-f)** when NaOH and acetonitrile were added to the solution. Sodium hydroxide was added to see the effect that pH has on the solution studies and on the deprotonation of the pyrrole nitrogens. The spectra show maxima at 648 and 714 nm.

The intensity of the maximum peak decreased compared to the original TPP band, while the 716 nm peak stayed unchanged in intensity. The intensities are wavelength dependent and there is a 4 nm and 5 nm shift of the maxima from 652 nm to 648 nm and from 719 nm to 714 nm, respectively. The emission spectra show more distribution between the spectrum at the maxima at 648 and 714 nm. The most intense band is exhibited when excited at 390 nm.

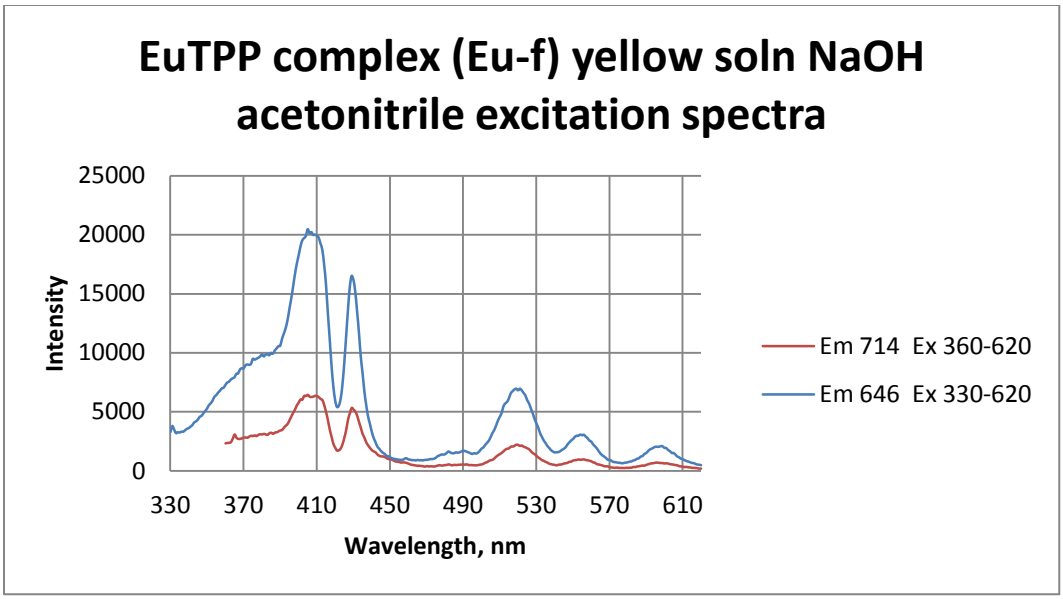

Figure 3.27. PL of EuTPP(TPP)(CH_3CN)**(Eu-f)** yellow solution in NaOH excitation spectra.

Figure 3.27 shows the excitation profile of the yellow solution of EuTPP **(Eu-f)**. The change in color occurred after one week of slow diffusion. The change in color is the indication for porphyrin complexes in aqueous solution that there is a change in the dielectric constant of the solvent. This change stabilizes the porphyrin and complex that was formed at various energy states. There is a change in the excitation profile compared to the previous purple colored solution. The maxima are shown at: shoulder 383, 401, 431, 519, 561, and 593 nm. There is a positive slope to the peak at 401 nm, while bypassing a maximum at 383 nm.

The 401 nm peak corresponds to a europium transition from $^7F_0 \rightarrow {}^5L_6$; this shows energetic interaction between the ligand and the lanthanide, europium. The 431 nm peak is blue shifted 9 nm from the original TPP at 440 nm and decreased in intensity where it appears in a region the original doesn't show luminescence intensity. The peaks at 519, 561, and 593 nm still show a decrease in intensity compared to the profile of TPP. The excitation spectra of Figure 3.27., shows two similar profiles differing in intensity. The most intense profile being monitored at 646 nm; the least intense profile was monitored at 714 nm.

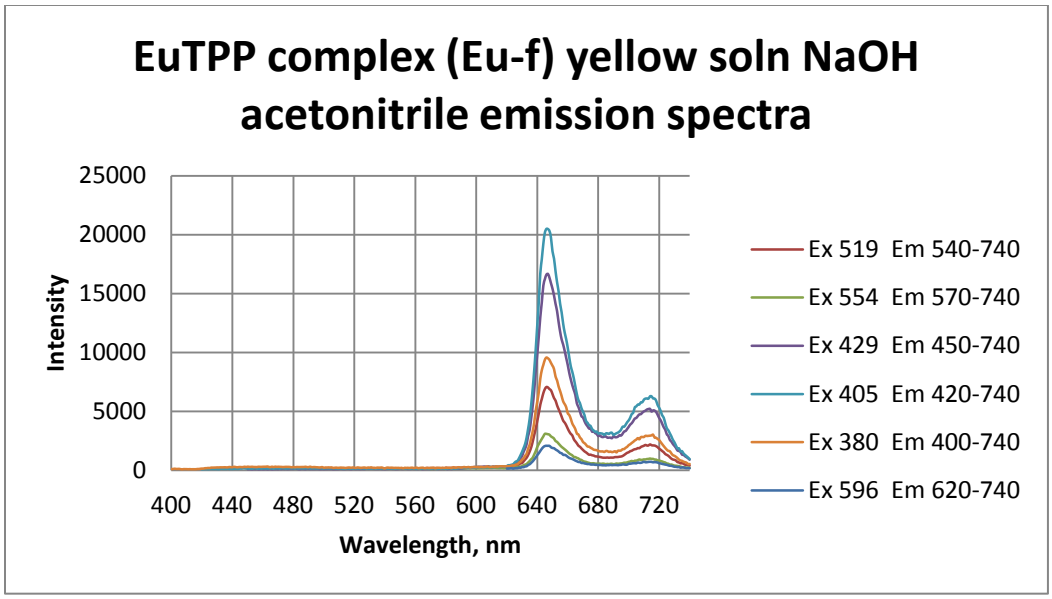

Figure 3.28. PL of Eu(TPP)(CH_3CN)**(Eu-f)** yellow solution in NaOH emission spectra.

Figure 3.28 exhibits the emission spectra showing no luminescence intensity from 400 to 630 nm, while traversing to the maxima at 646 and 714 nm. The intensities are wavelength dependent and show similar profiles to the original TPP spectra. The intensities are distributed in a uniform manner compared to other Ln(TPP) complexes. The most intense spectrum is excited at 405 nm; the least intense spectrum is excited at 596 nm. The peak at 405 nm corresponds to the europium $^7F_0 \rightarrow {}^5L_6$ transition. The peak at 714 nm shows more distribution in its intensities at various excitation wavelengths. The maxima are blue shifted 8 nm and 5 nm from 652 nm to 646 nm and 719 nm to 714 nm, respectively. The acetonitrile has an effect on the interaction between the europium and porphyrin to cause the blue shift in maxima.

The overall intensity is lower. With the addition of acetonitrile there is a greater affect on the intensity of the 714 nm peak with respect to excitation wavelength. The most intense spectrum results upon excitation with 405 nm band while the least intense spectrum results upon excitation at 596 nm. The lower maximum at 714 nm also decreases to almost no luminescence intensity.

3.4. PL of Dy(TPP) Complexes

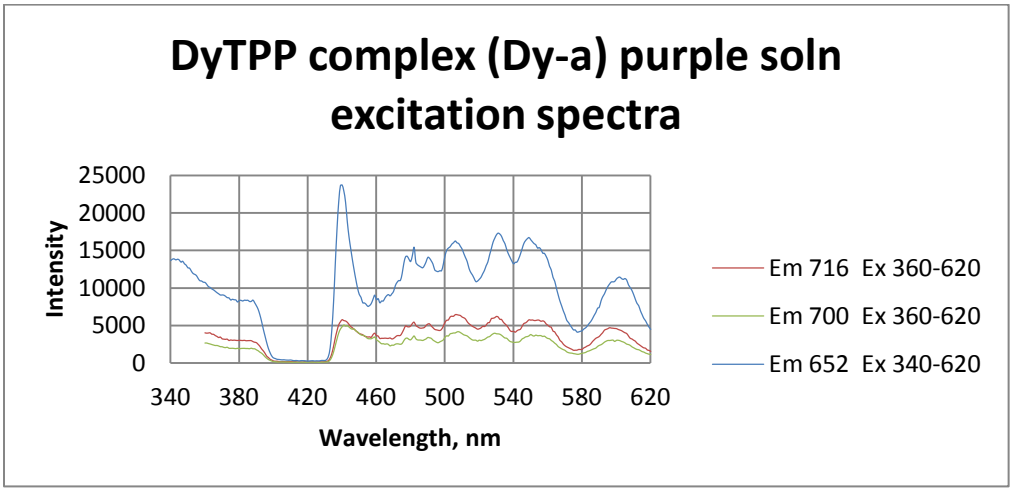

Figure 3.29. PL of Dy(TPP)**(Dy-a)** purple solution excitation spectra.

Figure 3.29., shows maxima at 347, 391, 440 (sharp), 506, 531, 550, and 600 nm. This spectrum shows the most similarity to the original TPP excitation spectra; the only major deviations are the 8 nm and 1 nm shift in maxima from 383 nm to 391nm and 440 nm to 441 nm. The peaks at 506, 531, and 550 nm are at the same intensity level. The intensity is wavelength dependent.

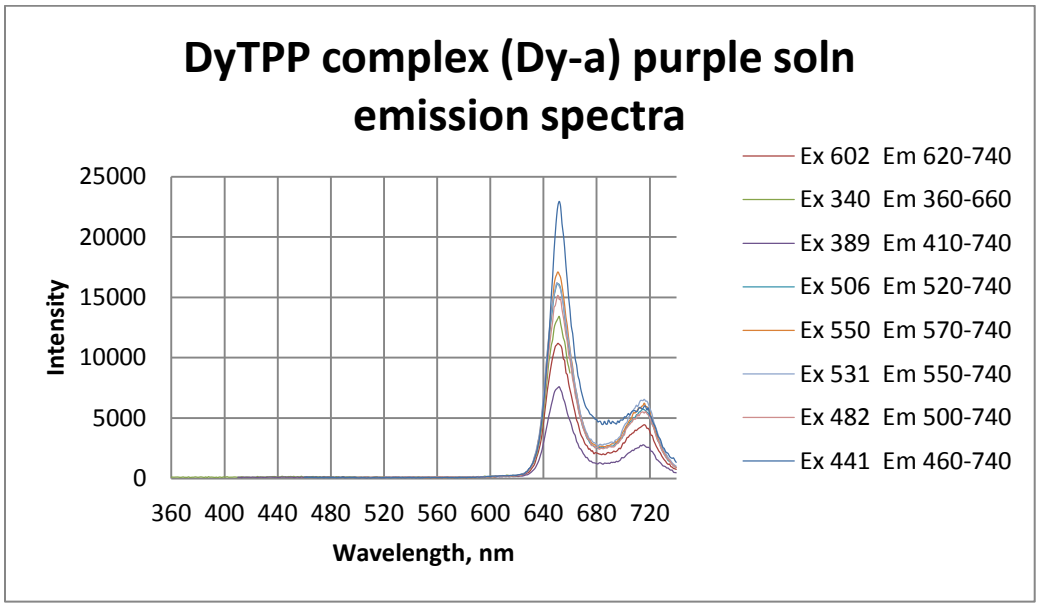

Figure 3.30. PL of Dy(TPP)**(Dy-a)** purple solution emission spectra.

Figure 3.30 shows maxima at 652 nm and 714 nm and a quiet front tail of the spectra from 360 to 630 nm showing no luminescence intensity. The emission maxima are consistent with that of the TPP emission profile. The intensity is wavelength dependent. The overall intensity has decreased in an uniformed manner.

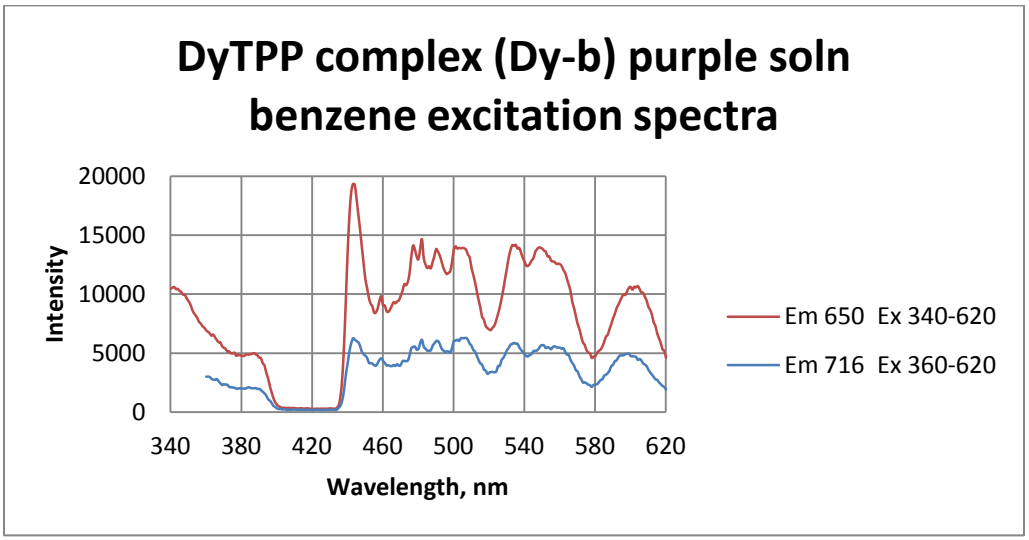

Figure 3.31. PL of Dy(TPP)(C_6H_6)**(Dy-b)** purple solution excitation spectra.

The excitation spectra shown in figure 3.31 has maxima at 346, 386, 443, 502, 535, 550, 600 nm. The spectra are consistent in their similarity to the excitation spectra of TPP. The negative slope from the 346 to 386 nm peak still persists. The differences arise in the 3 nm shift and intensity decrease of the maxima from 440 to 443 nm. The intensity of the peaks at 502, 535, and 550 nm are the same.

The spectrum is wavelength dependent. The two profiles are the result of being monitored at 650 and 716 nm. The most intense spectrum corresponds to the spectra monitored at 650 nm. There is a descending slope from the 346 nm peak to the 386 nm shoulder peak. The peak at 443 nm resumes its greater intensity over the longer wavelength maxima. The longer wavelength maxima resume comparable intensity without the consistent decrease as observed in the previous excitation spectra of the europium porphyrin complexes.

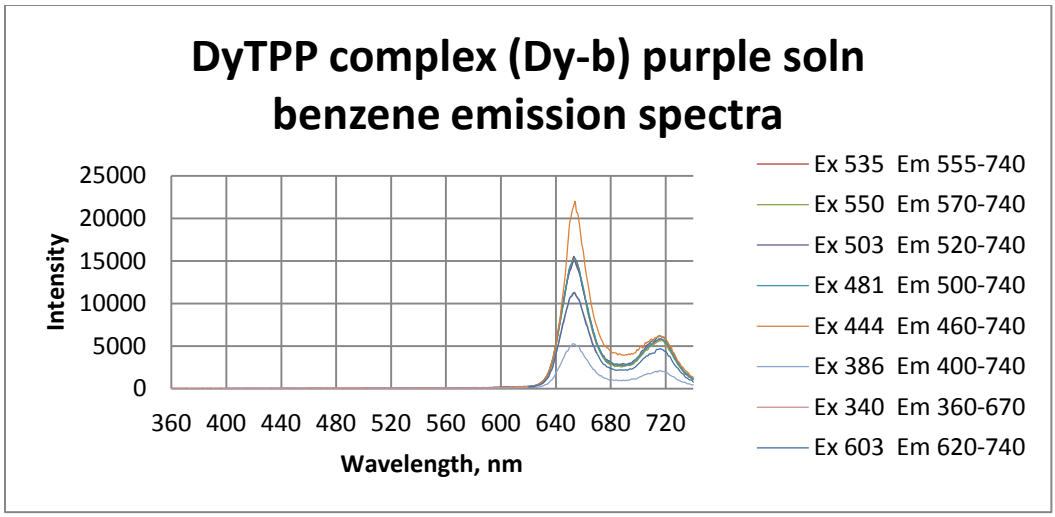

Figure 3.32. PL of Dy(TPP)(C_6H_6)**(Dy-b)** purple solution excitation spectra.

The spectra of Dy(TPP)(C_6H_6) **(Dy-b)** in figure 3.32 consist of the emission profile with maxima at 652 nm and 716 nm. The beginning shows no luminescence intensity and the emission intensity is wavelength dependent, with the most intense spectrum excited at 444 nm. The least intense spectrum is excited at 386 nm.

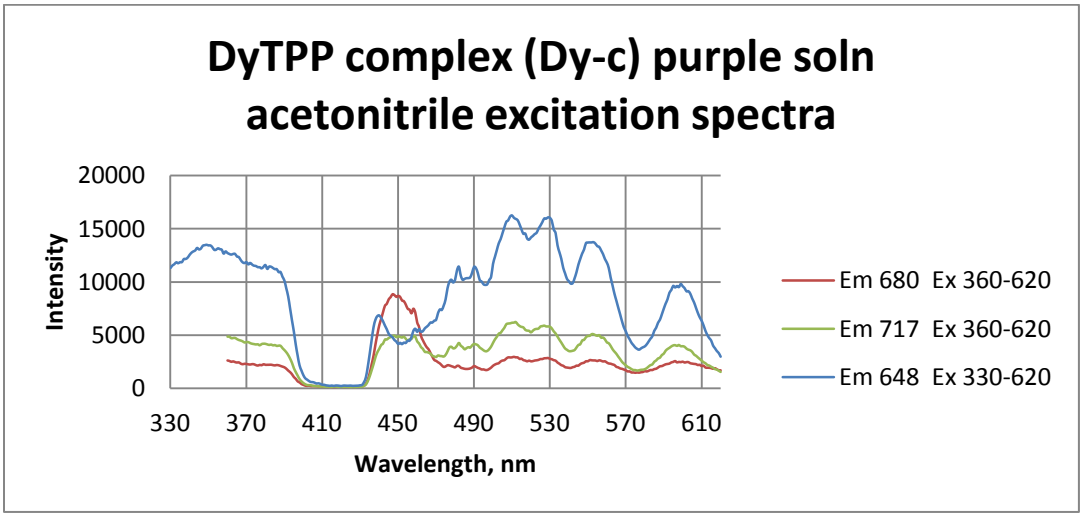

Figure 3.33. PL of Dy(TPP)(CH_3CN)**(Dy-c)** purple solution excitation spectra.

Figure 3.33., shows the excitation profile of Dy(TPP)(CH_3CN) **(Dy-c)** layered with acetonitrile. The spectra show maxima at 349, 384, 440, 448, 510, 530, 552, and 600 nm. The blue spectrum, monitored at 648 nm is more consistent with TPP excitation profile with regards to

the proximity of the 440 nm peak compared to 437 nm; its subsequent peaks are at similar wavelengths but deviate in that they descend in intensity unlike the original TPP excitation spectra. The intensity of the 440 nm peak is lower than every other peak on the spectrum when monitored at 648 nm. The red spectrum, monitored at 680 nm and green spectrum (monitored at 717 nm) are more consistent with the original TPP excitation spectra with regards to the same level intensity of the subsequent peaks, but they deviate from TPP in that the 440 nm peak is red shifted to 448 nm.

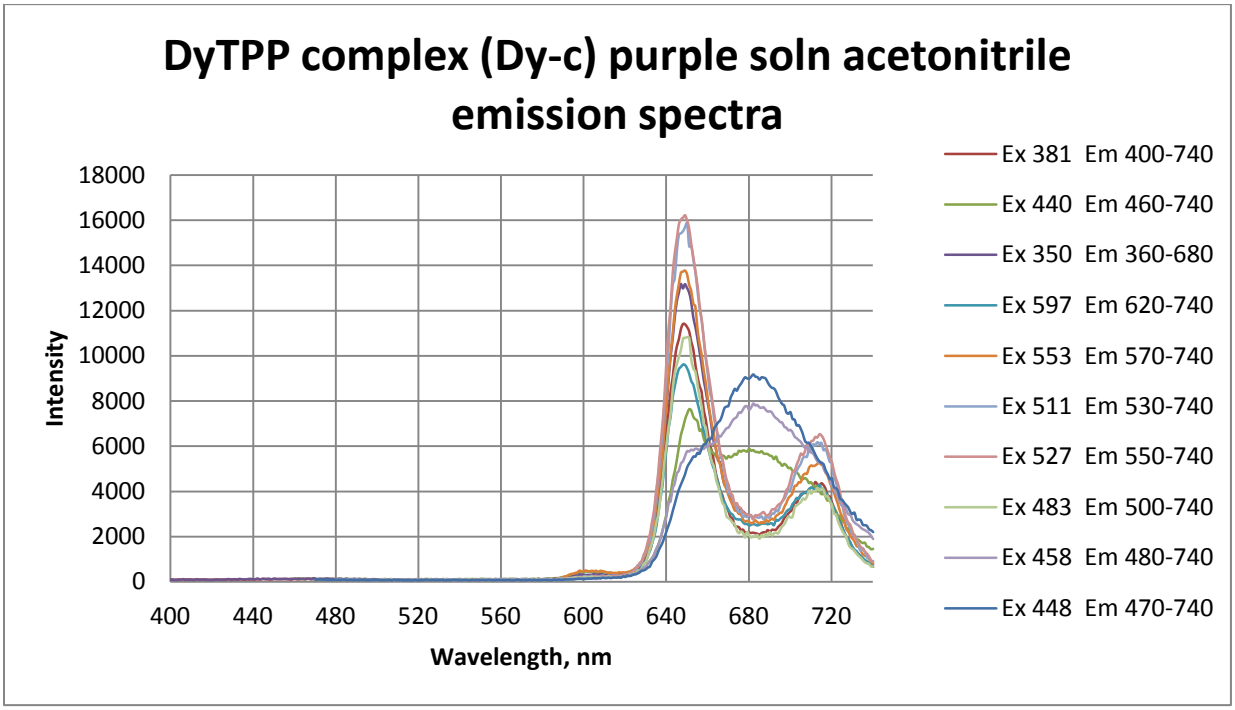

Figure 3.34. PL of Dy(TPP)(CH_3CN)**(Dy-c)** purple solution emission spectra.

The emission profile of Dy(TPP)(CH_3CN) **(Dy-c)** is shown in Figure 3.34. When layered with acetonitrile; the maxima are shown at 648, 680, and 717 nm. The emission spectra show two different wavelength dependent profiles. When excited at 440, 448, and 458 nm a broad peak at 680 nm appears on the emission profile; this indicates that there is a separate species in solution. When excited at the other wavelengths, the similar porphyrin spectrum is observed.

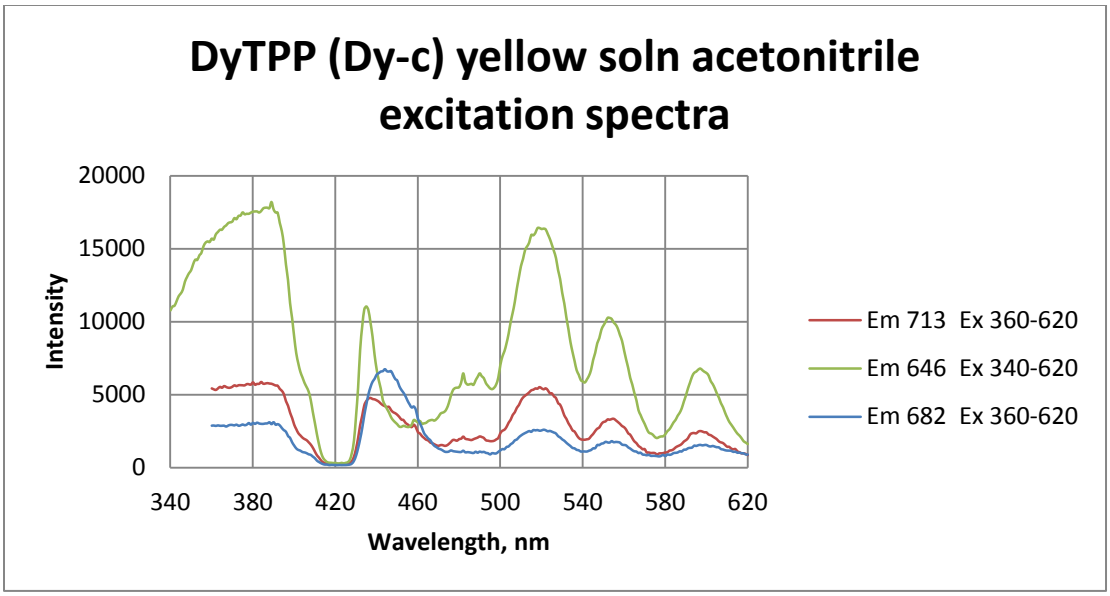

Figure 3.35. PL of Dy(TPP)(CH_3CN)**(Dy-c)** yellow solution excitation spectra.

The excitation profile of the yellow Dy(TPP)(CH_3CN) **(Dy-c)** solution in acetonitrile is shown in figure 3.35. The maxima are shown at 389, 406, 435, 444, 521, 554, and 597 nm. The overall intensity of the spectra has decreased. The peaks that were shown at 504 nm and 530 nm have disappeared and one peak at 521 nm is present. The subsequent peaks re-establish the descending intensity order compared to the equal intensity displayed in the TPP excitation spectra; this is owing to the greater interaction of the metal and porphyrin core. The positive slope is re-established with the changing dielectric constant. The peak at 435 nm has decreased in intensity to where it is now lower than the intensity of the 389 nm and 504 nm maxima.

Unlike previous spectra, the 389 nm peak is more intense than the rest of the peaks of the excitation spectra. The three spectra show similar profiles with only a slight change in the shape of the peak appearing around 440 nm. When monitored at 682 nm, there was the largest change of the peak with it red shifting to 444 nm and becoming broader while keeping the other profile characteristics. When monitoring at 682 nm, while keeping the overall spectral characteristics consistent, the shift to 444 nm is indicative of a species present similar to the main species.

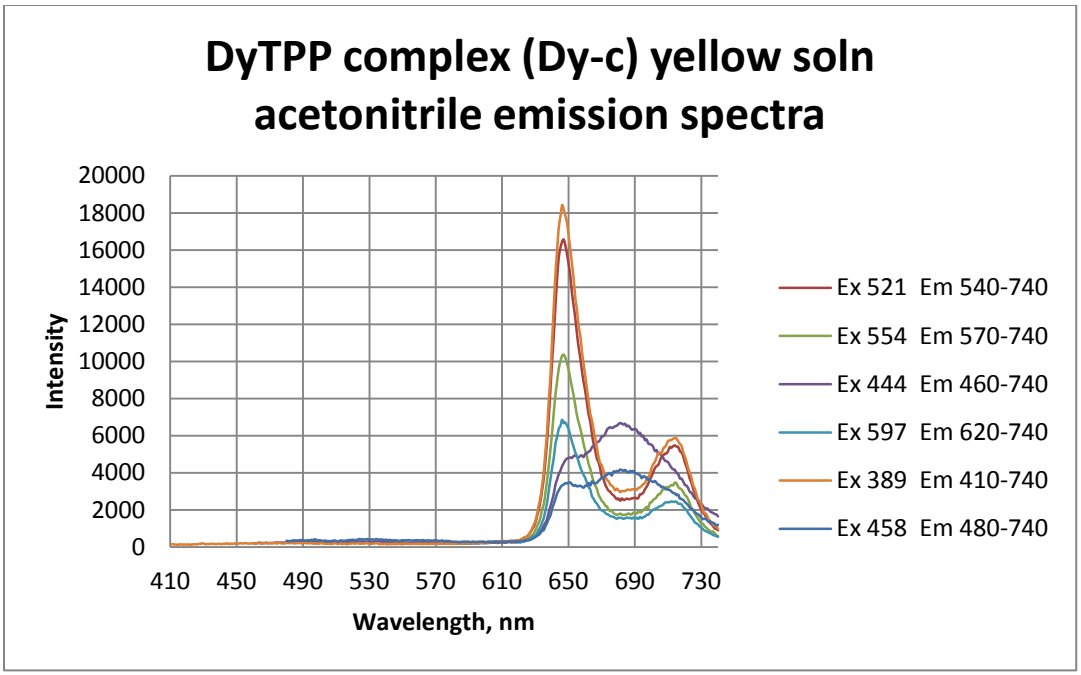

Figure 3.36. PL of Dy(TPP)(CH_3CN)**(Dy-c)** yellow solution emission spectra.

Figure 3.36 shows the emission profile of the yellow solution of Dy(TPP)(CH_3CN) **(Dy-c)**. Emission maxima are observed at 646, 682, and 713 nm. The emission profile displays two different spectral profile dependent upon the excitation wavelength. When excited at 444 nm and 458 nm there appears a broad peak at 682 nm. When excited at the other wavelengths, the spectra resume the similar TPP emission profile. The intensity of the major maxima is decreased in comparison to the intensity of the 652 nm peak of the TPP emission profile. The intensity of the lower maximum peak is relatively unchanged.

The beginning part of the emission spectrum from 410 to 630 nm shows no luminescent activity. The spectra with a maxima appearing at 682 nm when excited at 444 nm and 458 nm could be due to those excitation wavelengths stabilizing a different species in solution with the help of the addition of acetonitrile and the change in dielectric constant of the aqueous solution. The other species shows luminescent behavior different and independent of the original TPP spectra with a decrease in the 646 nm peak forming the 682 nm peak.

3.5. PL of Ce(TPP) Complexes

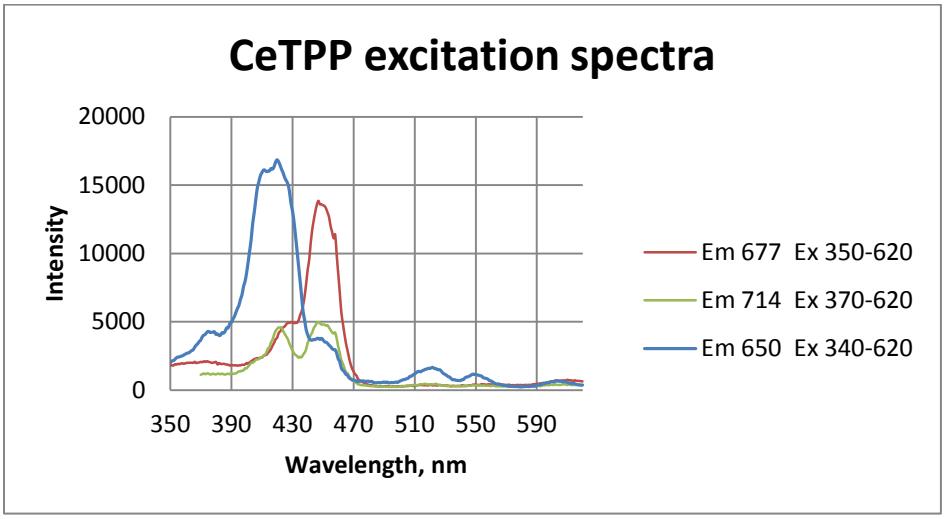

Figure 3.37. PL of Ce(TPP) excitation spectra.

In Figure 3.37 are shown the excitation peaks at 375, 418, 446, 522, 550, and 604 nm. There are three different excitation profiles depending on the monitoring wavelength. When monitored at 650 nm, the excitation profile shows a shoulder at 375 nm, broad peak maximum at 418 nm and smaller peaks at 446, 522, 550, and 604 nm. When monitored at 714 nm, which corresponds to the smaller porphyrin emission peak, the excitation profile shows maxima at 417 and 446 nm.

When monitored at 714 nm instead of 650 nm there is decrease in the intensity of the band at 418 nm and a slight increase in intensity of the broad band at 446 nm. The peaks at longer wavelengths are no longer present. When monitored at 677 nm, the excitation spectrum that is produced is similar in character to the spectrum that was monitored at 650 nm; the difference being the 28 nm red shift and disappearance of the 522, 550, and 604 nm peaks. There are two species in solution, one corresponding to the porphyrin maxima at 650 and 714 nm giving similar excitation spectra. The other profile corresponds to the other species in solution giving a different profile maximizing at 446 nm and vastly decreased longer wavelength maxima.

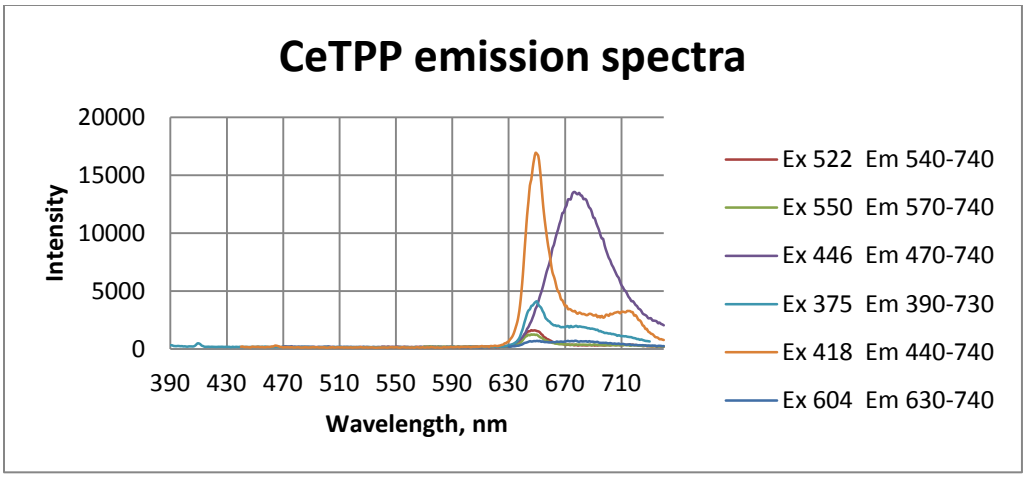

Figure 3.38. PL of Ce(TPP) emission spectra.

In Figure 3.38 the emission spectra of two different profiles is shown with maxima at 650, 677, and 714 nm. The standard porphyrin peak at 650 nm is still present, whereas the peak at 714 isn't present except when excited at 418 nm. When excited at 446 nm, there is a completely different emission profile that is produced, with a maximum at 677 nm.

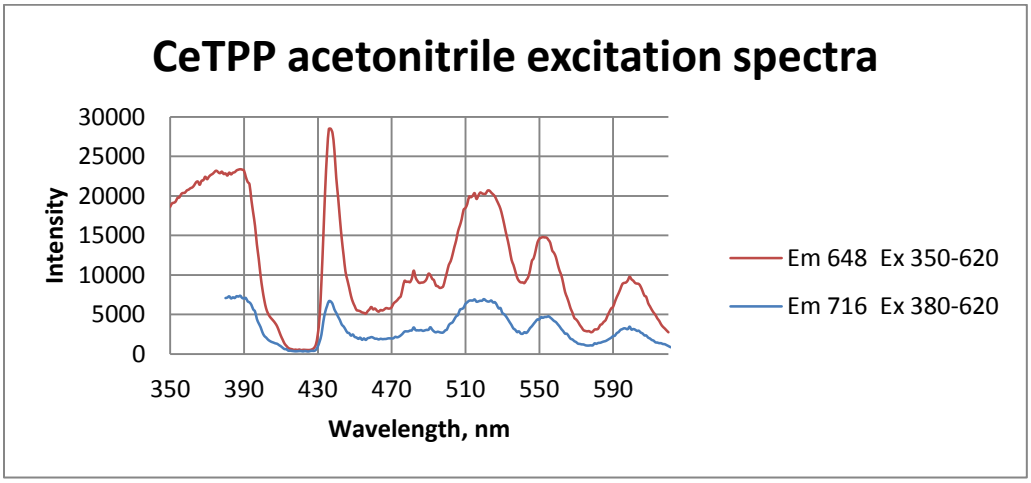

Figure 3.39. PL of Ce(TPP)(CH_3CN) excitation spectra.

The excitation spectra of Ce(TPP)(CH_3CN) in figure 3.39., more closely resembles that of lanthanide porphyrin complexes. The spectrum shows bands at 387, 436, 482, 519, 553, and 600 nm. Monitoring the excitation at 648 nm provides the most intense band than when monitored at 716 nm.

The two profiles show the same characteristic peaks. The 436 nm peak is the most intense peak with a small shoulder at 406 nm. The peaks at 519, 533, and 600 nm are similar to the TPP peaks but these are more distinct, red shift, combine and decrease in the intensity as the wavelength increases, showing interaction between the metal and the porphyrin core.

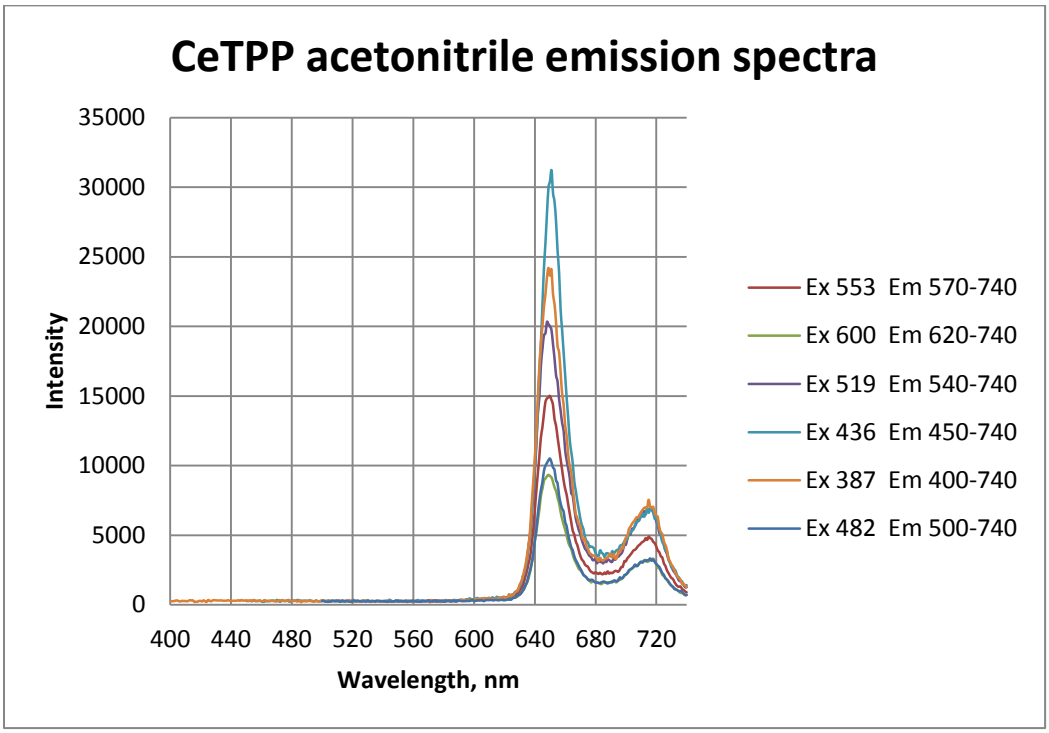

Figure 3.40. PL of Ce(TPP)(CH_3CN) emission spectra.

The spectra in Figure 3.40 exhibits the emission profile of Ce(TPP) when layered with acetonitrile. The maxima are shown at 648 nm and 714 nm. Compared to the original TPP emission profile the peaks are blue shifted 4 nm. The most intense band appears when excited at 436 nm. The emission profile is wavelength dependent.

There is no luminescent activity present in the beginning portion of the emission spectrum from 400 nm to 630 nm. The emission profile shows a uniformed distribution of intensity in the maxima of the spectra with respect to the excitation wavelength. The most intense spectrum appears when excited at 436 nm. The least intense spectrum appears when excited at 600 nm.

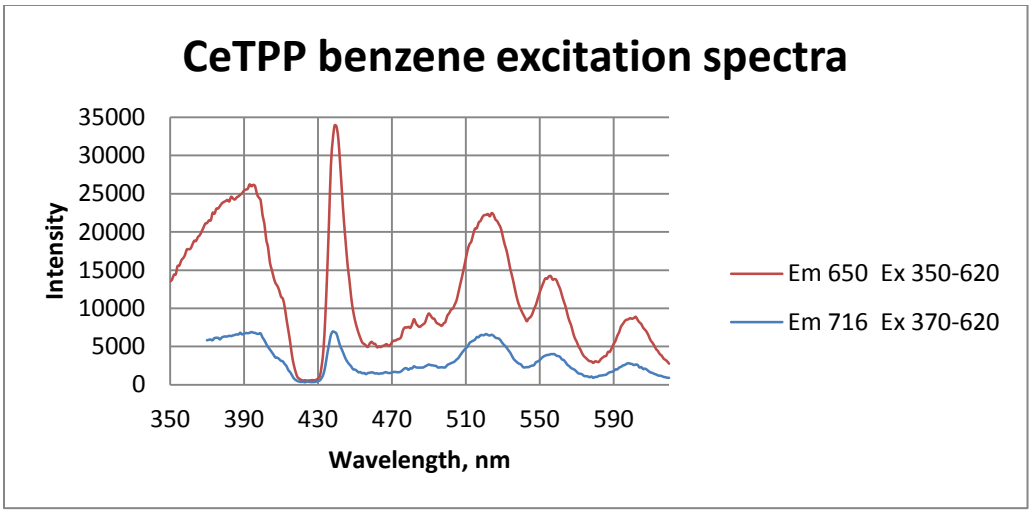

Figure 3.41. PL of Ce(TPP)(C_6H_6) excitation spectra.

Figure 3.41., the excitation profile exhibits maxima shown at 394, 440, 482, 490, 523, 555, and 600 nm. Although monitored at two different wavelengths, the profile is similar, varying in intensity. There is a small shoulder at 407 nm on the broad band of 394 nm.

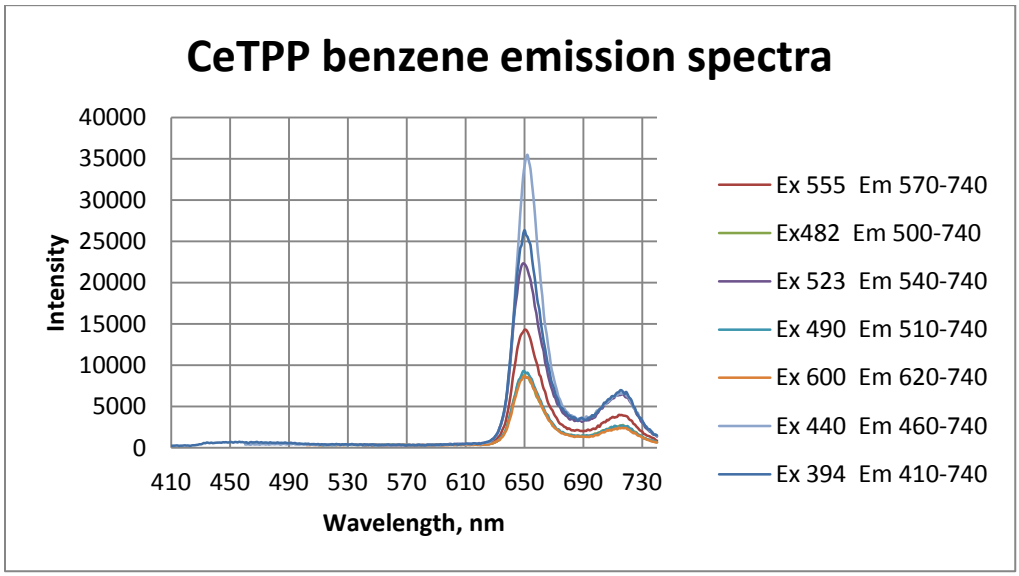

Figure 3.42. PL of Ce(TPP)(C_6H_6) emission spectra.

The spectra, shown in figure 3.42., exhibits emission maxima at 650 and 716 nm. The spectra show wavelength dependency and there is a slight 2 nm red shift in the spectrum that was excited at 440 nm. There is no luminescent activity in the beginning portion of the spectra.

3.6. PL of Gd(TPP) Complexes

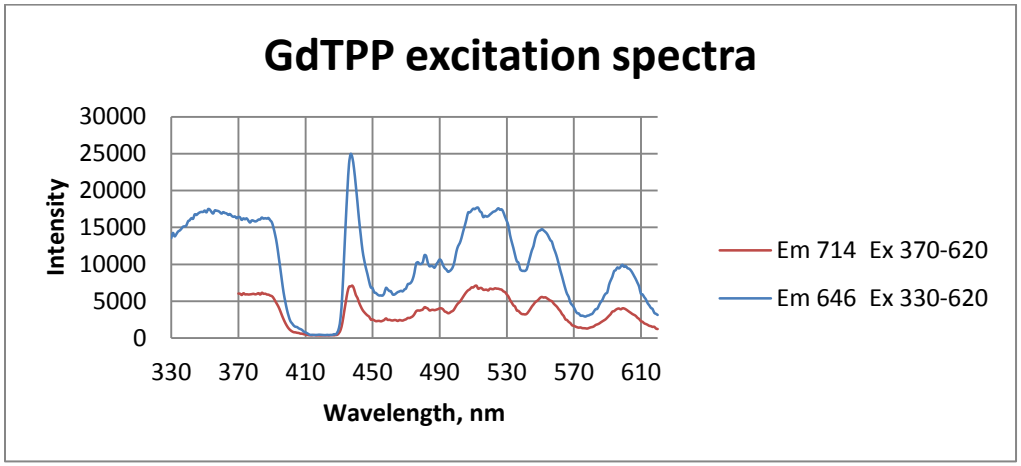

Figure 3.43. PL of Gd(TPP) excitation spectra.

The excitation spectra in figure 3.43., show maxima at 350, 386, 437, 480, 491, 512, 526, 550, and 600 nm. The peak at 437 nm is the most intense with the four peaks decreasing in intensity at 512, 526, 550, and 600 nm respectively. The two profiles are similar with the only difference being the luminescence intensity.

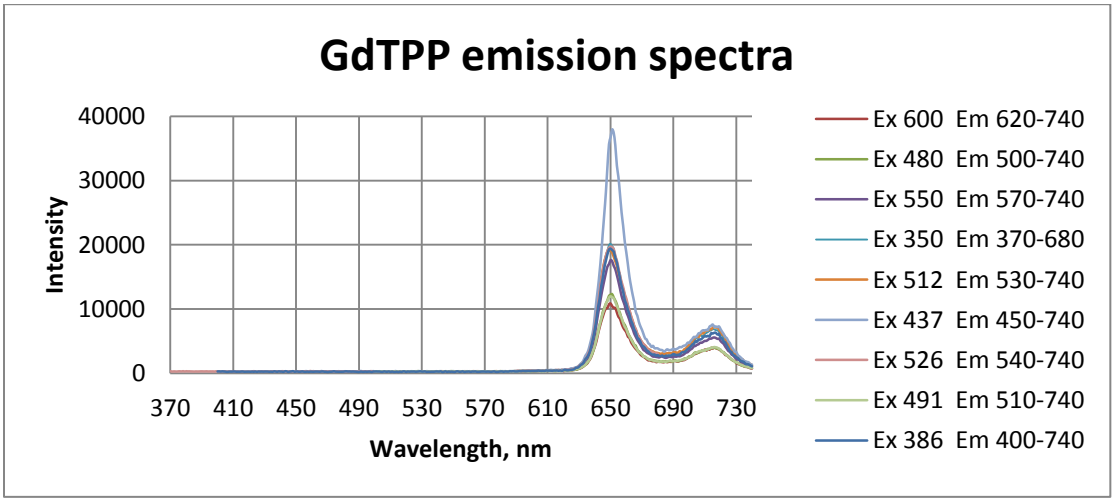

Figure 3.44. PL of Gd(TPP) emission spectra.

Figure 3.44 shows the emission spectra with maxima at 646 and 714 nm. When excited at 437 nm the spectrum red shifts 2 nm. Although wavelength dependent the spectra tend to group together instead of being evenly spread apart like the previous emission spectra.

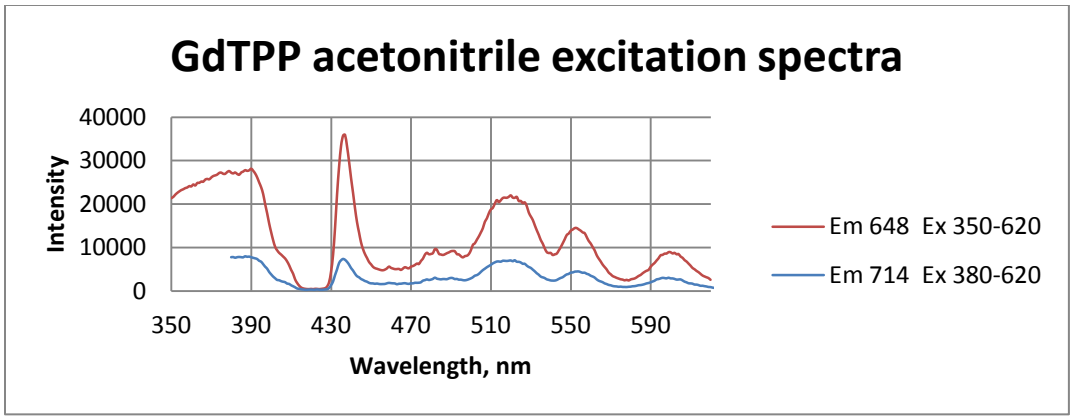

Figure 3.45. PL of Gd(TPP)(CH_3CN) excitation spectra.

In Figure 3.45 is shown the excitation spectra of Gd(TPP) when layered with acetonitrile. The spectra show maxima at 388, 405, 437, 482, 521, 552, and 600 nm. The most intense peak is observed at 437 nm. There is a reduction of 4 peaks to 3 peaks shown at 521, 552, and 600 nm. The two excitation profiles are similar with only differences in the intensity based on the monitoring wavelength.

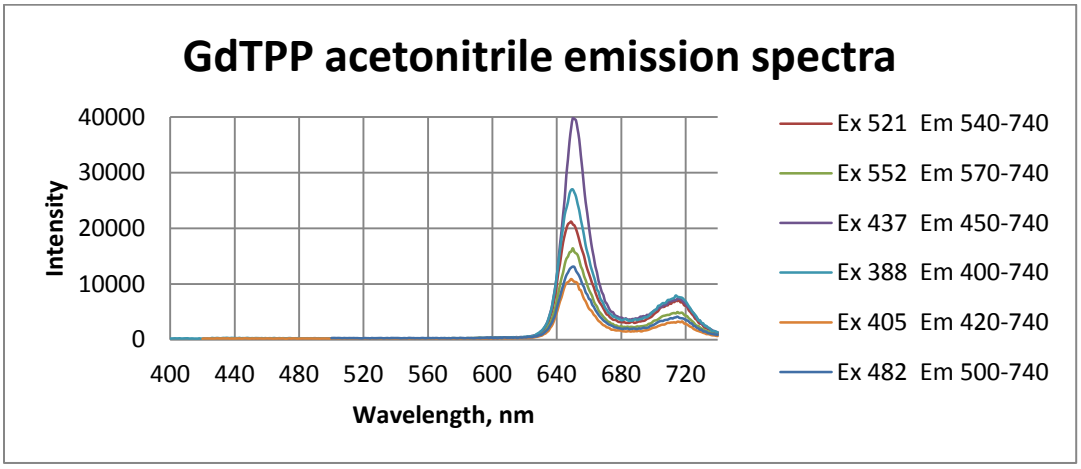

Figure 3.46. PL of Gd(TPP) (CH_3CN) emission spectra.

The maxima of the spectra in figure 3.46 consist of peaks at 648 and 714 nm. The emission spectra are wavelength dependent with the most intense band showing when excited at 437 nm. There is no luminescent activity in the beginning of the spectra with the most intense spectrum being excited at 437 nm.

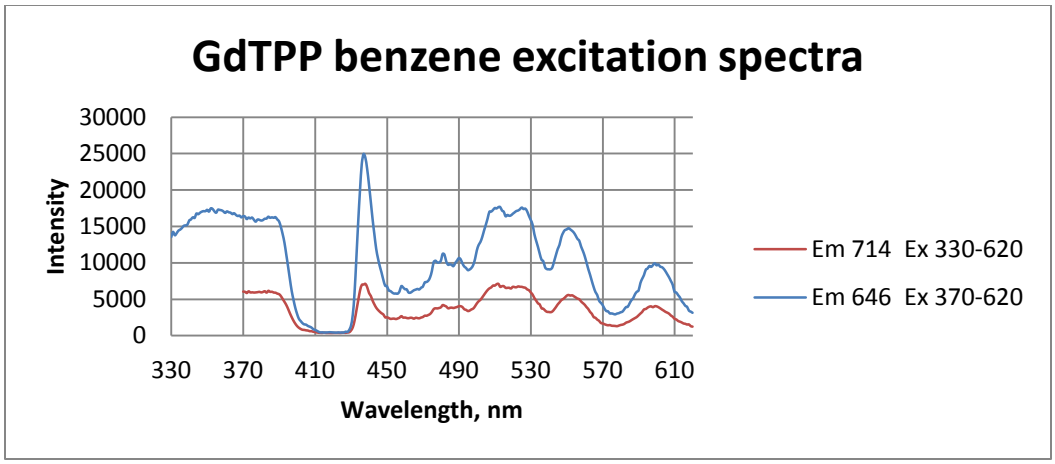

Figure 3.47. PL of Gd(TPP)(C_6H_6) excitation spectra.

In Figure 3.47is given the excitation spectra which show band maxima at 389, 442, 481, 490, 512, 533, 555, and 600 nm. The most intense band is at 442 nm. The spectra resume the similarity of the original TPP excitation spectra; the main difference is the red shifting and decrease in emission intensity.

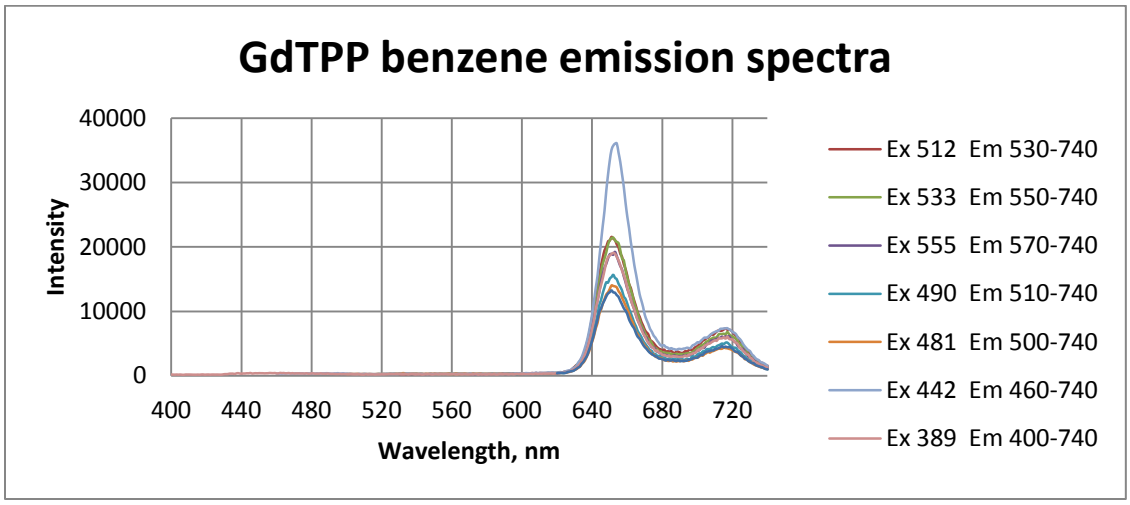

Figure 3.48. PL of Gd(TPP)(C_6H_6) emission spectra.

The emission spectra show maxima at 646 and 714 nm in figure 3.48. The spectral intensity is wavelength dependent but the intensity isn't spread evenly. The most intense band is the spectrum that was excited at 442 nm. There is no luminescence intensity in the beginning tail of the emission spectra from 400 to 630 nm.

3.7. PL of Ag(TPP) Complex

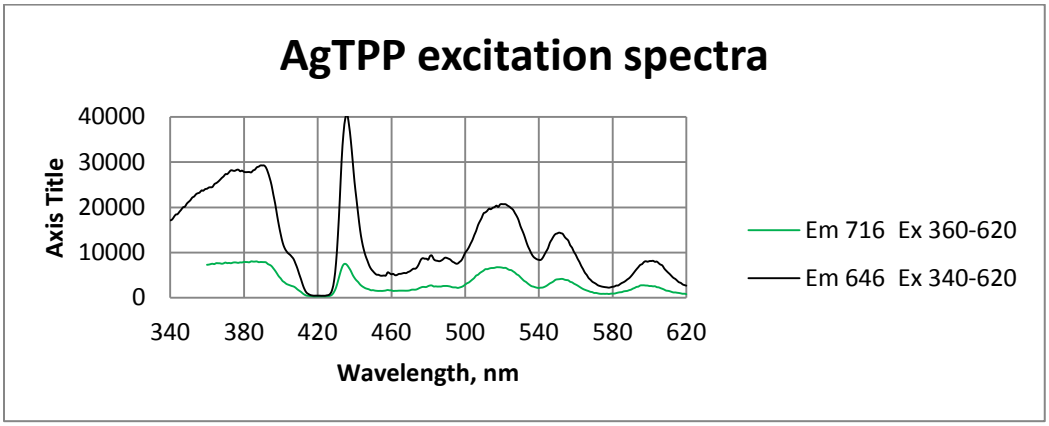

Figure 3.49. PL of Ag(TPP) excitation spectra.

The spectrum of Ag(TPP) excitation in figure 3.49., shows broad peaks at 386, 520, 551, 601 nm and a sharp peak at 436 nm. The 436 nm peak is of the highest intensity. There is a small shoulder on the 386 nm peak that appears at 405 nm. The three peaks occurring at 520, 551, and 601 nm decrease in intensity, unlike the excitation spectra of original TPP. The lower excitation spectrum is the result of being monitored at 716 nm.

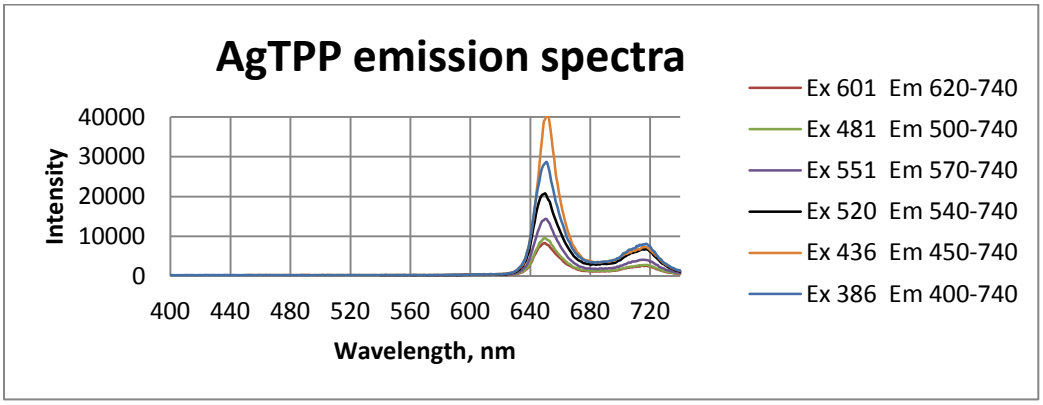

Figure 3.50. PL of Ag(TPP) emission spectra.

Figure 3.50 shows the emission spectrum of Ag(TPP) and its wavelength and intensity dependent characteristics. The peaks shown are at 646 nm and 716 nm. The largest peak observed is excited at 436 nm. There is an even distribution of spread between each spectrum shown in the

spectra. The beginning tail shows no luminescence activity from 400 to 630 nm, like previous Ln(TPP) complexes. The emission profile is similar in the appearance of the maxima at 646 nm and 716 nm which are both blue shifted from the original TPP emission profile. This proves that the smaller atomic radii and smaller charge of silver doesn't majorly affect the emission profile.

3.8. PL of Lanthanide (TPP) Combined Complexes

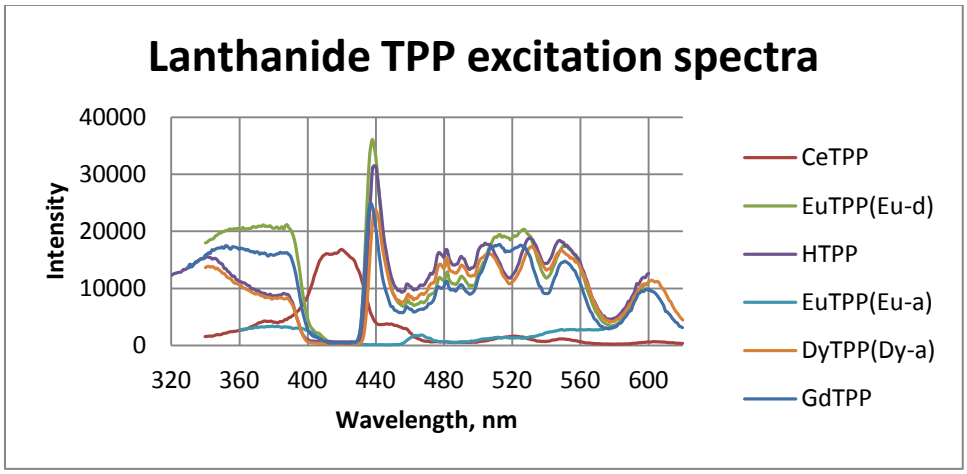

Figure 3.51. PL of Ln(TPP) combined excitation spectra.

The combined spectra of the lanthanides with TPP are illustrated in figure 3.51. The standard TPP spectrum is shown in purple with peaks at 340, 388, 436, 472, 482, 510, 530, 548, and 600 nm. The spectrum that most closely resembles the TPP is that of the DyTPP complex **(Dy-a)** purple solution, which was exposed to sodium hydroxide and retained its color. The Dy(TPP) complex **(Dy-a)** spectrum is close in intensity to the TPP except in relation to the 436 nm peak; there is a decrease in intensity and a slight red shift in the peak maximum.

The Gd(TPP) spectrum exhibits similar peak maxima as TPP; the differences arise in that the beginning peaks are higher in intensity and exhibit a different profile. The 348 nm peak has red shifted to 351nm and the 388 peak remains consistent with the original TPP although higher in intensity. The 436 nm peak has blue shifted and decreased in intensity compared to the original peak at 440 nm. The peaks at 472, 482, and 492 nm are the lowest of all the spectra, whereas the

peaks at 510, 526, 551, and 600 nm are only slightly less intense than the original TPP peaks at similar wavelengths. The Eu(TPP) complex **(Eu-d)** purple solution spectrum is similar to the original TPP being the differences are the beginning peaks intensities at 351 and 388 nm. The peaks of Eu(TPP) complex **(Eu-d)** purple solution are identical in position to the peaks of Gd(TPP), although higher in intensity. The 436 nm peak is blue shifted and more intense than the original peak located at 440 nm.

The Ce(TPP) spectrum shows maxima at 375, 418, 446, 522, 550, and 604 nm. Its spectrum shows its most intense luminescence where the other graphs have the lowest. The Eu(TPP) complex **(Eu-a)** green solution spectrum isn't consistent with the majority of the characteristic peaks, decreased intensity and no luminescent peak at 440 nm.

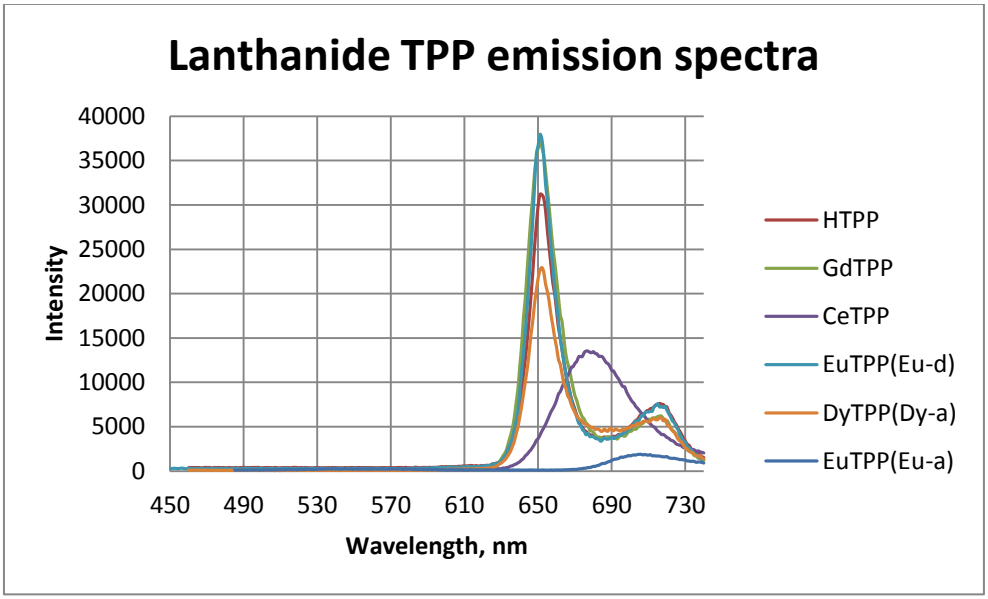

Figure 3.52. PL of Ln(TPP) combined emission spectra.

Figure 3.52 shows the combined lanthanides and TPP emission spectra with band maxima at 652 and 719 nm. The spectrum of the Eu(TPP) complex **(Eu-d)** maxima at 652 and 716 nm. The spectrum of Gd(TPP) shows maxima at 646 nm and 714 nm. The spectrum of Dy(TPP) complex **(Dy-a)** purple solution shows maxima at 652 nm and 714 nm.

The spectrum of Ce(TPP) shows a maximum at 677 nm. The spectrum of Eu(TPP) complex **(Eu-a)** green solution shows a maximum at 705 nm. The Ce(TPP) and Eu(TPP) complex **(Eu-a)** green solution changes the most from the original TPP spectrum. The intensity of the Eu(TPP) complex **(Eu-a)** green solution and Gd(TPP) is greater than the intensity of TPP original spectrum. There is no luminescence intensity in the beginning tail of the spectra.

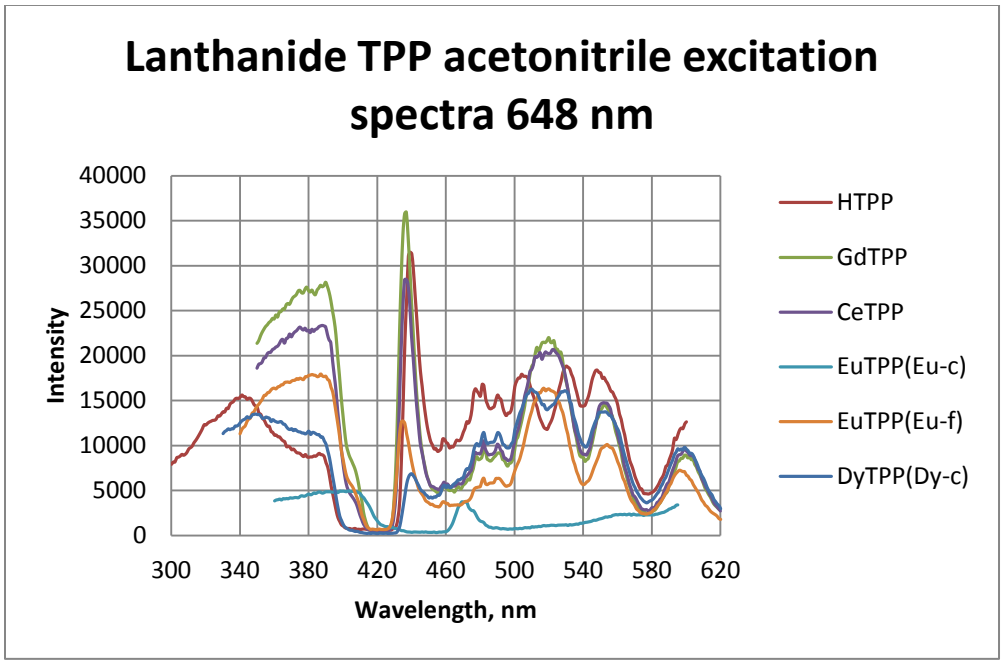

Figure 3.53. PL of Ln(TPP)(CH_3CN) excitation spectra.

In Figure 3.53 is shown a comparison of the excitation spectra of the lanthanides complexes in acetonitrile. The TPP spectrum shows maxima at 344, 388, 440, 472, 482, 505, 530, 550, and 600 nm. The emission profile of Gd(TPP) shows maxima at 388, 405, 437, 482, 521, 552, and 600 nm. The major peak is blue shifted from 440 nm to 437 nm and there is a combination of the 505 nm and 530 nm peaks to form the 521 nm broad peak. The beginning peak and structure changes from the TPP spectrum structure in that the 388 nm peak is more intense and there is a positive slope to 388 nm instead of a negative slope towards the 388 nm peak.

The emission profile of the Ce(TPP) spectrum layered with acetonitrile shows maxima at 387, 405, 436, 482, 519, 553, and 600 nm. The positive slope to the 388 nm peak is similar to the Gd(TPP) spectra only being lower in intensity. The major peak is also blue shifted from 440 nm to 436 nm; there is also a combination of the 505 and 530 nm peaks to form the 519 nm broad peak. There is a decrease in intensity from the 520, 550 and 600 nm peaks.

The emission profile of Eu(TPP) complex **(Eu-f)** purple solution layered with acetonitrile shows maxima at 365, 390, 405, 435, 482, 518, 554, and 597 nm. There is also a positive slope towards the peak at 390 nm; the major peak is blue shifted from 440 nm to 435 nm. There is also a combination of the 505 and 530 nm peaks to form the 518 nm. The major peak shows a decreased luminescence as well possibly due to the addition of sodium hydroxide.

The emission profile of Dy(TPP) complex **(Dy-c)** purple solution shows maxima at 350, 381, 440, 483, 511, 527, 553, and 597 nm. This profile is the most similar to the TPP spectrum being that the 350 and 381 nm peaks are consistent with each other and the major peak didn't blue shift although it decreased in intensity. The two peaks at 511 nm and 527 nm are similar to the TPP peaks at 505 nm and 530 nm. The cluster of peaks appearing from 470 nm to 490 nm is similar to the original and increased in intensity compared to the other Ln(TPP) acetonitrile complexes.

The emission profile of the Eu(TPP) complex **(Eu-c)** green solution shows maxima at 396, 470, 523, and 563 nm. This shows the largest change from the original TPP spectrum with a decrease luminescence profile and appearance of peaks. The 396 nm peak appears where all other complexes show no luminescent activity. The 470 nm peak is also uncharacteristic of porphyrin and lanthanide porphyrin complexes; this is reason for an energy transfer process and the result of the change in the solvent dielectric constant stabilizing at different energy states.

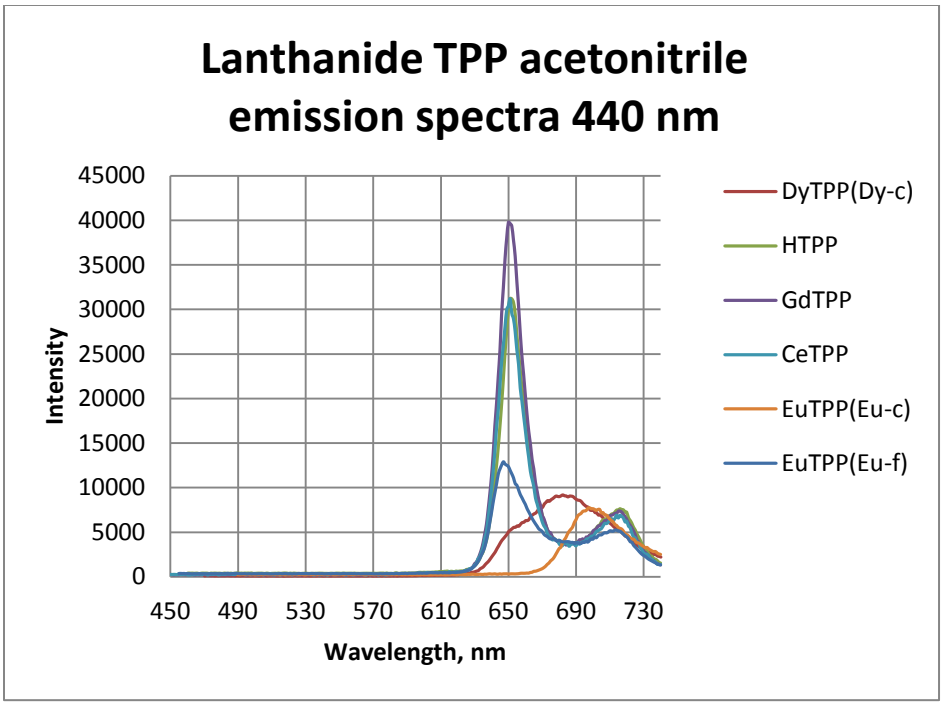

Figure 3.54. PL of Ln(TPP)(CH_3CN) emission spectra.

The spectra shown in figure 3.54 represent the emission profile of the Ln(TPP) layered with acetonitrile. The original TPP shows emission maxima at 652 nm and 719 nm. The emission profile of Ce(TPP) shows maxima at 648 nm and 714 nm; there is a 4 nm and 5 nm blue shift in the emission maxima respectively. The emission profile of Gd(TPP) shows maxima at 648 nm and 714 nm; the intensity is higher than the original TPP although the maxima are blue shifted 4 nm and 5 nm respectively.

The emission profile of Eu(TPP) **(Eu-f)** shows maxima at 648 nm and 714 nm; this is similar to the previous although the intensity is lower than the TPP emission spectrum. The emission profile of Dy(TPP) complex **(Dy-c)** purple solution shows maxima at 648 nm and 682 nm; the intensity is lower and there is a red shift in the major peak. There is a small shoulder at the 648 nm peak. The emission profile of Eu(TPP) complex **(Eu-c)** green solution shows maxima at 699 nm with no luminescence activity at 648 nm; the emission is centered closer the lower maximum due to the dielectric constant and other mechanisms occurring in solution.

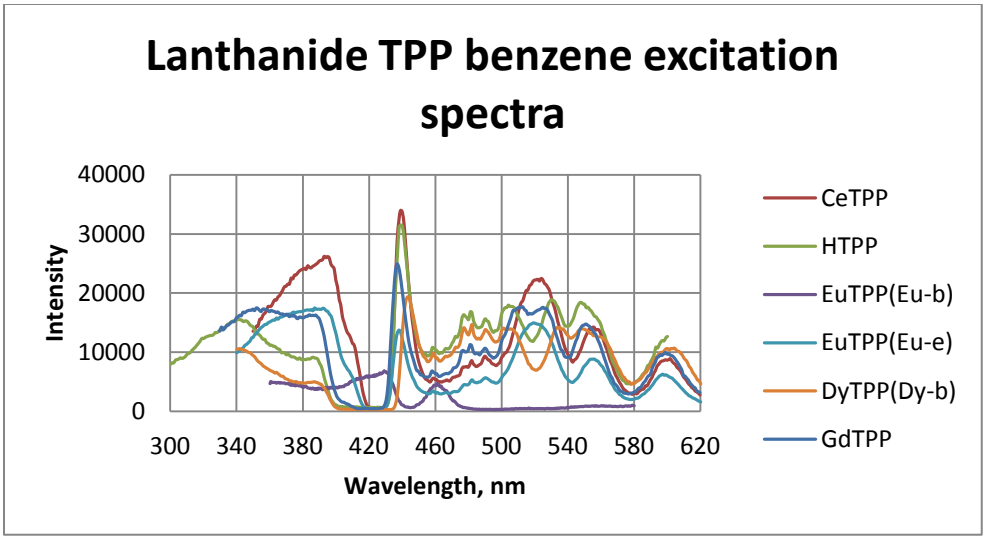

Figure 3.55. PL of Ln(TPP)(C_6H_6) excitation spectra.

Figure 3.55 shows the excitation spectra of Ln(TPP)(C_6H_6) complexes. The excitation profile of TPP shows maxima at 344, 386, 440, 481, 505, 529, 550, and 600 nm. There is a negative slope going from the 344 nm peak to the 386 nm peak. The major peak maxima shows at 440 nm and the peaks from 470 nm to 550 nm are comparable in intensity. There is no peak at 405 nm.

The excitation spectrum of Ce(TPP) shows maxima at 394, 405, 440, 482, 490, 523, 555, and 600 nm. There is a positive slope leading up to the 394 nm. The major peak at 440 nm is more intense than the TPP peak at 440 nm. The peaks at 505 and 529 nm were combined to form the 523 nm. There is a decrease in intensity from the 529 nm peak to the 600 nm peak.

The excitation spectrum of Gd(TPP) shows maxima at 350, 389, 442, 481, 490, 512, 533, 555, and 600 nm. There is a slight plateau from the 350 nm to the 389 nm peak. The major peak at 442 is red shifted from the original 440 nm wavelength and is less intense. The peaks at 502 nm and 535 nm haven't combined but are similar to the 505 nm and 529 nm peaks of the TPP excitation spectrum; where the TPP peaks are comparable in intensity, the Gd(TPP) excitation spectrum's 529 nm to 600 nm peaks decrease in intensity.

The excitation spectrum of Dy(TPP) complex **(Dy-b)** purple solution shows maxima at 346, 386, 443, 502, 535, 550, and 600 nm. The entire spectrum is most similar to the TPP spectrum in corresponding peak wavelengths, the difference being the decreased luminescence and 3 nm red shift of the major peak. The intensity of the 502 nm to 550 nm has the characteristics of a plateau just as the TPP spectrum. There is no peak at 405 nm like the other spectra.

The excitation spectrum of Eu(TPP) complex **(Eu-e)** purple solution shows maxima at 393, 406, 438, 519, 535, and 600 nm. The beginning part of the spectrum resumes the positive slope towards 393 nm and the shoulder at 406 nm returns. The major peak is blue shifted from 440 nm to 438 nm and is less intense than the TPP major peak at 440 nm. The peaks at 505 nm and 529 nm combine to form the 519 nm peak. The intensity of the 519 nm to 600 nm peaks decrease in intensity, unlike the TPP excitation spectrum. The intensity of the cluster of 470 nm to 490 nm peaks is lower than the TPP cluster.

The excitation spectrum of Eu(TPP) complex **(Eu-b)** green solution shows maxima at 373, 431, and 462 nm. This spectrum changes the most from the TPP spectrum and is the most consistent. The 431 and 462 nm peaks are most intense when the other spectra are least intense. This shows that even with the addition of benzene the profile stays consistent and maintains the peaks at 373 and 462 nm which are blue shifted compared to the same complex with acetonitrile added. This excitation spectrum shows that there is a direct energy transfer coupled with another intricate process occurring between the europium and the porphyrin; this intricate process is still consistent with the involvement of benzene on the excitation spectra for lanthanides and porphyrin. This observation would make the europium porphyrin complex a candidate for the sensor for benzene and acetonitrile.

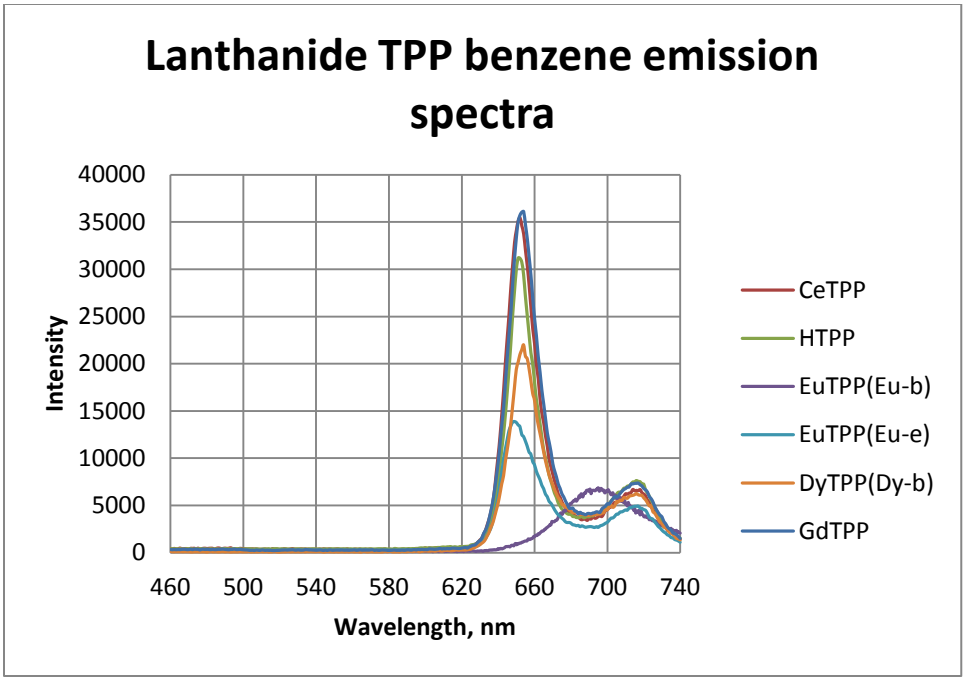

Figure 3.56. PL of Ln(TPP)(C_6H_6) emission spectra.

In Figure 3.56 the emission profile of the lanthanides, TPP, and benzene complexes are given. The emission profile of TPP shows maxima at 652 and 719 nm, while the emission profile of Ce(TPP) shows maxima at 650 and 716 nm. The emission profile of Gd(TPP) shows maxima at 646 and 714 nm. The emission profile of Dy(TPP) complex **(Dy-b)** purple solution shows maxima at 652 and 716 nm.

The emission spectrum of Eu(TPP) complex **(Eu-e)** purple solution shows maxima at 648 and 714 nm. The emission profile of Eu(TPP) complex **(Eu-b)** green solution shows a maximum at 698 nm. Aside from blue shifts of the major peak, the complex that shows the greatest change is Eu(TPP) complex **(Eu-b)** green solution; there is no luminescence activity at the 648 nm peak but shifts from the 716 nm to shorter wavelength at 698 nm. The 714 to 719 nm peak is consistent in its intensity although different lanthanides were used; the major difference is in the major peak intensities with Ce(TPP) and Gd(TPP) being more intense than the TPP emission profile with respect to the maxima occurring at 650 and 646 nm, respectively.

3.9. PL of (TBSP)

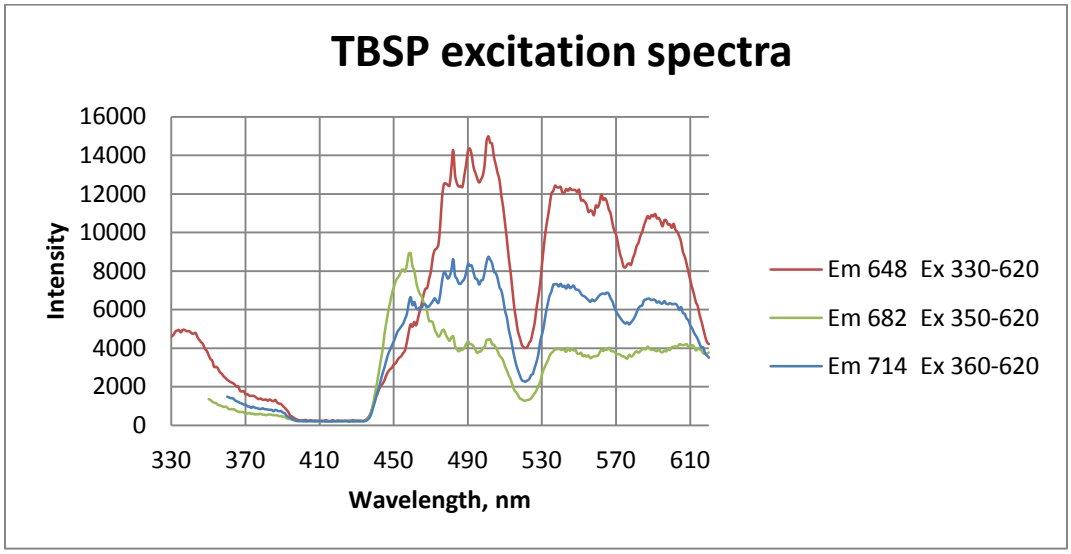

Figure 3.57. PL of TBSP excitation spectra.

The excitation spectra of TBSP, seen in figure 3.57 have maxima at 336, 388, 459, 478, 482, 490, 501, 538, 563, and 587 nm. The excitation spectra show two different profiles; when monitored at 648 nm and 714 nm similar spectra are produce, but when monitored at 682 nm, a different profile has emerged. When monitored at 682 nm, the peak at 459 is more prominent than in the other excitation profiles. The peaks at 482, 490, and 501 nm are decreased in relative intensity compared to the 459 nm peak; those peaks show comparable intensity unlike the other excitation profile that is shown.

The intensity of the excitation profile when monitored at 648 nm is the most intense compared to the similar profile when monitored at 714 nm. The intensity of the excitation profile when monitored at 682 nm is lower than the profile monitored at 714 nm at all points except for the maxima at 459 nm. Although there are differences between the 450 nm to 520 nm portion of the graph, all three spectra show similar excitation profile character from 530 nm to 610 nm. Peaks and remnants of the same peaks can be seen in all three spectra; all descend in a negative slope after 610 nm. All three show no luminescence activity from the 390 nm to 430 nm range.

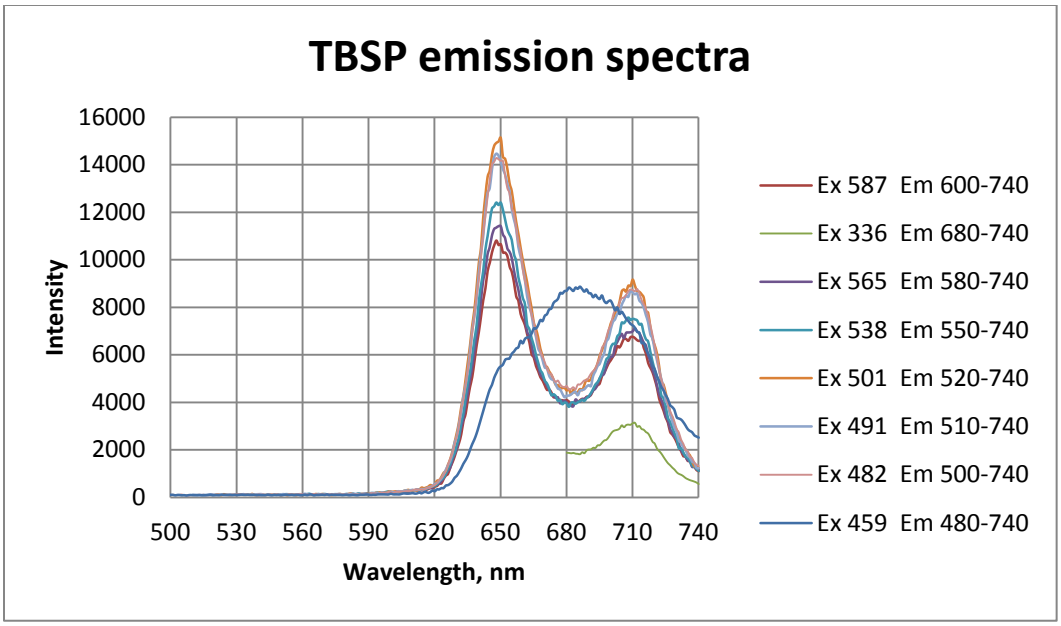

Figure 3.58. PL of TBSP emission spectra.

In Figure 3.58 is given the emission profile of TBSP and its maxima at 648, 682, and 714 nm. The beginning portion of the emission spectra doesn't show any luminescence intensity from 500 to 620 nm. There are two emission profiles seen in the spectra; one being two dominant peaks at 648 nm and 714 nm, and the other profile with a dominant peak at 682 nm and a small shoulder at 650 nm. When excited at 459 nm, the emission spectrum with a maximum at 682 nm is produced, indicating a new species is stabilized at the excitation wavelength. When excited at all other peak wavelengths, the emission profile with maxima at 648 nm and 714 nm is produced; the most intense spectrum is excited at 501 nm.

With the first profile showing maxima at 648 nm and 714 nm, there isn't a great deviation in the emission intensity compared to that of the TPP emission spectra. The ratio between the height of the 648 nm and 714 nm maxima isn't as large as the TPP; this is due to the electron withdrawing sulfonyl groups. The other profile showing a maximum at 682 nm is still persistent although this porphyrin is different than the tetraphenylporphyrin; this shows that the other species is still present and stabilized at that excitation wavelength.

3.10. PL of Lanthanide (TBSP) Combined Complexes

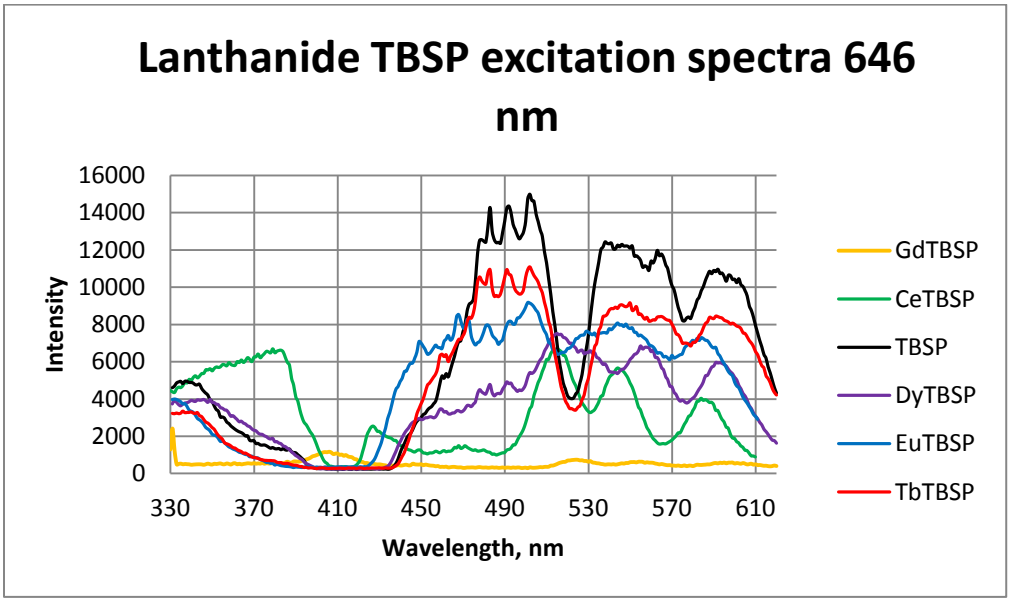

Figure 3.59. PL of Ln(TBSP) excitation spectra.

The excitation profile of Ln(TBSP) when monitored at 646 nm is shown in figure 3.59. The TBSP spectrum shows maxima at 336, 388, 478, 482, 490, 501, 538, 563, and 587 nm. There is a small broad band at 336 nm. There are three other broad bands with the first having three distinctive sharp maxima peaks. There is a decrease in intensity between the three intense broad bands.

The Tb(TBSP) excitation spectrum is most consistent with the TBSP excitation spectra, thus showing maxima at 338, 457, 478, 482, 490, 501, 549, 563, and 591 nm. The intensity of the Tb(TBSP) spectra is lower than the TBSP. There are four broad bands in total, with the most intense three broad bands being of comparable intensity.

The Eu(TBSP) excitation spectrum shows maxima at 338, 458, 478, 482, 490, 501, 512, 554, and 591 nm. This excitation spectrum is similar to the TBSP spectrum in the beginning portion from 338 nm to 388 nm; afterwards, it changes from the original profile character. It develops prominent peaks at 512, 554, and 591 nm.

The Dy(TBSP) excitation spectrum shows maxima at 345, 389, 458, 476, 482, 490, 501, 511, 531, 554, and 592 nm. The excitation profile shows a similar negative slope from 345 nm to 389 nm; there is then no luminescence activity until a peak maximum occurs at 458 nm. The similar cluster of maxima at 476, 482, and 501 nm are shown. Three prominent peak maxima emerge at 511, 554, and 592 nm with a small shoulder appearing at 531 nm. Unlike the previous excitation spectra, the three prominent peaks are more intense than the cluster of maxima at the 470 nm to 501 nm range. This alteration of the excitation spectrum shows that there is an observable reaction occurring changing the excitation spectrum.

The excitation spectrum of Ce(TBSP) shows maxima at 393, 437, 523, 553, and 593 nm. This excitation profile deviates from the most from the others. There is a positive slope going from 330 nm to the peak maximum at 393 nm. There is also a small broad band at 437 nm where in the other lanthanide TBSP spectra there was luminescence inactivity. The cluster of bands that had showed up at the 470 nm to 501 nm range is absent while there are three distinct broad bands that decrease in intensity, arise at 523, 553, and 593 nm. This shows a greater interaction between the cerium and porphyrin in the way that it alters and decreases the spectrum as in the previous lanthanide porphyrin complexes in aqueous solution.

The excitation spectrum of Gd(TBSP), yellow spectrum, shows maxima at 331, 403, 523, 553, and 595 nm. This spectrum is the least intense of all the spectra and differ the most from all the other spectra. There is a small broad peak at 403 nm and three small remnants of broad peaks at 523, 553, and 595 nm. The maximum at 403 nm is intense where the other profiles don’t show luminescence intensity. There is a small sharp band at 331 nm. The difference in this spectrum compared to the rest shows the direct interaction and alteration of spectrum due to gadolinium and porphyrin interaction, thus quenching the excitation and altering the profile the most.

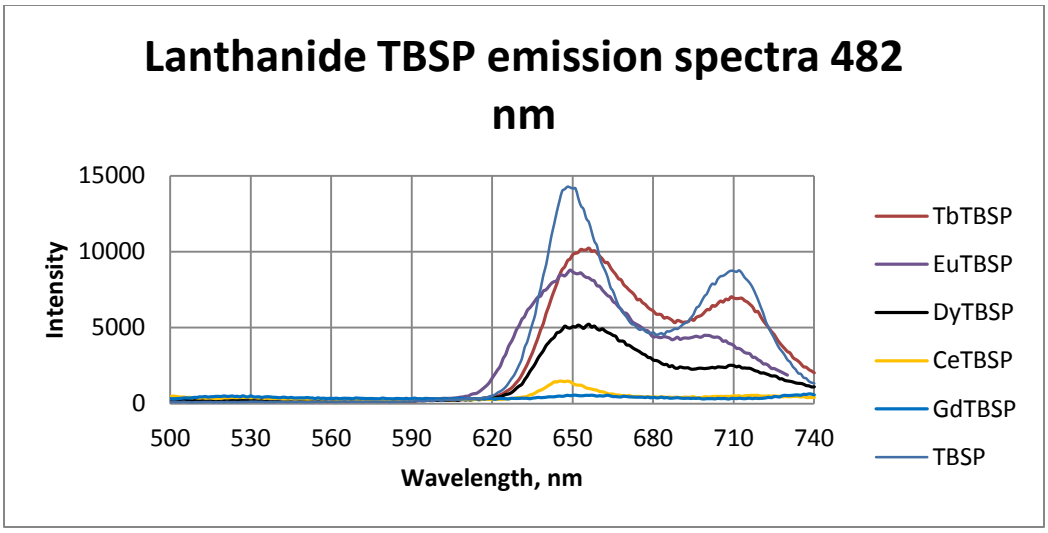

Figure 3.60. PL of Ln(TBSP) emission spectra excited at 482 nm.

The emission spectra of Ln(TBSP) shown in figure 3.60 has the emission maxima at 648 nm and 712 nm. The emission profile of Tb(TBSP) shows maxima at 657 nm and 712 nm; this is a 9 nm red shift in the most intense peak. The emission spectrum of Eu(TBSP) shows maxima at 649 nm and 700 nm; this is a 1 nm red shift and 12 nm blue shift respectively. The emission profile of Dy(TBSP) shows emission maxima at 653 nm and 709 nm; this is a 5 nm red shift and 3 nm blue shift respectively. The emission profile of Ce(TBSP) shows a maximum at 645 nm; this is a 3 nm blue shift. The emission spectrum of Gd(TBSP) shows a maximum at 656 nm; this is an 8 nm red shift.

The intensity of the highest maxima decreases in intensity from the TBSP, Tb(TBSP), Eu(TBSP), Dy(TBSP), Ce(TBSP), and Gd(TBSP) respectively. The intensity of the smaller maxima also decreases until disappearance, as seen in the Ce(TBSP) and Dy(TBSP). Based on the emission profile, Ce(TBSP) and Gd(TBSP) quench the emission most compared to the other complexes. The beginning portion of the emission spectra shows no luminescence activity from 500 nm to 600 nm, just like previously seen in the other lanthanide porphyrin complexes whether acetonitrile, benzene or no additional solvent was added to the reaction mixture.

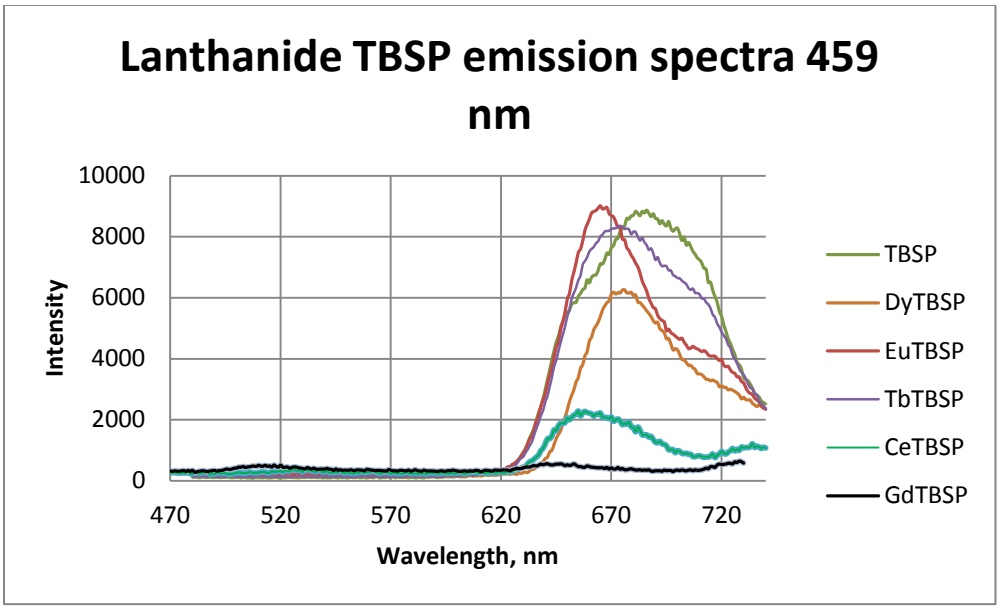

Figure 3.61. PL of Ln(TBSP) emission spectra excited at 459 nm.

The above spectra figure 3.61., show the emission profile of lanthanide TBSP complexes. The emission TBSP shows a maximum at 687 nm. The spectrum of Eu(TBSP) shows a maximum of 665 nm. The emission of Tb(TBSP) shows a maximum at 672 nm. The Dy(TBSP) emission spectrum shows a maximum at 674 nm. The emission profile of Ce(TBSP) shows a maximum at 657 nm. The emission profile of Gd(TBSP) shows a maximum at 645 nm. The emission profiles of cerium and gadolinium TBSP are quenched and blue shifted the most compared to the other spectra. All of the emission spectra of lanthanide TBSP complexes have blue shifted maxima emission profiles when excited at 459 nm.

All of the lanthanide TBSP complexes show a decrease in intensity being Tb(TBSP), Dy(TBSP), Ce(TBSP), and Gd(TBSP). The only complex that enhances the luminescence spectrum profile is that of the Eu(TBSP); this shows that there is energy transfer from the metal to the porphyrin. The single maximum appearing is consistent whether lanthanides are added to the porphyrin. This shows that the stabilized species is still prevalent with the addition of lanthanides in the solution when it is excited at 459 nm.

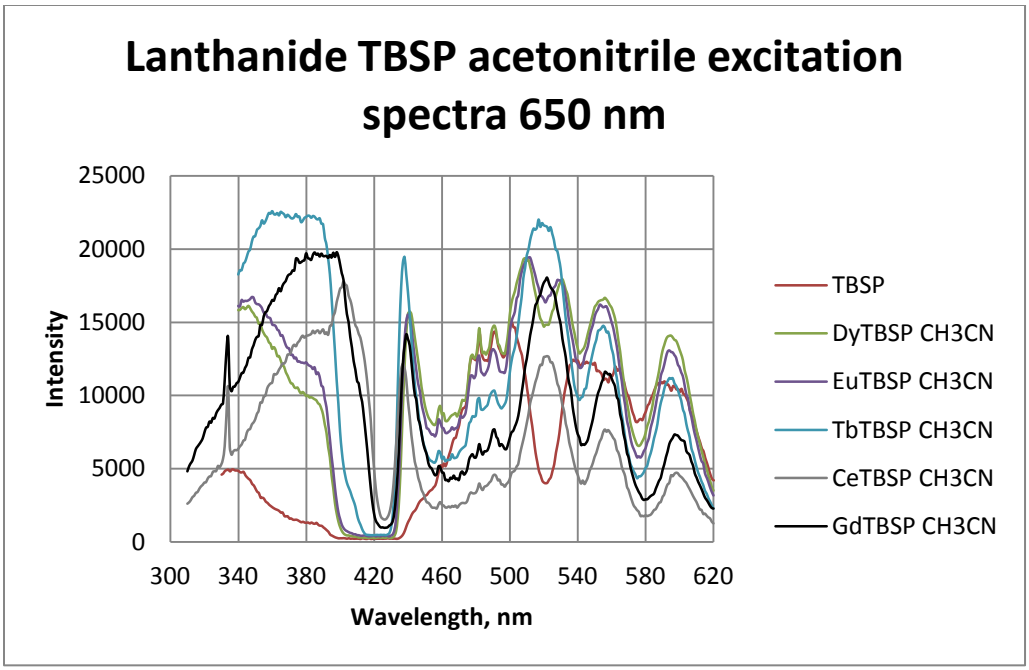

Figure 3.62. PL of Ln(TBSP)(CH_3CN) excitation spectra.

In Figure 3.62 is shown the excitation profile of the combined lanthanide, TBSP and acetonitrile complexes. This spectrum shows three different excitation profiles. One profile is that of the TBSP which shows a negative slope in the beginning peak, no peak in the 440 nm area, and three broad bands including the intense cluster peaks. The second profile shows positive slopes to a maximum peak, intense sharp peak at 440 nm region, and the emergence of three distinct broad peaks with the decrease in cluster peaks intensity. The third profile shows negative slope from one maximum to another, a sharp peak in the 440 nm region, relatively comparable cluster intensity, and four distinct broad peaks with decreasing luminescence intensity.

The TBSP spectrum shows maxima at 336, 388, 478, 482, 490, 501, 538, 563, and 587 nm. There is a small broad band at 336 nm with negative slope and a trough at 520 nm.. There are three other broad bands with the first having three distinctive sharp maxima peaks. There is a decrease in intensity between the three intense broad bands, but there isn't a uniform conformity between the three peaks of the TBSP excitation spectrum.

The excitation spectrum of Tb(TBSP) shows maxima at 360, 388, 437, 482, 490, 516, 554, and 594 nm. There is a broad, plateau, band from 360 nm to 388 nm. There is a sharp intense peak at 437 nm; the cluster of peaks from 470 nm to 490 nm is still prevalent. There are three distinct broad peaks descending in intensity at 516, 554, and 594 nm. This spectrum is the most intense of the compared lanthanide, TBSP, acetonitrile complexes.

The excitation spectrum of Gd(TBSP) shows maxima at 333, 395, 438, 482, 490, 521, 556, and 597 nm. There is a sharp band at 333 nm, followed by a positive slope to a maximum at 395 nm. There is a sharp peak at 438 nm. The small cluster of peaks from 470 nm to 490 nm remains. There are three distinct broad peaks descending in intensity with maxima at 521, 556, and 597 nm.

The excitation spectrum of Ce(TBSP) shows maxima at 334, 388, 401, 437, 482, 490, 521, 556, and 595 nm. The spectrum shows a sharp peak at 334 nm, followed by a positive slope to two maxima at 388 nm and 401 nm. There is a sharp peak at 437 nm followed by three distinct broad peaks at 521, 556, and 595 nm. The three peaks descend in intensity.

The excitation spectrum of Dy(TBSP) shows maxima at 344, 380, 440, 482, 490, 511, 530, 553, and 593 nm. There is a negative slope from the 344 nm peak to the 380 nm shoulder. There is a sharp peak at 440 nm, followed by the cluster of peaks at 472 nm and 482 nm. There are four distinct broad peaks at 511, 530, 553, and 593 nm. These four peaks also descend in intensity.

The excitation spectrum of Eu(TBSP) shows maxima at 347, 379, 439, 482, 490, 511, 530, 553, and 593 nm. There is a negative slope from the 347 nm peak to the 379 nm shoulder. There is a sharp peak at 439 nm, followed by the cluster of peaks at 472, 472, and 490 nm. There are four large, descending peaks at 511, 530, 553, and 593 nm.

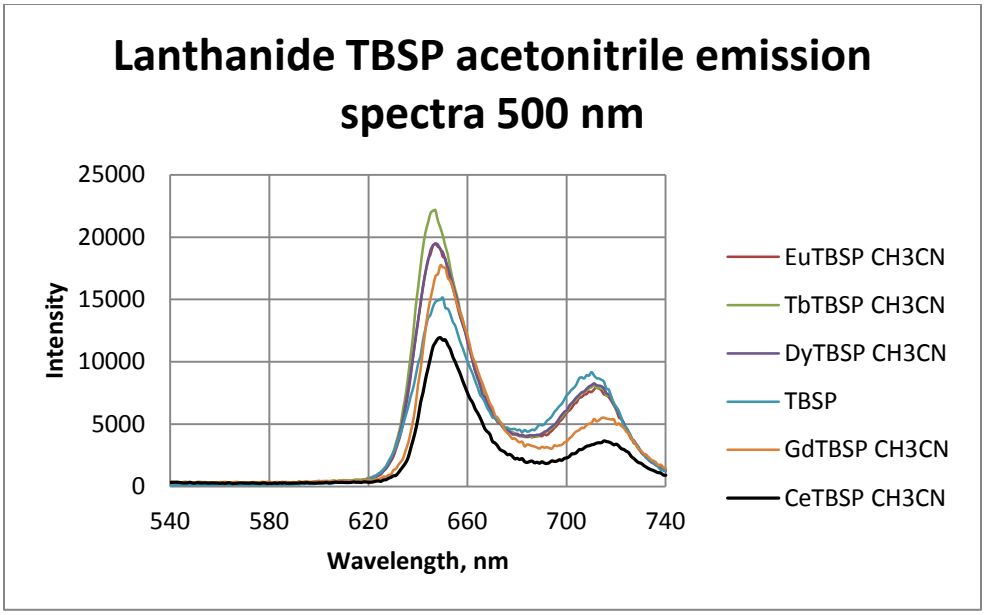

Figure 3.63. PL of Ln(TBSP)(CH_3CN) emission spectra

The above emission spectra figure 3.63 show the lanthanide, TBSP, acetonitrile complexes. The spectra show one type of emission profile with two distinct maxima. The TBSP emission spectrum shows maxima at 650 nm and 710 nm. The Tb(TBSP) emission spectrum shows maxima at 647 nm and 711 nm. The emission spectrum of Eu(TBSP) shows maxima at 647 nm and 711 nm. The emission spectrum of Dy(TBSP) shows maxima at 647 nm and 711 nm. The emission spectrum of Gd(TBSP) shows maxima at 649 nm and 715 nm. The emission spectrum of Ce(TBSP) shows maxima at 649 nm and 717 nm. All of the lanthanide, TBSP, acetonitrile complexes show a blue shift in the major maximum peak; the latter peak is red shifted.

The beginning portions of the emission spectra show no luminescent activity from 540 nm to 610 nm. The intensity of the major maximum is decreased for the Ce(TBSP) acetonitrile layered and the lower maxima is red shifted compared to the original TBSP emission spectrum. The intensity of the major maximum is increased for the Gd(TBSP), Dy(TBSP), Eu(TBSP), and Tb(TBSP) acetonitrile complexes.

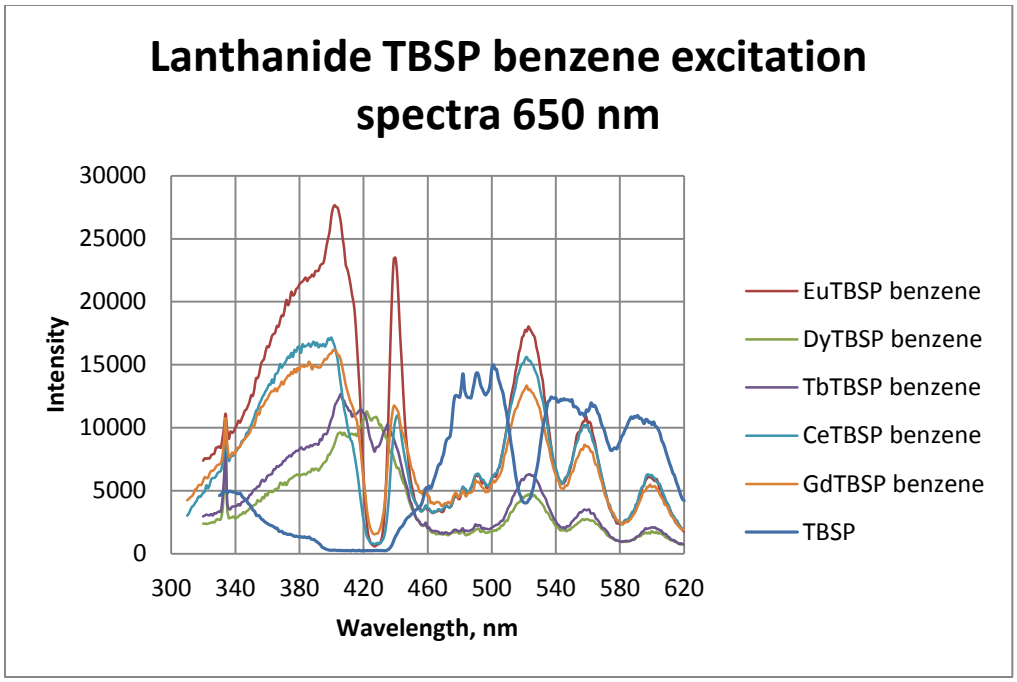

Figure 3.64. PL of Ln(TBSP)(C_6H_6) excitation spectra.

The figure 3.64 corresponds to the excitation profiles of lanthanide, TBSP, benzene complexes. The spectra show three different profiles; one being of the original TBSP, the second profile containing Dy(TBSP) and Tb(TBSP), and the third profile containing Eu(TBSP), Ce(TBSP), and Gd(TBSP). The first profile of the TBSP spectrum shows maxima at 336, 388, 478, 482, 490, 501, 538, 563, and 587 nm. There is a small broad band at 336 nm. There are three other broad bands with the first having three distinctive sharp maxima peaks. There is a decrease in intensity between the three intense broad bands.

The excitation profile of the Eu(TBSP) shows maxima at 383, 401, 439, 521, 555, and 598 nm. There is a positive slope leading to the maxima at 383 nm and 401 nm. The peak at 401 nm corresponds to a europium excitation peak. There is a sharp peak at 439 nm, followed by the reduced intensity of cluster peaks from 470 nm to the 490 nm range. There are three distinct broad peaks descending in intensity from 521, 555, and 598 nm wavelengths. This spectrum is more intense than the TBSP spectrum.

The excitation profile of the Ce(TBSP) shows maxima at 381, 398, 441, 521, 558, and 598 nm. There is a positive slope leading to maxima at 381 nm and 398 nm. The maximum at 398 isn't as pronounced as the broad peak at 401 nm of the Eu(TBSP) spectrum. There is a sharp peak at 441 nm, followed by a reduced intensity cluster peaks. There are three distinct broad bands appearing at 521, 558, and 598 nm.

The excitation spectrum of Gd(TBSP) shows maxima at 386, 401, 438, 521, 558, and 598 nm. There is also a positive slope leading from the 386 nm peak to the 401 peak. There is a sharp peak at 438 nm and the cluster of peaks from 470 nm to 490 nm. There are three distinct broad peaks descending in intensity from the 521, 558, and 598 nm wavelengths.

The excitation spectrum of Tb(TBSP)shows maxima at 380, 405, 417, 433, 521, 558, and 598 nm. There are three distinct broad peaks at 598, 558, and 521 nm. The cluster peaks have been reduced to show almost no luminescence activity. There is no peak at the 440 nm wavelength, but a peak at 433 nm appears along with two maxima at 417 nm and 405 nm corresponding to a terbium excitation peak. There is also a shoulder at 380 nm.

The excitation spectrum of Dy(TBSP) shows maxima at 388, 404, 420, 426, 521, 558, and 598 nm. There are three distinct broad peaks descending in intensity at 521, 558, and 598 nm. The cluster peaks intensity has been reduced and no peak is shown at the 440 nm area. There are maxima at 420, 404, and a shoulder at 388 nm.

Although there are three different profiles shown in the excitation spectra, all of the lanthanide TBSP benzene complexes show a sharp excitation peak at 333 nm, and three distinct broad peaks at 521, 558, and 598 nm. These alterations show that benzene molecule may causes a consistent deviation of spectra of the lanthanide TBSP from the original TBSP excitation profile; this is due to the stabilizing of the higher energy state of porphyrin by benzene.

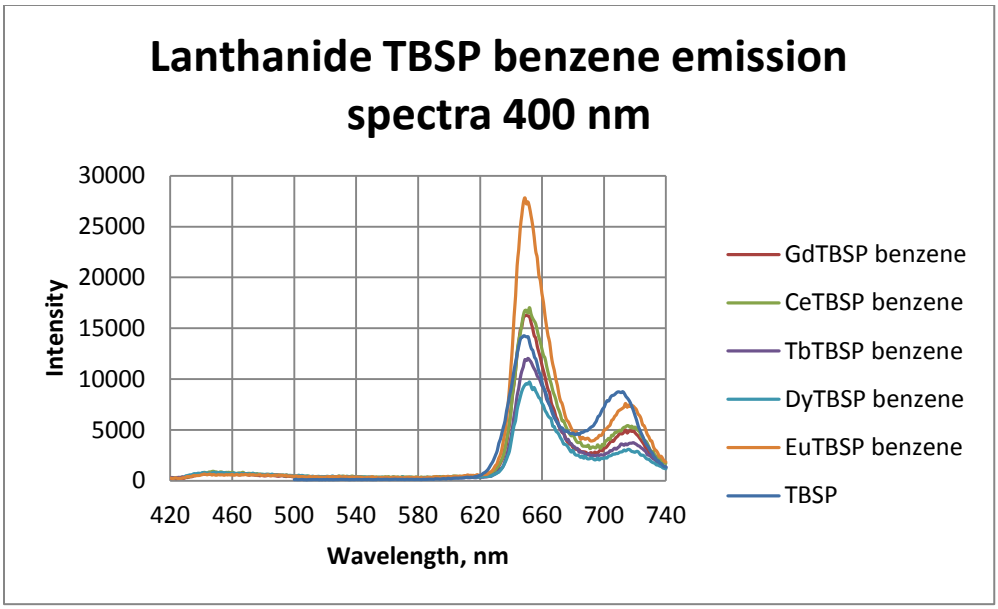

Figure 3.65. PL of Ln(TBSP)(C_6H_6) emission spectra excited at 400 nm.

The above spectra in figure 3.65 show the emission profiles of the TBSP alone and of the lanthanide TBSP benzene complexes while excited at 400 nm. The TBSP emission profile shows maxima at 648 nm and 710 nm. The Eu(TBSP) complex emission profile shows maxima at 648 nm and 711 nm. The Ce(TBSP) complex emission profile shows maxima at 651 nm and 713 nm. The Gd(TBSP) complex emission profile shows maxima at 650 and 713 nm.

The Tb(TBSP) complex emission profile shows maxima at 650 nm and 713 nm. The Dy(TBSP) complex emission profile shows maxima at 652 nm and 713 nm. The most intense major band corresponds to the Eu(TBSP) complex. All of the lanthanide TBSP complexes show a red shift in the major emission peak maxima and the lower emission peak maxima. The beginning portion of the emission spectra shows very little luminescence activity from 420 to 620 nm, with a broad band maximizing at 438 nm, when excited at 400 nm. The ratio between the maxima peaks at 648 nm and 710 nm is larger compared to when the complexes are exposed to acetonitrile or no solvent at all. With no solvent added, acetonitrile added, and benzene added the ratios between the maxima are 2.09, 2.05, and 4.72 respectively.

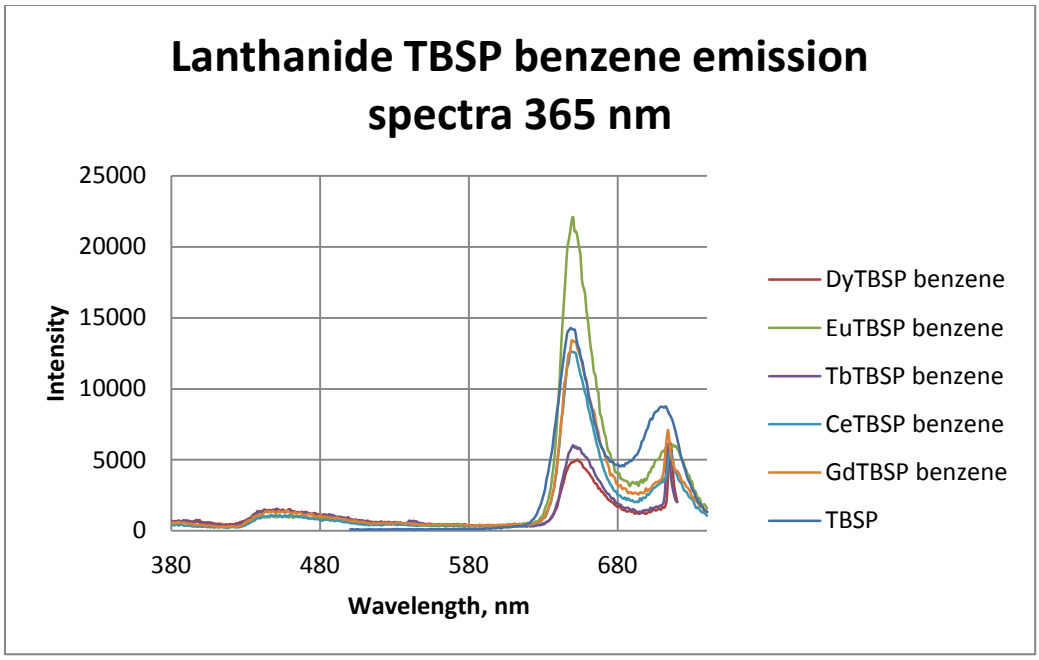

Figure 3.66. PL of Ln(TBSP)(C_6H_6) emission spectra excited at 365 nm.

The above spectra figure 3.66., show the emission profile of TBSP alone and of the lanthanide, TBSP, benzene complexes when excited at 365 nm. The TBSP emission profile shows maxima at 648 nm and 710 nm. The Eu(TBSP) complex shows maxima at 648 nm and 711 nm. The Ce(TBSP) complex emission spectrum shows maxima at 651 nm and 713 nm. The Gd(TBSP) complex emission spectrum shows maxima at 650 nm and 713 nm.

The Tb(TBSP) complex emission spectrum shows maxima at 650 nm and 713 nm. The Dy(TBSP) complex emission spectrum shows maxima at 652 nm and 713 nm. The emission spectra of TBSP and Eu(TBSP) benzene complex don't show a sharp peak maximum at 713 nm; they show a round broad peak at 711 nm. The emission spectra of Ce(TBSP), Gd(TBSP), Tb(TBSP), and Dy(TBSP) benzene complexes show a sharp peak maximum at 713 nm. There is luminescence activity at the beginning of the spectra in a broad band with a maximum at 438 nm. The most intense spectra are listed in order from Eu(TBSP), TBSP, Gd(TBSP), Ce(TBSP), Tb(TBSP), and Dy(TBSP) benzene complexes. The Eu(TBSP) is much more intense compared to

the rest of the spectra. The TBSP, Ce(TBSP), and Gd(TBSP) benzene complexes are comparable in intensity where the Tb(TBSP) and Dy(TBSP) benzene complexes are the least intense among the compared spectra. There is luminescent activity in the beginning portion of the emission spectra, a broad band and smaller other peaks.

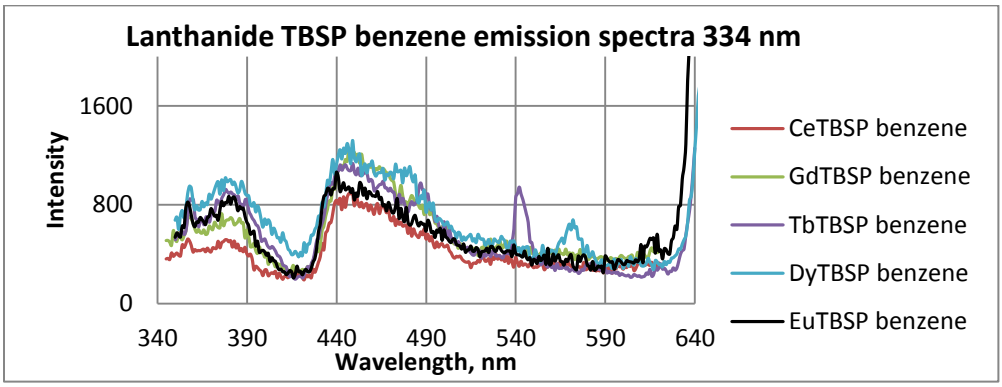

Figure 3.67. PL spectra of Ln(TBSP)(C_6H_6) emission spectra excited at 334 nm.

The above spectra in figure 3.67 reveal the similarities of the emission spectra of lanthanide TBSP benzene complexes when excited at 334 nm. The spectra show consistent peak maxima at 358, 380, and 443 nm. There is a sharp peak at 358 nm, broad band at 380 nm and broad band at 443 nm. The most intense spectrum corresponds to the Dy(TBSP) benzene complex, also show a characteristic dysprosium band at 571 nm. The second most intense band corresponds to the Tb(TBSP) benzene complex, displaying a characteristic terbium band at 542 nm. The third most intense band corresponds to the Eu(TBSP) benzene complex showing a characteristic europium band at 615 nm. The two least intense bands correspond to the Gd(TBSP) and Ce(TBSP) benzene complexes, respectively.

The presence of the lanthanide peaks show that the projected lanthanide was present in the system and that its luminescence was greatly reduced. The lanthanide energy is transferred to the TBSP ligand and the benzene layered environment allows for some lanthanide emission to be observed.

3.11. UV-Vis Spectroscopy of Lanthanide (TPP) Combined Complexes

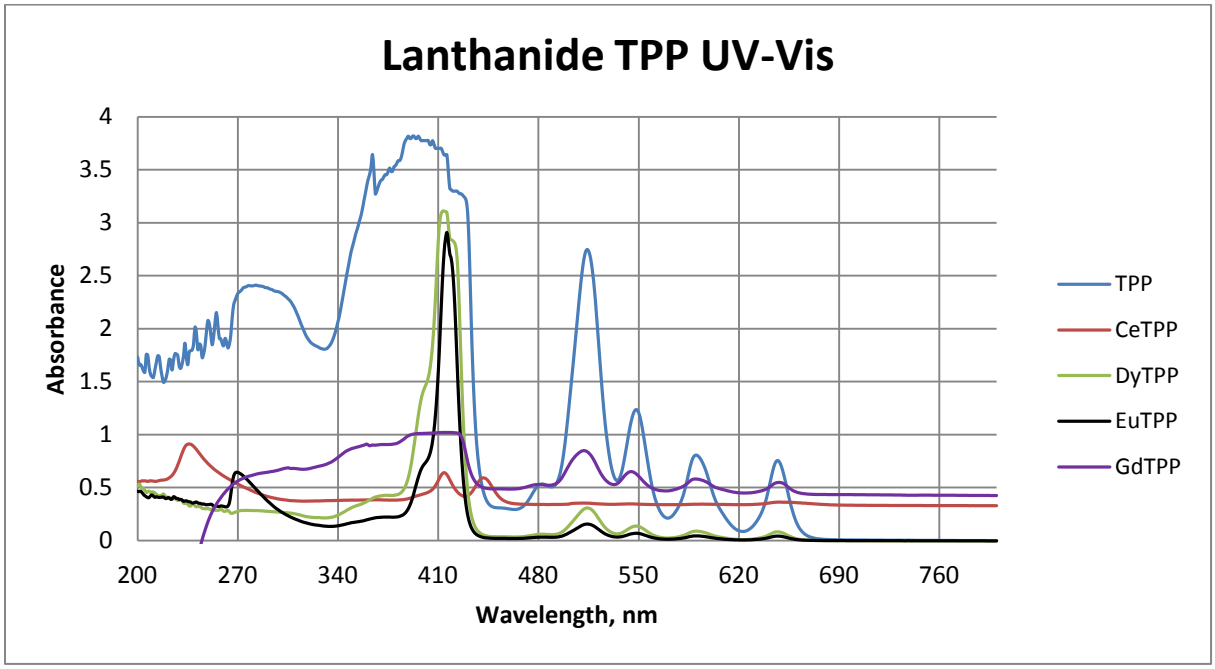

Figure 3.68. UV-Vis spectroscopy of Ln(TPP) complexes

The above spectra in figure 3.68 show the UV-Vis spectroscopic, absorbance peaks of TPP and lanthanide TPP complexes. The absorbance of TPP shows characteristic maxima at 281, 364, 395, 421, 513, 549, 586, and 647 nm. The Ce(TPP) shows maxima at 238, 414, and 434 nm. There are no absorbent peaks shown after the 434 nm peak. The Dy(TPP) shows maxima at 374, 401, 414, 416, 513, 549, 586, and 647 nm. There is no broad peak at 281 nm, but there is a small shoulder at 374 nm followed by a narrow soret peak at 416 nm with small shoulders at 401 nm and 416 nm. The characteristic peaks at 513, 549, 586, and 647 nm are greatly reduced in absorbance compared to the TPP absorbance spectrum.

The Eu(TPP) spectrum shows maxima at 270, 401, 414, 513, 549, 586, and 647 nm. There is a small broad peak at 270 nm, followed by a sharp peak with a small shoulder at 401 nm. There is no broadening of the 414 nm peak. The 513, 549, 586, and 647 nm peaks are reduced in absorbance compared to the TPP absorbance spectrum.

The Gd(TPP) absorbance spectrum shows maxima at 305, 360, 386, 513, 549, 586, and 647 nm. There is a single large broad band with three small maxima at 305, 360, and 386 nm. There is no evidence of a sharp peak at 414 nm but the Gd(TPP) spectrum does show the characteristic Q band peaks at 513, 549, 586, and 647 nm.

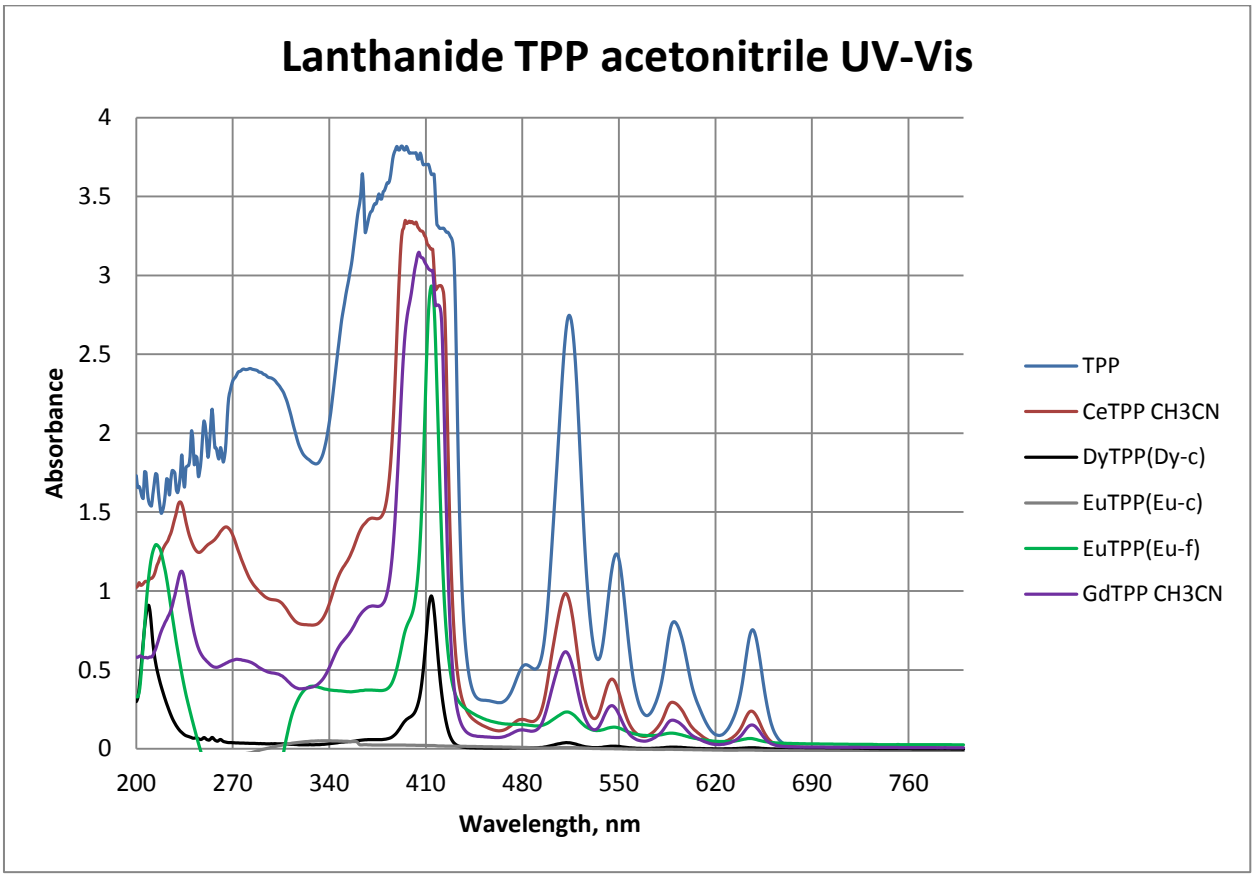

Figure 3.69. UV-Vis spectroscopy of Ln(TPP)(CH_3CN) complexes

The above spectra in figure 3.69., show the UV-Vis spectroscopic, absorbance peaks of TPP and lanthanide TPP acetonitrile complexes. The absorbance of TPP shows characteristic maxima at 281, 364, 395, 421, 513, 549, 586, and 647 nm. The Ce(TPP) spectrum shows maxima at 231, 267, 375, 395, 415, 512, 545, 588, and 647 nm. There are two small peaks at 231 nm and 267 nm. There is a large peak at 395 nm with small shoulders at 375 nm and 415 nm. The characteristic peaks show at 512, 545, 588, and 647 nm.

The Gd(TPP) spectrum shows maxima at 233, 273, 372, 407, 420, 512, 545, 588, and 647 nm. There is a broad peak at 233 nm and a small broad peak at 273 nm. There is a large broad peak at 407 nm with small shoulders at 372 nm and 420 nm. The characteristic peaks are decreased in absorbance and observed at 512, 545, 588, and 647 nm.

The Eu(TPP) complex **(Eu-f)**, sodium hydroxide added, yellow solution spectrum shows maxima at 214, 327, 415, 512, 545, 588, and 647 nm. There is a broad peak at 214 nm and at 327 nm. There is a sharp soret band peak at 415 nm followed by the characteristic decreased Q band absorbance peaks at 512, 545, 588, and 647 nm. The Dy(TPP) complex **(Dy-c)**, sodium hydroxide added, purple solution spectrum shows maxima at 206, 415, 512, 545, 588, and 647 nm. There is a broad band at 206 nm followed by a large single peak at 415 nm and the characteristic peaks at 512, 545, 588, and 647 nm. There is a decrease in the absorbance of the last four peaks.

For the TPP organic ligand, a decrease in the absorbance of the last four peaks shows efficient coordination of a metal in the porphyrin core center. The decrease is also attributed to the increase in the symmetry that is formed when the lanthanide coordinates to the porphyrin core. The symmetry of the porphyrin complex transitions from D_2h to D_4h symmetry.

The narrowing of the major band around 412 nm shows that a metal is coordinated at the center of the pyrrole ring of porphyrin ligands. The addition of acetonitrile causes the cerium and gadolinium complexes to resume the characteristic profile of a porphyrin UV-Vis spectrum, although there is still broadening in the 415 nm soret band peak. With the addition of other lanthanides, the broad peak that shows up at 281 nm is no longer present as shown in the original TPP UV-Vis spectrum. Of all the lanthanide porphyrin acetonitrile combinations that were conducted, the Dy(TPP) complex showed the best and greatest deviation in that it was coordinated better 281 nm peak disappeared the most and reduction in Q band peaks.

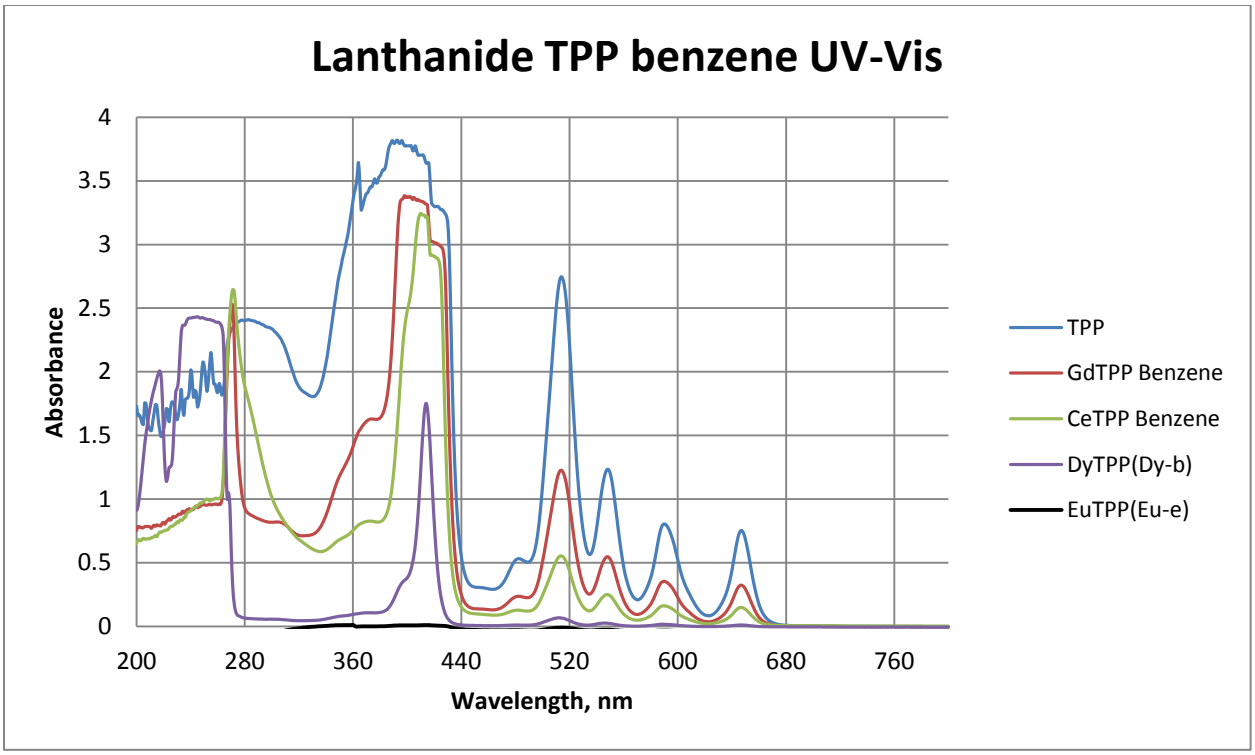

Figure 3.70. UV-Vis spectroscopy of Ln(TPP)(C_6H_6) complexes.

The above spectra in figure 3.70 show the UV-Vis spectroscopic, absorbance peaks of TPP and lanthanide TPP benzene complexes. The absorbance of TPP shows characteristic maxima at 281, 364, 395, 421, 513, 549, 586, and 647 nm. The Gd(TPP) complex shows maxima at 269, 374, 402, 416, 514, 549, 586, and 647 nm. There is a broad band with a sharp intense absorbance peak at 269 nm, followed by a large broad peak at 402 nm with shoulders at 374 nm and 416 nm. The decreased absorbent characteristic peaks occur at 514, 549, 586, and 647 nm.

The Ce(TPP) complex shows maxima at 269, 374, 410, 416, 514, 549, 586, and 647 nm. There is a broad band with a sharp intense peak at 269 nm followed by a large broad peak at 410 nm with shoulders at 374 nm and 416 nm. The decreased, absorbent, characteristic Q band peaks are observed at 514, 549, 586, and 647 nm. The last four peaks are decreasing in absorbance and the broadening of the 415 nm soret peak is decreased. The shoulder at 374 nm has decreased in intensity and the 415 nm peak is comparable to the Gd(TPP) complex 415 nm peak absorbance.

The Dy(TPP) complex **(Dy-b)**, sodium hydroxide added, purple solution shows maxima at 216, 241, 371, 415, 514, 549, 586, and 647 nm. There is a sharp peak at 216 nm, followed by a broad band with a maximum at 241 nm. There is sharp single peak at 415 nm with a shoulder at 371 nm. The last four characteristic Q band peaks at 514, 549, 586, and 647 nm have diminished in absorbance to almost baseline. With the most decreased absorbance of the last four peaks and the single sharp peak at 415 nm, the Dy(TPP) complex **(Dy-b)**, sodium hydroxide added, purple solution is a good candidate for a sensor for benzene.

3.12. UV-Vis Spectroscopy of Lanthanide (TBSP) Combined Complexes

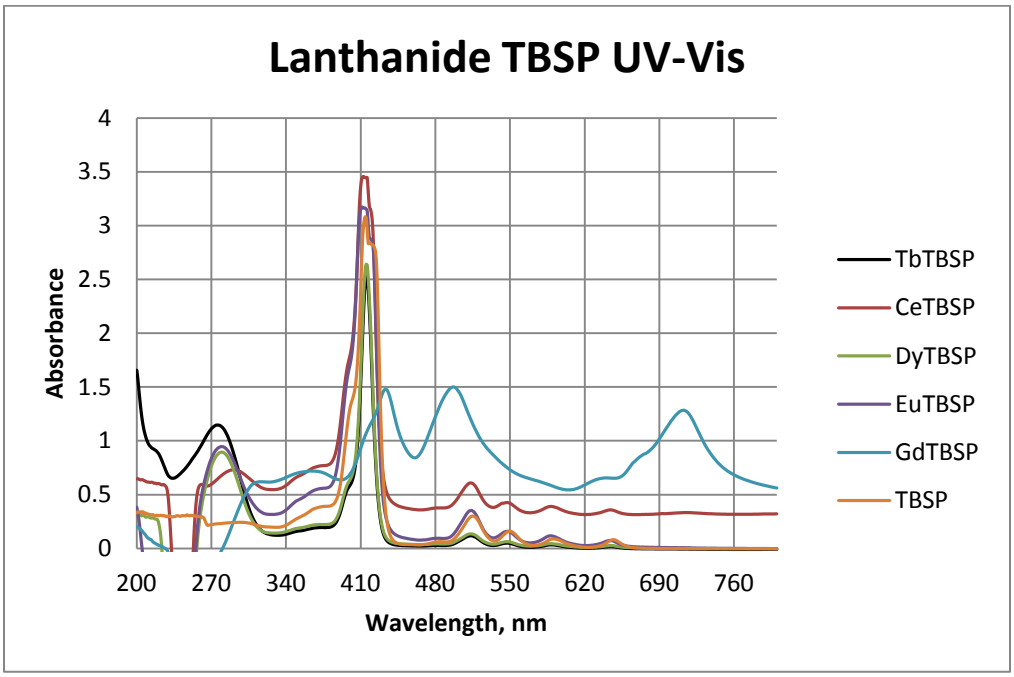

Figure 3.71. UV-Vis spectroscopy of Ln(TBSP) complexes.

The UV-Vis spectra of TBSP in figure 3.71 show band maxima at 405, 413, 416, 516, 550, 587, and 650 nm. There is a large peak that corresponds to the soret peak at 413 nm with shoulders at 405 nm and 416 nm. There are four characteristic Q band peaks at 516, 550, 587, and 650 nm. The Tb(TBSP) complex spectrum shows maxima at 217, 274, 417, 514, 547, 588, and 647 nm. There is a large broad peak at 274 nm with a small shoulder at 217 nm.

There is a sharp, single peak at 417 nm, corresponding to the soret band, followed by the decreased, absorbent peaks at 514, 547, 588, and 647 nm. This spectrum shows a narrower 417 nm band with decreased subsequent bands compared to the TBSP spectrum. According to the profile, the Tb(TBSP) would be a good candidate based on the altering of the soret band and Q peaks.

The Eu(TBSP) complex spectrum shows maxima at 280, 371, 400, 411, 416, 514, 547, 588, and 647 nm. There is a broad band at 280 nm, followed by shoulders at 371, 400, and 416 nm. There is large broad band with a maximum at 411 nm corresponding to the soret band, followed by the four subsequent bands at 514, 547, 588, and 647 nm. This spectrum shows a broader 416 nm peak than the TBSP original spectrum; it also shows that the subsequent peaks are similar in absorbance intensity. There is peak at 280 nm that isn't present in the original TBSP spectrum.

The Dy(TBSP) complex spectrum shows maxima at 280, 417, 514, 547, 588, and 647 nm. The broad band at 280 nm is still consistently present with a sharp, narrow 417 nm peak. The subsequent peaks have been diminished in absorbance intensity. These characteristics show that the combination of dysprosium and TBSP leads to more efficient energy transfer in the complex along with the increase in the symmetry of the resulting complex in solution.

The Ce(TBSP) complex spectrum shows maxima at 291, 378, 400, 411, 416, 514, 547, 588, and 647 nm. The absorbance of this spectrum doesn't start at the baseline like the other lanthanide (TBSP) spectra. The broad peak that was at 280 nm is red shifted to 291 nm with a large, broad, soret peak at 411; the peaks at 400 nm and 416 nm are shoulders. The subsequent Q band peaks at 514, 547, 588, and 647 nm are higher in absorbance than the TBSP spectrum. There is also a broadening of the 416 nm peak with an increase in the intensity of the soret band.

The Gd(TBSP) complex spectrum shows maxima at 312, 359, 433, 498, and 713 nm. This spectrum differs from the other spectra due to its large, broad bands at 433, 498, and 713 nm. The broad peak at 359 nm is similar to the other spectra that have broad bands in the 370 nm range. Further studies will be conducted to account for the Gd(TBSP) deviation in UV-Vis spectrum.

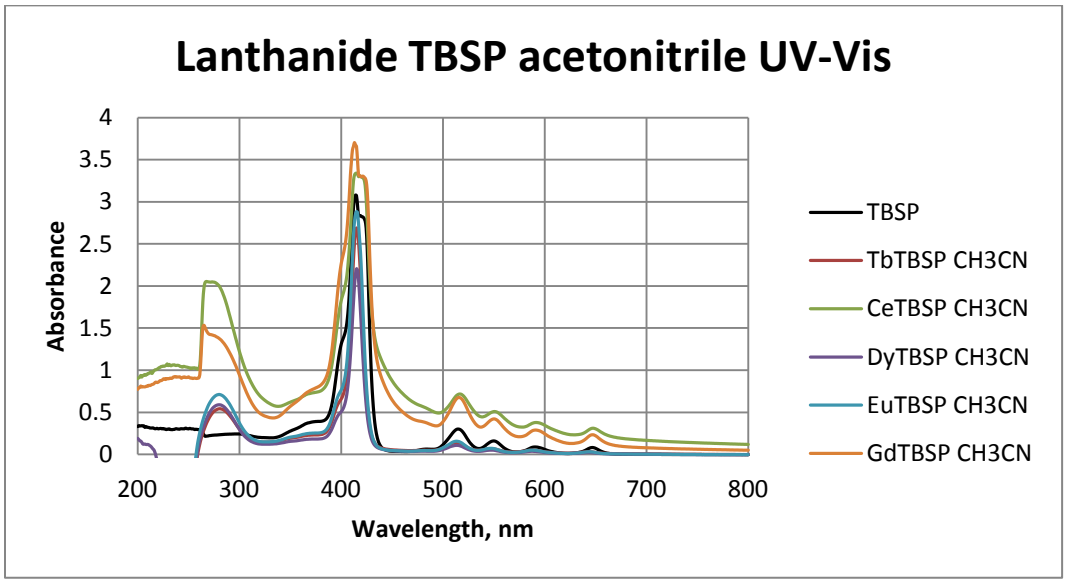

Figure 3.72. UV-Vis spectroscopy of Ln(TBSP)(CH_3CN) complexes.

The UV-Vis spectroscopy of TBSP in figure 3.72., shows maxima at 405, 413, 416, 516, 550, 587, and 650 nm. There is a soret peak at 413 nm with shoulders at 405 nm and 416 nm. There are four characteristic peaks at 516, 550, 587, and 650 nm. The Ce(TBSP) complex shows maxima at 266, 370, 412, 516, 550, 587, and 650 nm. There is a large, broad peak at 266 nm, followed by a shoulder at 370 nm. There is a large peak at 412 nm, followed by the subsequent bands at 516, 550, 587, and 650 nm.

The spectrum of the Gd(TBSP) complex shows maxima at 264, 370, 415, 417, 516, 550, 587, and 650 nm. There is a broad band at 264 nm followed by a shoulder at 370 nm and 417 nm. The large peak is observed at 415 nm, which is then followed by the intense, absorbent, subsequent peaks at 516, 550, 587, and 650 nm.

The Eu(TBSP) complex spectrum shows maxima at 279, 416, 516, 550, 587, and 650 nm. The broad band at 279 nm is much less absorbent than the cerium and gadolinium complexes spectra. There is a soret band at 416 nm with the observed peaks at 516, 550, 587, and 650 nm representing the Q bands. The Dy(TBSP) and Tb(TBSP) complexes spectra show the same profile as that of the Eu(TBSP) with differences being the lower intensity 416 nm peak. The narrowing of the 416 nm peak, decreased absorbance intensity of subsequent peaks and consistent precision between Eu(TBSP), TBSP, Dy(TBSP), and Tb(TBSP) complexes imply that these could be used as sensors for acetonitrile.

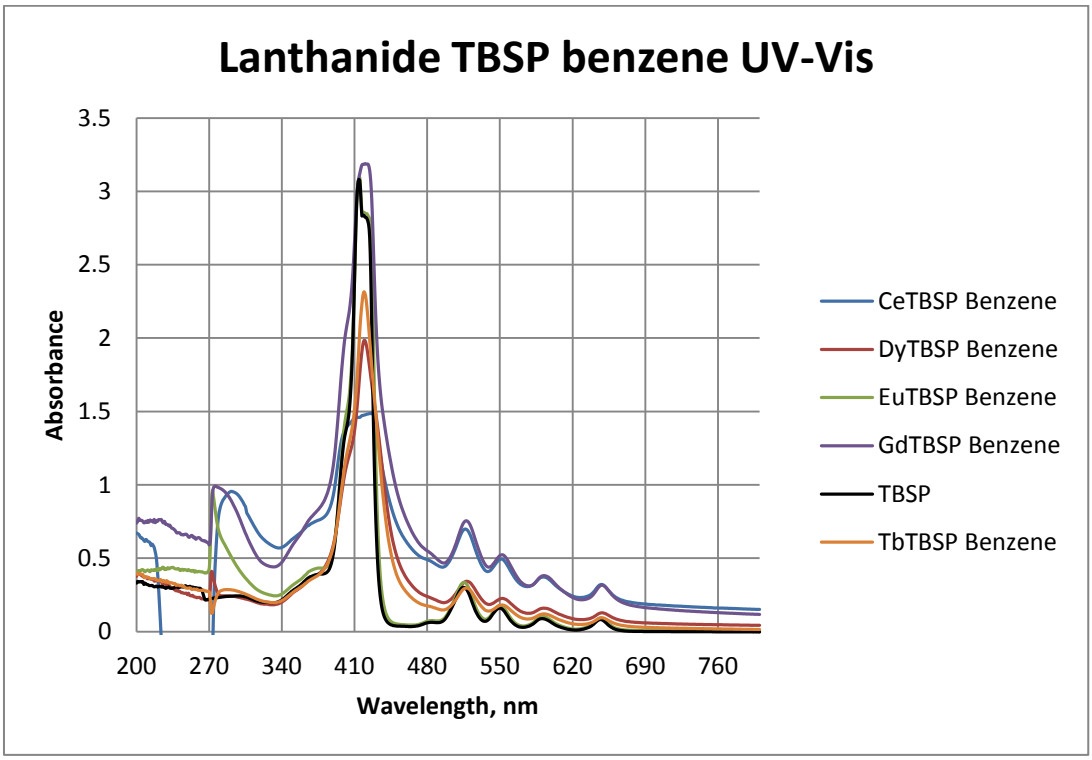

Figure 3.73. UV-Vis spectroscopy of Ln(TBSP)(C_6H_6) complexes.

Figure 3.73 shows the UV-Vis spectra of lanthanide TBSP benzene complexes. The UV-Vis spectroscopy of TBSP shows maxima at 405, 413, 416, 516, 550, 587, and 650 nm. There is a large soret peak at 413 nm with shoulders at 405 nm and 416 nm. There are four characteristic Q band peaks at 516, 550, 587, and 650 nm. The Gd(TBSP) complex shows maxima at 275, 364,

403, 421, 518, 552, 593, and 648 nm. There is a broad band at 275 nm, followed by shoulders at 364 nm and 403 nm. There is a large broad peak at 421 nm observed, followed by Q band peaks at 518, 552, 593, and 648 nm. The 275 nm peak isn't observed in the TBSP UV-Vis spectrum; the subsequent peaks are of higher absorbance intensity. The spectrum of Gd(TBSP) when exposed to benzene re-established its conformity to a similar profile as the TBSP.

The Ce(TBSP) complex shows maxima at 295, 375, 400, 425, 516, 552, 593, and 648 nm. There is broad band at 295 nm, followed by shoulders at 375 nm and 400 nm; a broad major peak is observed at 425 nm along with the subsequent peaks at 516, 552, 593, and 648 nm. The Eu(TBSP) complex shows maxima at 273, 375, 403, 413, 417, 514, 552, 593, and 648 nm. The sharp band at 273 nm is followed by shoulders at 375, 403, and 417 nm. There is a large peak at 413 nm, followed by peaks at 514, 552, 593, and 648 nm.

The Tb(TBSP) complex shows maxima at 405, 420, 515, 553, 593, and 648 nm. The shoulder is observed at 405 nm with a large, single peak soret band at 420 nm and subsequent peaks at 515, 553, 593, and 648 nm. The Dy(TBSP) complex shows maxima at 270, 405, 419, 519, 553, 593, and 648 nm. There is a small peak at 270 nm, followed by a shoulder at 405 nm and a large single peak at 419 nm. The subsequent Q band peaks at 519, 553, 593, and 648 nm are of reduced intensity but are of higher absorbance intensity than the TBSP spectrum subsequent peaks.

This UV-Vis spectra shows how the interaction of the lanthanide, porphyrin, and benzene behave compared to the acetonirile and no volatile organic compound added spectra. The benzene, due to the Hard Acid Soft Base Theory, HSAB, would interact with the porphyrin more than the lanthanide to create a change in the UV-Vis spectra. The acetonitrile which interacts through its nitrogen atom would be classified more as a hard base to interact with the lanthanide.

3.13. UV-Vis Spectroscopy of Metallo (TPP) and (TBSP) Complexes

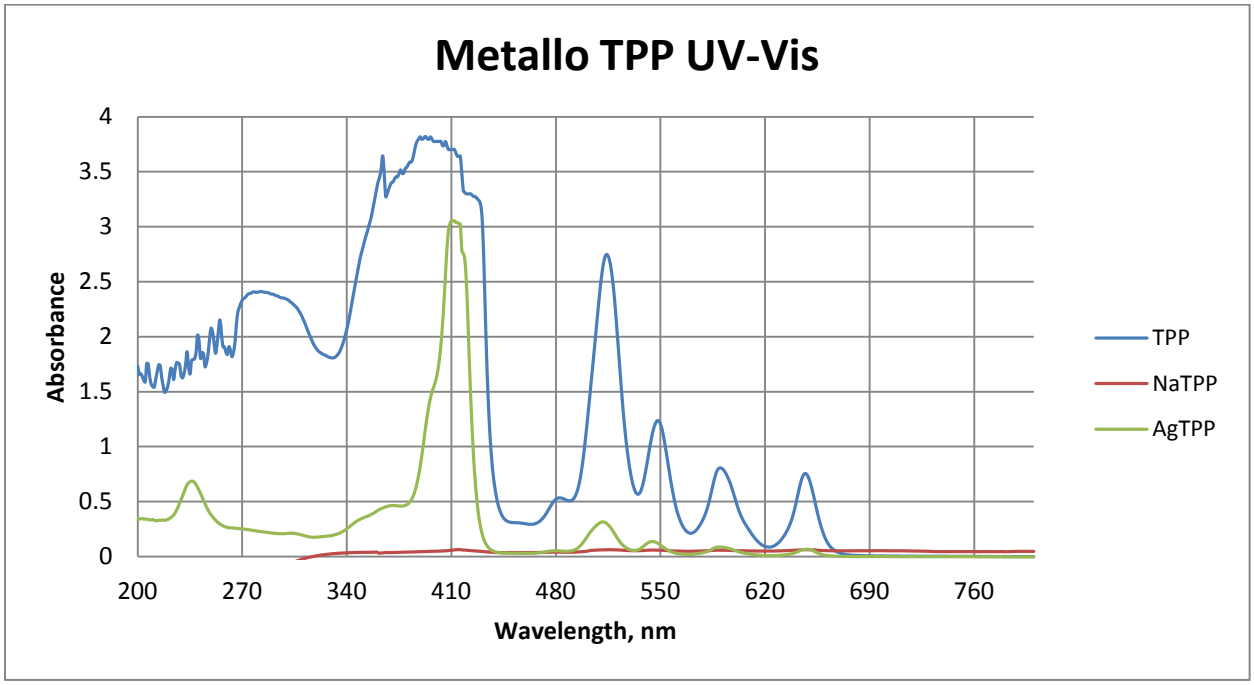

Figure 3.74. UV-Vis spectroscopy of metallo(TPP) complexes.

In Figure 3.74 is shown the UV-Vis spectrum of TPP, Ag(TPP), and Na(TPP) complexes. The TBSP shows maxima at 405, 413, 416, 516, 550, 587, and 650 nm. There is a large peak at 413 nm, the soret band with shoulders at 405 nm and 416 nm. There are four characteristic peaks at 516, 550, 587, and 650 nm.

The Na(TPP) has completely quenched absorbance spectrum, where as the Ag(TPP) spectrum shows maxima at 236, 372, 400, 410, 512, 545, 586, and 646 nm. There is a small broad peak at 236 nm, a small shoulder at 372 nm, a large peak soret band peak at 410 nm and the decreased, absorbent Q bands at 512, 545, 586, and 646 nm.

The Ag(TPP) complex was used due to silver having a smaller radius than the lanthanides, thus it is able to sit inside of the porphyrin core and affect the UV-Vis spectra. The soret band is narrowed and the Q bands are decreased showing the interaction between the metal and the porphyrin. This spectrum is similar to the lanthanide porphyrin UV-Vis spectra.

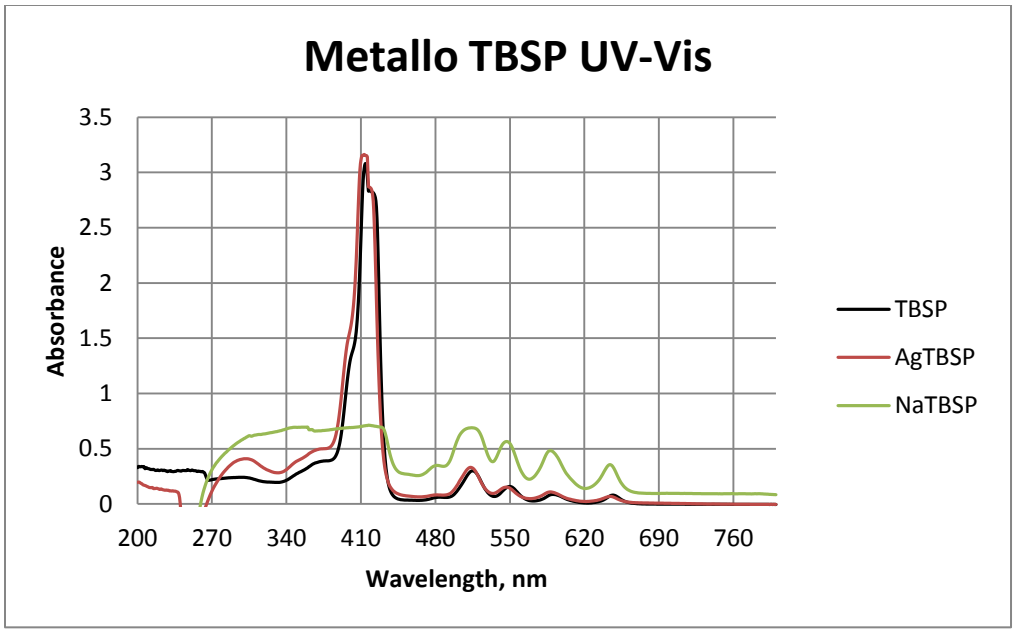

Figure 3.75. UV-Vis spectroscopy of metallo(TBSP) complexes.

Figure 3.75 shows the UV-Vis spectra of the TBSP and metallo(TBSP) complexes maxima. The TBSP shows maxima at 405, 413, 416, 516, 550, 587, and 650 nm. There is a large peak at 413 nm corresponding to the soret band, with shoulders at 405 nm and 416 nm. There are four characteristic Q band peaks at 516, 550, 587, and 650 nm.

The Ag(TBSP) shows almost identical spectrum to the TBSP in the only difference is the appearance of a broad peak at 302 nm, absent broad peak at 230 nm, and increased absorbance at the 405 nm shoulder. It doesn't show the difference in the profile as shown in the Ag(TPP) UV-Vis spectrum.

The Na(TBSP) shows a different profile than the previous two spectra. The Na(TBSP) shows maxima at 310, 357, 418, 512, 547, 586, and 644 nm. There is no large peak in the 416 nm range, corresponding to the soret band, but there is a leveling off of a broad band at 418 nm. The 512 nm peak is broader than the 512 nm peak of TBSP and Ag(TBSP) complexes. The last four peaks at 512, 547, 586, and 644 nm are consistent with TBSP but have a higher absorbance; this could be due to the sodium interaction with the sulfonyl groups as well.

3.14. X-ray Diffraction of (TPP)

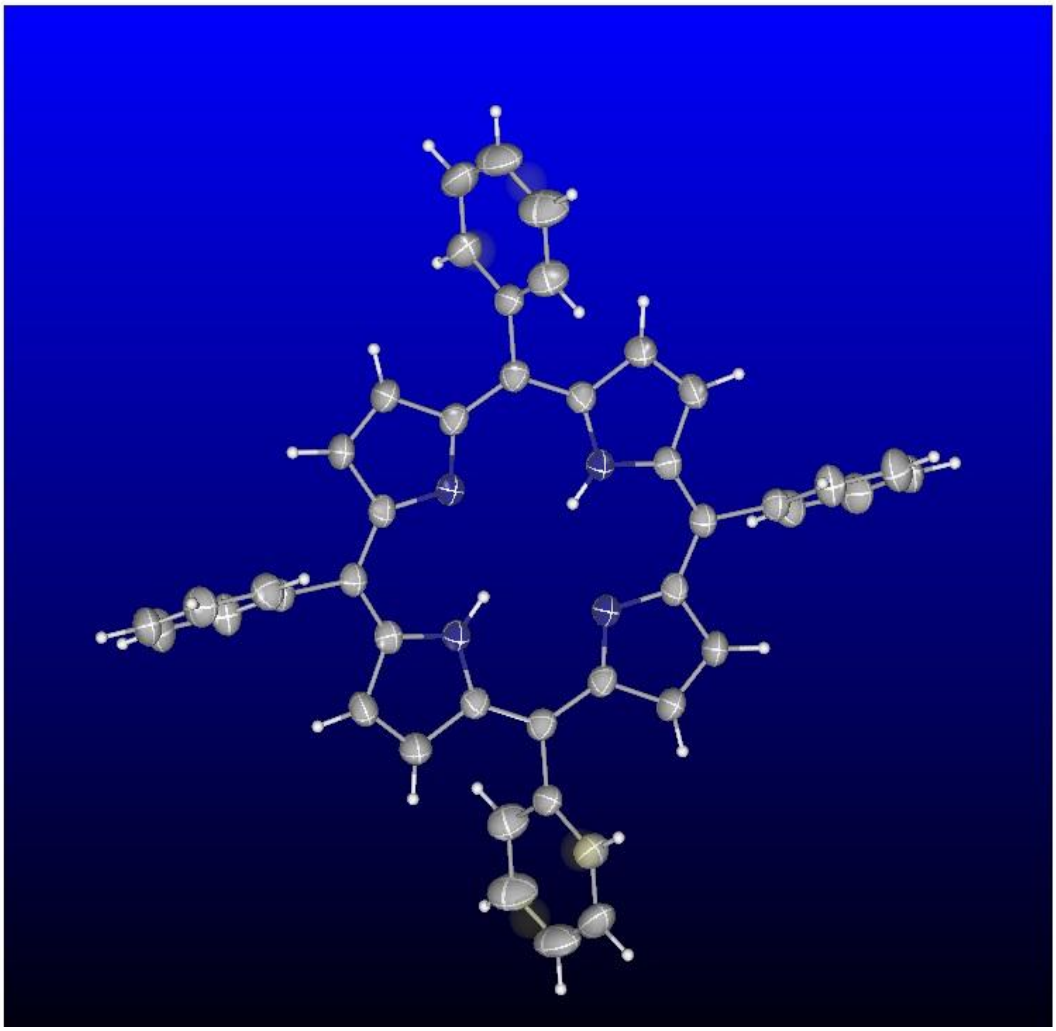

Figure 3.76. X-ray diffraction of TPP.

The x-ray crystallography diffraction result that was collected is shown in figure 3.76. The figure shows with clarity the pyrrole ring system with the blue atoms labeled as nitrogen, grey atoms as carbon, and white atoms as hydrogen. The black shaded areas around the carbon-carbon bonds indicate areas for more refinement to be done. The pyrrole ring system is in one plane with no distortion or puckering due to the resonance stabilization. The figure also shows the phenyl rings in the meso position of the porphyrin ring. The phenyl rings are in perpendicular planes to one another. The phenyl rings in the five and fifteen position are in the same plane; the phenyl

rings in the ten and twenty position are in the same plane and orientation as one another. Two of the pyrrole nitrogens have hydrogens attached and the other two nitrogens are unprotonated. This particular x-ray structure doesn't show the double bonds of the pyrrole rings nor phenyl rings of the system.

Table 2

X-ray Crystallography data of TPP

Chemical formula	$C_{44}H_{32}N_4$
Crystal system	Triclinic
Space group	P-1
Unit cell dimensions	a= 6.434, b= 10.441, c= 12.358 α= 95.881°, β= 99.302°, γ= 101.194°
Z	1
F(000)	324
Reflections collected	14714
Goodness-of-fit	1.037
Final R indices	2171 data; I>2σ(I) R_1= 0.0416, wR_2= 0.1185

Table 2., shows the crystal data that was collected; the TPP crystallized as triclinic and a P-1 space group. The unit cell dimensions such as the length and angles validate the space group and crystal system. The Z parameter signifies that only one monomeric TPP unit that is composed in the unit cell of the crystal. The R_1 value is 4.16% with a wR_2 value of 11.85%. A total of 14,714 reflections collected from this x-ray crystal structure.

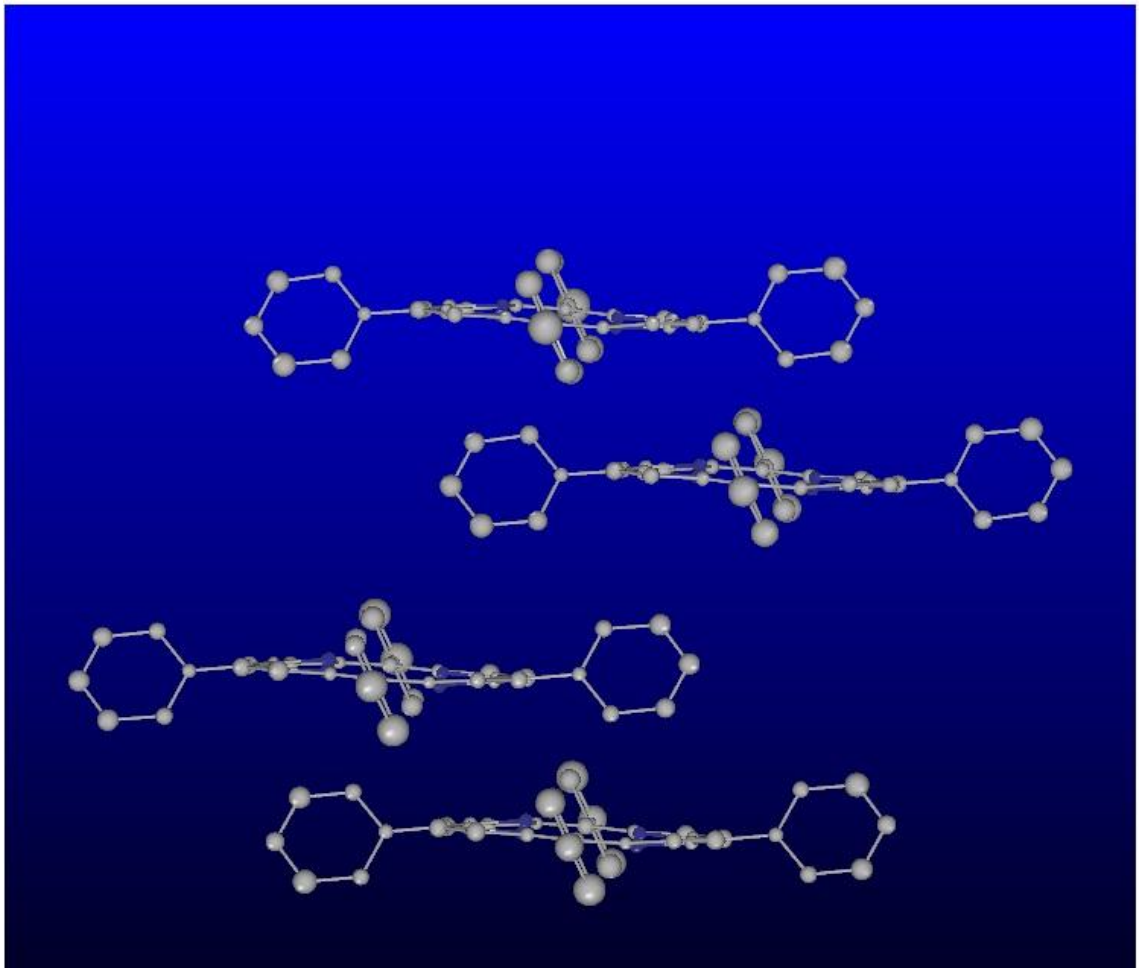

Figure 3.77. X-ray diffraction pattern of side view TPP stacking.

The x-ray diffraction crystallography result that was collected is shown in figure 3.77. The figure shows four TPP molecules in a stacked arrangement with the first and fourth directly above and below one another. The second and third are shifted from alignment to the right and left respectively. In each of the four TPP molecules, the phenyl rings in the five and fifteen position are in the same plane and orientation. The phenyl rings in the ten and twenty position are in the same plane and orientation as one another. The pyrrole ring system is still in one plane and no puckering occurred due to resonance stabilization. This side view of the stacking arrangement shows where possible benzene and acetonitrile compounds can interact with the porphyrin and alter the luminescence properties.

Table 3

X-ray Crystallography data of TPP stacking

Chemical formula	$C_{44}H_{32}N_4$
Crystal system	Triclinic
Space group	P-1
Unit cell dimensions	a= 12.383, b= 12.855, c= 20.898 α= 101.067°, β= 95.740°, γ= 99.315°
Z	4
F(000)	1296
Reflections collected	39380
Goodness-of-fit	1.076
Final R indices	1600 data; I > 2σ(I) R_1= 0.1090, wR_2= 0.4083

Table 3 shows the x-ray crystallography data for the TPP crystal. The compound crystallizes in a triclinic system and the space group is P-1. The unit cell dimensions a, b, c, α, β, and γ are given in the table. The Z value states that there are 4 repeating monomeric units in the unit cell. The R1 value is at 10.90 %. There were 39380 reflections collected for this particular structure.

CHAPTER 4

Conclusion

Lanthanide porphyrin aqueous complexes were successfully synthesized in the formation of sensors for benzene and acetonitrile. The blue shifts in the major emission peak (648 nm), change in the profile of the excitation spectra, the narrowing of the soret band (416 nm) and decrease of the Q bands in the UV-Vis spectra show how benzene and acetonitrile affect lanthanide porphyrin complexes. A decrease and narrowing of the soret band along with a decrease of intensity in Q bands show coordination between metal and porphyrin core. Shifts in the emission spectra show interaction between voc and lanthanide complex. X-ray diffraction data shows the stacking profile of TPP and the possible channels in which acetonitrile and benzene can affect the characterization results. Gaussian studies shown in the Appendix section show the electron densities and energies of the two HOMO and two LUMO states. The Dieke diagram is also referenced in the Appendix section correlating the energy of the porphyrin with those of the lanthanides and substantiating the reasoning for benzene facilitating the energy transfer from an excited state porphyrin to the various lanthanides.

CHAPTER 5

Lanthanide Dual Donor Systems

5.1. PL of $KLa[Pt(CN)_4]_2 \cdot 8.75H_2O$ Complex

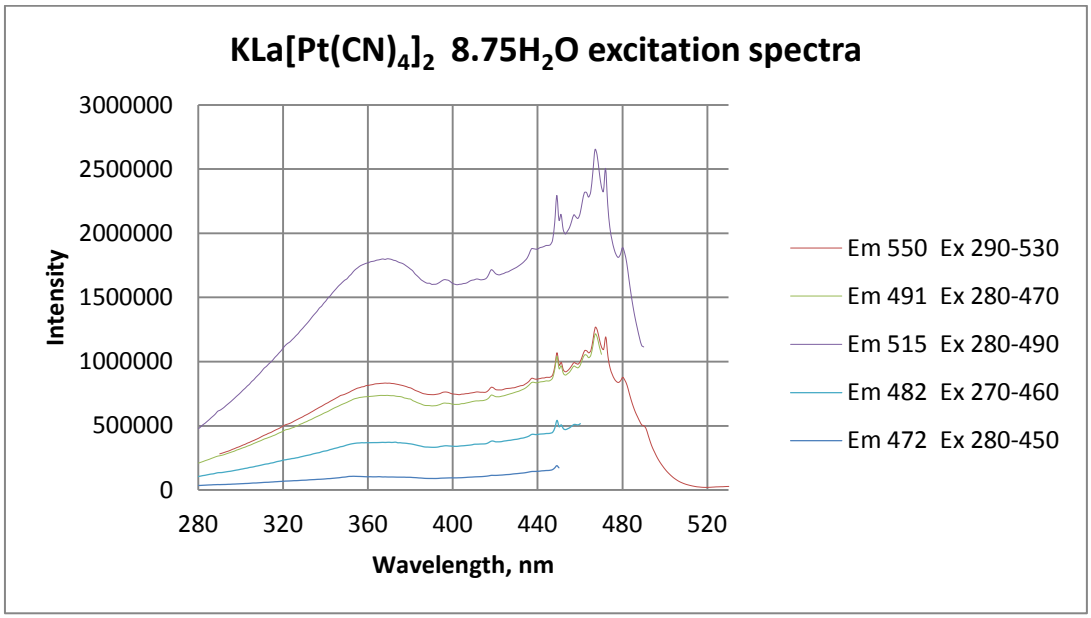

Figure 5.1. PL of $KLa[Pt(CN)_4]_2 \cdot 8H_2O$ complex excitation spectra.

Figure 5.1 shows the excitation spectra of the $KLa[Pt(CN)_4]_2 \cdot 8H_2O$ complex. The broad band maximum at 367 nm corresponds to the tetracyanoplatinate excitation peak. The sharper peaks are of the Lanthanum moiety; these peaks appearing at 450, 469, and 480 nm. The five spectra are similar in character and peak position with the only difference being the intensity which was dependent on the monitoring wavelength.

The most intense excitation peak was monitored at 515 nm which was the maxima of the emission spectrum corresponding to the tetracyanoplatinate species. The two next most intense excitation spectra were monitored at 550 nm and 491 nm. The two lowest intensity excitation spectra were monitored at 482 nm and 472 nm. Each of the excitation spectra were monitored at different wavelengths of the same single broad emission peak spectrum. This was done to see if there was a major change in the excitation profile based on the monitoring wavelength.

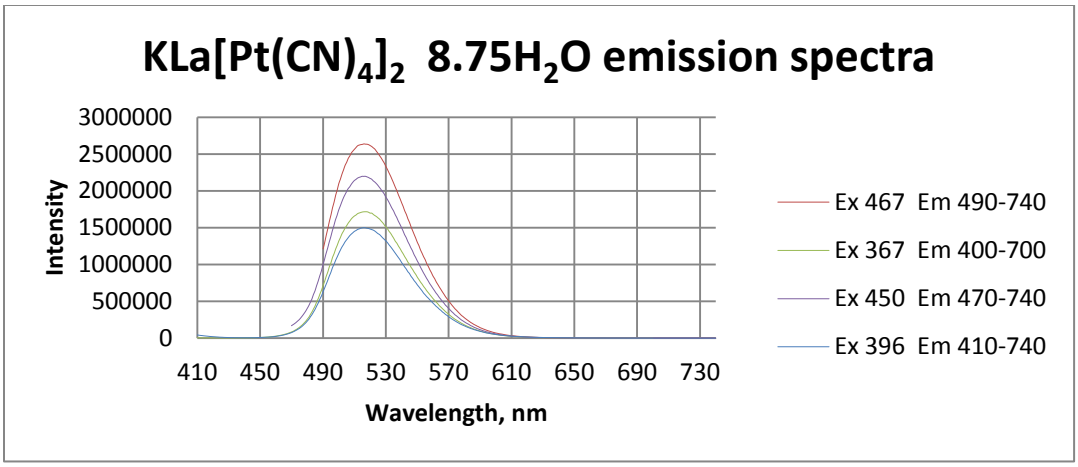

Figure 5.2. PL of $KLa[Pt(CN)_4]_2 \cdot 8H_2O$ complex emission spectra.

Figure 5.2., is the emission spectrum of the $KLa[Pt(CN)_4]_2 \cdot 8H_2O$ complex. The spectra show a broad peak with a maximum at 515 nm. The intensity of the peak maxima is affected by the exciting wavelength, with the most intense being excited at 467 nm. When excited at 450, 367, and 396 nm, the intensity of the emission peak maximum decreases. The broad peak at 515 nm corresponds to the tetracyanoplatinate.

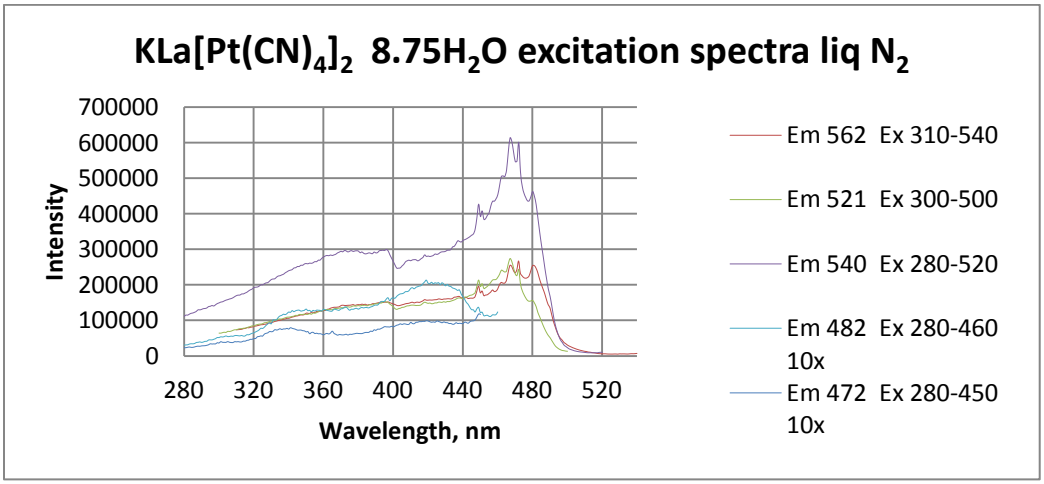

Figure 5.3. PL of $KLa[Pt(CN)_4]_2 \cdot 8H_2O$ complex excitation spectra liquid nitrogen temperature.

The excitation spectra of the $KLa[Pt(CN)_4]_2 \cdot 8H_2O$ complex at liquid nitrogen temperature is shown in figure 5.3. The spectra show that same profiles as those of the room temperature spectra with minor variations such as the increase in intensity of the spectra monitored at 482 nm;

its intensity is comparable to the spectra monitored at 562 and 521 nm. The spectrum monitored at 482 nm has developed an enhanced band at 419 nm when exposed to liquid nitrogen temperatures. The spectrum monitored at 562 nm shows an enhanced peak at 480 nm at liquid nitrogen temperature compared to room temperature.

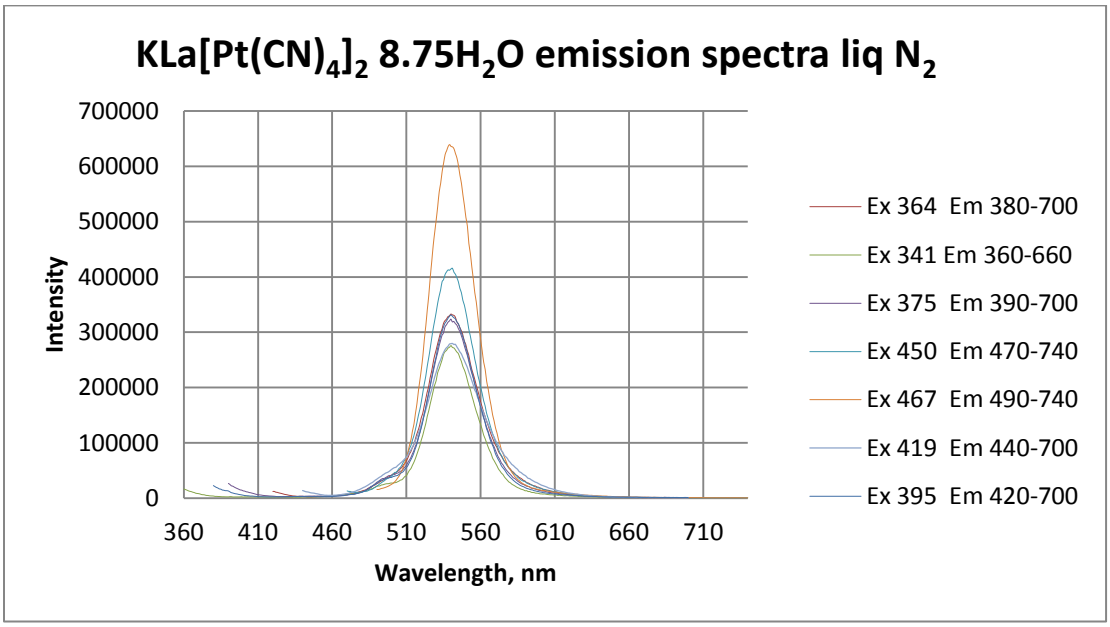

Figure 5.4. PL of $KLa[Pt(CN)_4]_2 \bullet 8H_2O$ complex emission spectra liquid nitrogen temperature.

The emission profile of $KLa[Pt(CN)_4]_2 \bullet 8H_2O$ complex at liquid nitrogen temperature is shown in figure 5.4. All of the spectra show a maximum at 540 nm. The most intense spectrum was produced when excited at 467 nm. The intensity decreases as excited at 450, 364, 395, 375, 419, and 341 nm.

The spectra show a 25 nm red shift in the maximum position from 515 nm to 540 nm. This red shift is a common phenomenon that happens with tetracyanoplatinate complexes. This shift was induced by the liquid nitrogen temperature creating a smaller stacking distance of the tetracyanoplatinate arrangement. This smaller arrangement causes a red shift in the emission maximum compared to at room temperature, where the stacking profile of the tetracyanoplatinate is farther apart from one another.

5.2. PL of $K_2[Dy(H_2O)_4(Pt(CN)_4)_2](Au(CN)_2)\cdot 2H_2O$ Complex

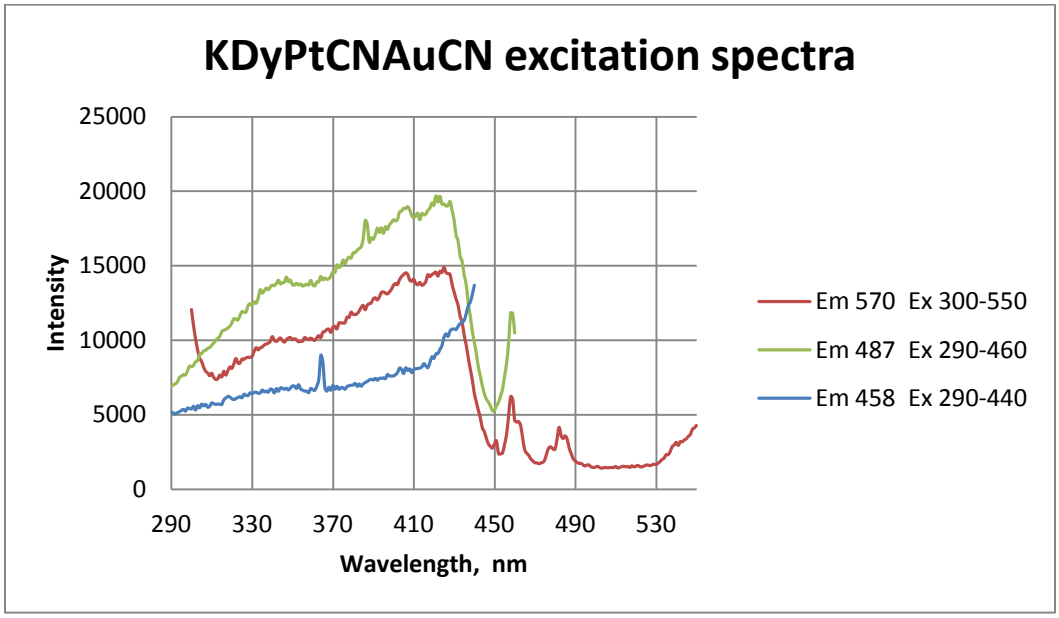

Figure 5.5. PL of $K_2[Dy(H_2O)_4(Pt(CN)_4)_2](Au(CN)_2)\cdot 2H_2O$ excitation spectra.

Figure 5.5 shows the $K_2[Dy(H_2O)_4(Pt(CN)_4)_2](Au(CN)_2)\cdot 2H_2O$ complex excitation spectra. The most intense spectrum was monitored at 487 nm, where the second most intense spectrum was monitored at 570 nm wavelength. The characteristics and profile of the two spectra are similar with differences being the intensity and extension of the spectrum monitored at 570 nm.

The excitation spectrum shows characteristic broad band at 350 nm corresponding to tetracyanoplatinate peak, a broad band at 420 nm corresponding to the gold dicyanide, and smaller, sharper peaks at 459 nm and 482 nm corresponding to the dysprosium excitation peaks from the $^6H_{15/2} \rightarrow {}^4I_{15/2}$ and $^6H_{15/2} \rightarrow {}^4F_{9/2}$ transitions. The tetracyanoplatinate and gold cyanide bands are more intense than the lanthanide excitation transitions. The more intense and overlap of donor ligands give rise to a better opportunity for ligand to metal energy transfer to take place. These ligands overlap the $^6H_{15/2} \rightarrow {}^4M_{15/2} + {}^6P_{7/2}$ (351 nm) and $^6H_{15/2} \rightarrow {}^4G_{11/2}$ (428 nm) transitions of dysprosium.

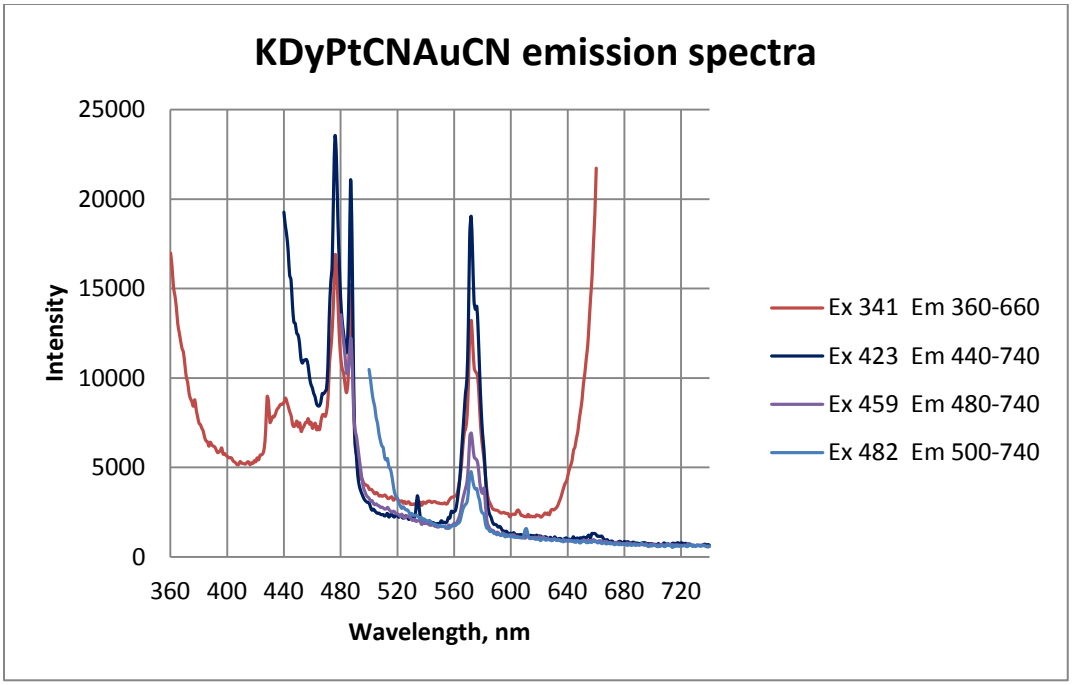

Figure 5.6. PL of the $K_2[Dy(H_2O)_4(Pt(CN)_4)_2](Au(CN)_2)\bullet 2H_2O$ complex emission spectra.

The room temperature emission spectra of the $K_2[Dy(H_2O)_4(Pt(CN)_4)_2](Au(CN)_2)\bullet 2H_2O$ complex is shown in figure 5.6. The spectra show sharp peaks at 476, 487, and 572 nm. These sharp peaks correspond to the dysprosium emission peaks from the $^4F_{9/2} \rightarrow {}^6H_{15/2}$ and $^4F_{9/2} \rightarrow {}^6H_{13/2}$, transitions respectively. The 476 nm peak is more intense than the 487 nm maximum, and both are more intense than the 572 nm transition.

The 572 nm shows an intense single peak at room temperature. The 572 nm transition shows increased intensity dependent on the excitation wavelength; this is due to the intensity of the exciting source wavelength and the profile of this peak doesn't change with increasing intensity. There is a small broad band at 440 nm corresponding to the gold dicyanide moiety in the complex. The intensity decreases when excited at 423, 341, 459, and 482 nm. When the spectrum is excited at 341 nm there is a large upward increase; this is due to the instrumental constraints of the fluorimeter approaching a limit based on the excitation wavelength and ending wavelength on the spectrum x-axis.

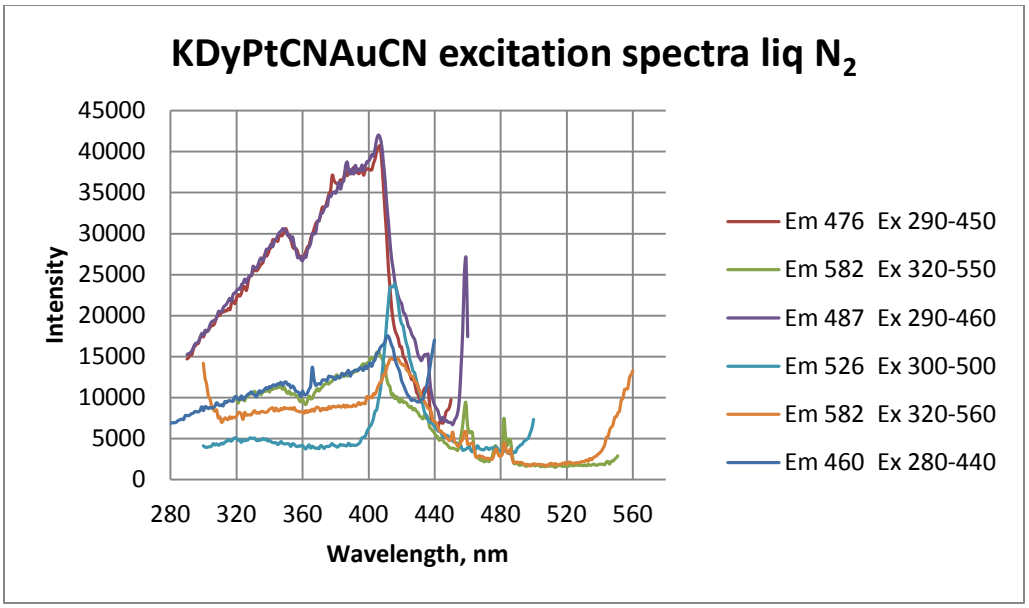

Figure 5.7. PL of the $K_2[Dy(H_2O)_4(Pt(CN)_4)_2](Au(CN)_2)\bullet 2H_2O$ complex excitation spectra at liquid nitrogen temperature.

In figure 5.7., it shows the $K_2[Dy(H_2O)_4(Pt(CN)_4)_2](Au(CN)_2)\bullet 2H_2O$ complex excitation spectra at liquid nitrogen temperatures. The profile shows similar spectra that have maxima at 350, 416, 420, 458, and 482 nm. The 350 nm broad band corresponds to the tetracyanoplatinate, the 416 nm and 420 nm bands correspond to the gold dicyanide. The intensity of the tetracyanoplatinate and gold dicyanide bands increased in the liquid nitrogen temperature profile, where as the intensity of the dysprosium bands stayed relatively constant as in the room temperature profile.

The excitation spectra at liquid nitrogen temperature show two different profiles. One profile shows dominant broad peaks at 350 nm and 416 nm, where as the other profile shows absent luminescence in that region and a broad peak maximizing at 420 nm followed by the dysprosium transitions at 458 nm and 482 nm. This is evident of temperature still affecting the tetracyanoplatinate and bridging ligands by enhancing and creating excitation spectra with two different profiles, while keeping the dysprosium transitions relatively constant.

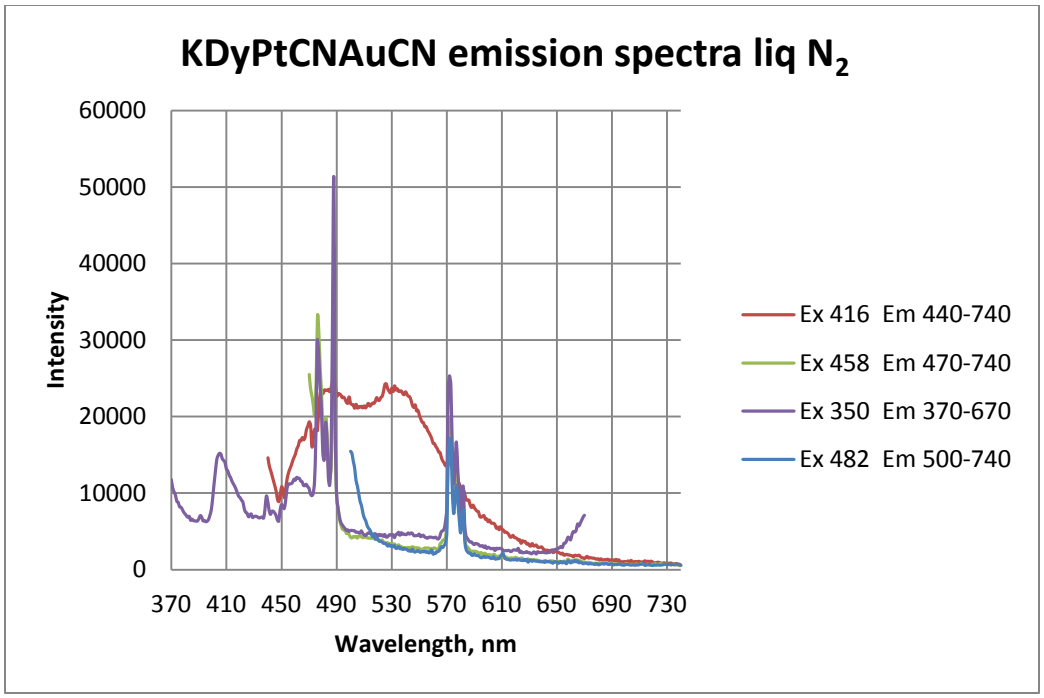

Figure 5.8. PL of the $K_2[Dy(H_2O)_4(Pt(CN)_4)_2](Au(CN)_2)\bullet 2H_2O$ complex emission spectra at liquid nitrogen temperature.

Figure 5.8., shows the photoluminescence emission spectra of the $K_2[Dy(H_2O)_4(Pt(CN)_4)_2](Au(CN)_2)\bullet 2H_2O$ complex at liquid nitrogen temperatures. The emission spectra shows two different profiles; one profile with the sharp peaks attributed to the dysprosium emission transitions, the other profile shows that of the tetracyanoplatinate at 540 nm and gold cyanide ligand at 460 nm and 480 nm with quenched dysprosium emission. This shows that at liquid nitrogen temperature there is some energy transfer as well as a complete quenching of lanthanide emission based on excitation wavelength.

The profile which shows the dysprosium transitions shows a change in the peaks of the $^4F_{9/2} \rightarrow {}^6H_{15/2}$ and the $^4F_{9/2} \rightarrow {}^6H_{13/2}$ transitions. In the room temperature spectrum the 572 nm transition was a single peak but at liquid nitrogen temperatures the single peak is split into a triplet. In the room temperature spectrum the 487 nm peak was a doublet with the first peak more intense than the latter; now at liquid nitrogen temperature the latter peak is more intense than the

first peak of the 487 nm transition. This is significant, due to a change in temperature the same complex can go from all dysprosium lanthanide emission to a combination emission of both lanthanide and ligand emission. This change in major emission peaks observed is also based on the excitation wavelength. The tetracyanoplatinate ligand still shows the 25 nm red shift along with enhanced gold dicyanide emission.

References

A.S., Kovacs. A; Konings. R.J.M.; Booij. (1995). *Vib. Spectrosc, 10*, 65.

Baker, E., E.W. and Palmer, S.E. (1978). Geochemistry of Porphyrins. *The Porphyrins, 1*, 545.

Basova, T., Gürek, A. G., Ahsen, V., & Ray, A. K. (2007). Electrical properties of dysprosium phthalocyanine films. *Organic Electronics, 8*(6), 784-790. doi: http://dx.doi.org/10.1016/j.orgel.2007.06.008

Bequerel, J. (1907). *Le Radium, 4*, 329.

Bequerel, J. (1908). *Physik. Z., 8*, 632.

Bessiere, Aurelie, Lecointre, Aurelie, Benhamou, Rajia Ait, Suard, Emmanuelle, Wallez, Gilles, & Viana, Bruno. (2013). How to induce red persistent luminescence in biocompatible Ca3(PO4)2. *Journal of Materials Chemistry C, 1*(6), 1252-1259.

Binnemans, K. (2009). Lanthanide-based luminescent hybrid materials. *Chem Rev, 109*(9), 4283-4374. doi: 10.1021/cr8003983

Bunzli, J.C.; Kuzmina, N.; Gunnlaugsson, T.; Stomeo, F. . (2008). *J. Phys. Chem, 112*(16), 3614-3626.

Bunzli, Jean-Claude G., & Piguet, Claude. (2005). Taking advantage of luminescent lanthanide ions. *Chemical Society Reviews, 34*(12), 1048-1077.

Burrows, Nathan D., Hale, Christopher R. H., & Penn, R. Lee. (2012). Effect of Ionic Strength on the Kinetics of Crystal Growth by Oriented Aggregation. *Crystal Growth & Design, 12*(10), 4787-4797. doi: 10.1021/cg3004849

Cario, G; Franck, J. (1922). *Physik 11*, 161.

Carletti, R., & Romano, D. (2002). Assessing health risk from benzene pollution in an urban area. *Environ Monit Assess, 80*(2), 135-148.

Case Studies in Environmental Medicine: Benzene Toxicity. (2000) (pp. 1-32). Atlanta, GA 30333: U.S. Department of Health and Human Services.

Chen, K. M., El-Bayoumy, K., Cunningham, J., Aliaga, C., Li, H., & Melikian, A. A. (2004). Detection of nitrated benzene metabolites in bone marrow of B6C3F1 mice treated with benzene. *Chem Res Toxicol, 17*(3), 370-377. doi: 10.1021/tx030039s

Cotton, Simon. (2006). *Lanthanide and actinide chemistry* (Vol. 17): Wiley.

De Saja, J. A., & Rodríguez-Méndez, M. L. (2005). Sensors based on double-decker rare earth phthalocyanines. *Advances in Colloid and Interface Science, 116*(1–3), 1-11. doi: http://dx.doi.org/10.1016/j.cis.2005.03.004

Dolg, M. (1998). The Encyclopedia of Computational Chemistry (pp. 1478).

Duque, Juan G., Pasquali, Matteo, Cognet, Laurent, & Lounis, Brahim. (2009). Environmental and Synthesis-Dependent Luminescence Properties of Individual Single-Walled Carbon Nanotubes. *ACS Nano, 3*(8), 2153-2156. doi: 10.1021/nn9003956

Girard, James. (1994). *Chemistry: An Environmental Perspective* (P. Buell Ed.). Englewood Cliffs, New Jersey 07632: Prentice Hall.

Goldberg Marvin, C., & Weiner Eugene, R. (1989). The Science of Luminescence *Luminescence Applications* (Vol. 383, pp. 1-22): American Chemical Society.

Greenberg, Mark. (1999). *Toxicological Review of Acetonitrile* (pp. 35).

Grimvall, Göran. (1981). *The electron-phonon interaction in metals* (Vol. 16): North-Holland Amsterdam.

Harris, Daniel C. (2007). Quantitative Chemical Analysis. In J. Fiorillo (Ed.), (7th ed., pp. 663). New York, New York 10010: Craig Bleyer.

Harvey, Edmund Newton. (1957). *A history of luminescence from the earliest times until 1900* (Vol. 44): American Philosophical Society.

He, Shuzhong, Li, Hongguang, Yip, Yuk-Wang, Yeung, Chi-Tung, Fung, Yuen On, Kong, Hoi-Kuan, Wong, Wing-Tak. (2011). Responsive Two-Photon Induced Europium Emission as Fluorescent Indicator for Paralytic Shellfish Saxitoxin. *Organic Letters, 13*(19), 5036-5039. doi: 10.1021/ol2018246

Hebbink, Gerald. (2002). *Luminescent Materials based on Lanthanide Ions.* (Ph.D. Ph.D. Thesis), University of Twente, Enschede, Netherlands.

Jackson, Derek A., & Dicks, Andrew P. (2012). The Five Senses of Christmas Chemistry. *Journal of Chemical Education, 89*(10), 1267-1273. doi: 10.1021/ed300231z

Jones, E., Fox, V., Elliott, B. M., & Moore, N. P. (2001). The mutagenic potential of acetonitrile in the bone marrow and peripheral blood of the mouse. *Mutagenesis, 16*(2), 151-154.

Kalf, G. F. (1987). Recent advances in the metabolism and toxicity of benzene. *Crit Rev Toxicol, 18*(2), 141-159. doi: 10.3109/10408448709089859

Kamruzzaman, M., Alam, A. M., Lee, S. H., Kim, Y. H., & Kim, S. H. (2012). A terbium-sensitized spectrofluorimetric method for determination of catecholamines in a serum sample with micelle medium. *Luminescence, 27*(1), 84-90. doi: 10.1002/bio.1332

Kirubaharan, C. Joseph, Kalpana, D., Lee, Yang Soo, Kim, A. R., Yoo, Don Jin, Nahm, Kee Suk, & Kumar, G. Gnana. (2012). Biomediated Silver Nanoparticles for the Highly Selective Copper(II) Ion Sensor Applications. *Industrial & Engineering Chemistry Research, 51*(21), 7441-7446. doi: 10.1021/ie3003232

Kong, H., & Jang, J. (2008). Synthesis and antimicrobial properties of novel silver/polyrhodanine nanofibers. *Biomacromolecules, 9*(10), 2677-2681. doi: 10.1021/bm800574x

Kujawinski, Elizabeth B., Kido Soule, Melissa C., Valentine, David L., Boysen, Angela K., Longnecker, Krista, & Redmond, Molly C. (2011). Fate of Dispersants Associated with the Deepwater Horizon Oil Spill. *Environmental Science & Technology, 45*(4), 1298-1306. doi: 10.1021/es103838p

Lanza, G., Varga, Z., Kolonits, M., & Hargittai, M. (2008). On the effect of 4f electrons on the structural characteristics of lanthanide trihalides: computational and electron diffraction study of dysprosium trichloride. *J Chem Phys, 128*(7), 074301. doi: 10.1063/1.2828537

Lente, G.; Espenson, J.H. (2004). *International Journal of Chemical Kinetics*(36), 449.

Lim, J., Turkbey, B., Bernardo, M., Bryant, L. H., Jr., Garzoni, M., Pavan, G. M., . . . Kobayashi, H. (2012). Gadolinium MRI contrast agents based on triazine dendrimers: relaxivity and in vivo pharmacokinetics. *Bioconjug Chem, 23*(11), 2291-2299. doi: 10.1021/bc300461r

Lin, Z. J., Yang, Z., Liu, T. F., Huang, Y. B., & Cao, R. (2012). Microwave-assisted synthesis of a series of lanthanide metal-organic frameworks and gas sorption properties. *Inorg Chem, 51*(3), 1813-1820. doi: 10.1021/ic202082w

Liu, Yu, Pan, Mei, Yang, Qing-Yuan, Fu, Lei, Li, Kang, Wei, Shi-Chao, & Su, Cheng-Yong. (2012). Dual-Emission from a Single-Phase Eu–Ag Metal–Organic Framework: An Alternative Way to Get White-Light Phosphor. *Chemistry of Materials, 24*(10), 1954-1960. doi: 10.1021/cm3008254

Luo, J., Li, X., Hou, Q., Cao, Y. (2007). High-Efficiency White Light Emission from a Single Copolymer: Fluorescent Blue, Green, and Red Chromophores on a Conjugated Polymer Backbone., *19*(8), 1113-1117. doi: 10.1002/adma.200601241

Maduraiveeran, G., & Ramaraj, R. (2009). Potential sensing platform of silver nanoparticles embedded in functionalized silicate shell for nitroaromatic compounds. *Anal Chem, 81*(18), 7552-7560. doi: 10.1021/ac900781d

Maldiney, Thomas, Lecointre, Aurélie, Viana, Bruno, Bessière, Aurélie, Bessodes, Michel, Gourier, Didier, Scherman, Daniel. (2011). Controlling Electron Trap Depth To Enhance Optical Properties of Persistent Luminescence Nanoparticles for In Vivo Imaging. *Journal of the American Chemical Society, 133*(30), 11810-11815. doi: 10.1021/ja204504w

Maynard, B. A., Smith, P. A., Ladner, L., Jaleel, A., Beedoe, N., Crawford, C., . . . Sykora, R. E. (2009). Emission enhancement through dual donor sensitization: modulation of structural and spectroscopic properties in a series of europium tetracyanoplatinates. *Inorg Chem, 48*(14), 6425-6435. doi: 10.1021/ic900149v

Muniyappan, R. (1955). Porphyrins in petroleum. *Journal of Chemical Education, 32*(5), 277. doi: 10.1021/ed032p277

Nyalala, S. O., Petersen, M. A., & Grout, B. W. W. (2011). Acetonitrile (methyl cyanide) emitted by the African spider plant (Gynandropsis gynandra L. (Briq)): Bioactivity against spider mite (Tetranychus urticae Koch) on roses. *Scientia Horticulturae, 128*(3), 352-356. doi: http://dx.doi.org/10.1016/j.scienta.2011.01.036

Ornatska, Maryna, Sharpe, Erica, Andreescu, Daniel, & Andreescu, Silvana. (2011). Paper Bioassay Based on Ceria Nanoparticles as Colorimetric Probes. *Analytical Chemistry, 83*(11), 4273-4280. doi: 10.1021/ac200697y

Ozawa, T., Santos, R. A., Lamborn, K. R., Bauer, W. F., Koo, M. S., Kahl, S. B., & Deen, D. F. (2004). In vivo evaluation of the boronated porphyrin TABP-1 in U-87 MG intracerebral human glioblastoma xenografts. *Mol Pharm, 1*(5), 368-374.

Que, Emily L., & Chang, Christopher J. (2006). A Smart Magnetic Resonance Contrast Agent for Selective Copper Sensing. *Journal of the American Chemical Society, 128*(50), 15942-15943. doi: 10.1021/ja065264l

Risovany, V. D., Zakharov, A. V., Muraleva, E. M., Kosenkov, V. M., & Latypov, R. N. (2006). Dysprosium hafnate as absorbing material for control rods. *Journal of Nuclear Materials, 355*(1–3), 163-170. doi: http://dx.doi.org/10.1016/j.jnucmat.2006.05.029

Rosenkranz, H.S.; McCoy, E.C.; Sanders, D.R. (1980). *Science, 209*, 1039-1043.

RusCic, B., Goodman, G. L., & Berkowitz, J. (1983). Photoelectron spectra of the lanthanide trihalides and their interpretation@f[sup a]@f[sup)]. *The Journal of Chemical Physics, 78*(9), 5443-5467.

Santos, Júlio G., Dutra, José Diogo L., Junior, Severino A., Freire, Ricardo O., & da Costa Junior, Nivan B. (2012). Theoretical Spectroscopic Study of Europium Tris(bipyridine) Cryptates. *The Journal of Physical Chemistry A, 116*(17), 4318-4322. doi: 10.1021/jp300707v

Santos, Tracy Dos, Morandeira, Ana, Koops, Sara, Mozer, Attila J., Tsekouras, George, Dong, Ying, . . . Durrant, James R. (2010). Injection Limitations in a Series of Porphyrin Dye-Sensitized Solar Cells. *The Journal of Physical Chemistry C, 114*(7), 3276-3279. doi: 10.1021/jp908401k

Singh, M. P., Mishra, M., Sharma, A., Shukla, A. K., Mudiam, M. K., Patel, D. K., . . . Chowdhuri, D. K. (2011). Genotoxicity and apoptosis in Drosophila melanogaster exposed to benzene, toluene and xylene: attenuation by quercetin and curcumin. *Toxicol Appl Pharmacol, 253*(1), 14-30. doi: 10.1016/j.taap.2011.03.006

Sreeremya, Thadathil S., Thulasi, Kunnambeth M., Krishnan, Asha, & Ghosh, Swapankumar. (2011). A Novel Aqueous Route To Fabricate Ultrasmall Monodisperse Lipophilic

Cerium Oxide Nanoparticles. *Industrial & Engineering Chemistry Research, 51*(1), 318-326. doi: 10.1021/ie2019646

Szabadvary, Ferenc. (1998). *Handbook of the Chemistry and Physics of the Rare Earths* (Vol. 11): Elsevier Science Publishers.

Tokmakoff, Andrei. (2011). Time-dependent Quantum Mechanics and Spectroscopy. from www.mit.edu/~tokmakof/TDQMS/Notes/12.%20Applications.pdf

Vij, D.R. (1998). *Luminescence of Solids*: Plenum Press.

Voet, D., Pratt, C.W., & Voet, J.G. (2008). *Fundamentals of Biochemistry, Binder Ready Version: Life at the Molecular Level*: John Wiley & Sons.

Wang, C., Dai, Y., Feng, G., He, R., Yang, W., Li, D., . . . Tan, L. (2011). Addition of porphyrins to cigarette filters to reduce the levels of benzo[a]pyrene (B[a]P) and tobacco-specific N-nitrosamines (TSNAs) in mainstream cigarette smoke. *J Agric Food Chem*, *59*(13), 7172-7177. doi: 10.1021/jf200966p

Wiedemann, E. . (1888). *Ann. der. Physik, 34*, 446-449.

Wohrle, D.; Pomogailo, A.D. (2008). Metal complexes and Metals in Macromolecules. *Mater. Chem*(18), 23-40.

Wu, F. G., Wang, N. N., Tao, L. F., & Yu, Z. W. (2010). Acetonitrile induces nonsynchronous interdigitation and dehydration of dipalmitoylphosphatidylcholine bilayers. *J Phys Chem B, 114*(39), 12685-12691. doi: 10.1021/jp104190z

Wulfsberg, G. (2000). *Inorganic Chemistry*: Univ Science Books.

Xie, M. H., Yang, X. L., Zou, C., & Wu, C. D. (2011). A Sn(IV)-porphyrin-based metal-organic framework for the selective photo-oxygenation of phenol and sulfides. *Inorg Chem*, *50*(12), 5318-5320. doi: 10.1021/ic200295h

Ye, Zhiqiang, Wang, Guilan, Chen, Jinxue, Fu, Xiaoyan, Zhang, Wenzhu, & Yuan, Jingli. (2010). Development of a novel terbium chelate-based luminescent chemosensor for time-resolved luminescence detection of intracellular Zn2+ ions. *Biosensors and Bioelectronics, 26*(3), 1043-1048. doi: http://dx.doi.org/10.1016/j.bios.2010.08.056

Zhang, D.L.; Tao, Y.; Gao, J.T.; Zhang, C.N.; Rohdewald, P.; Ahao, B.L. (2002). Pycnogenol in cigarette filters scavenges free radicals and reduces mutagenicity and toxicity of tobacco smoke in vivo. *Toxicology, Industry Health, 18*, 215-224.

Appendix

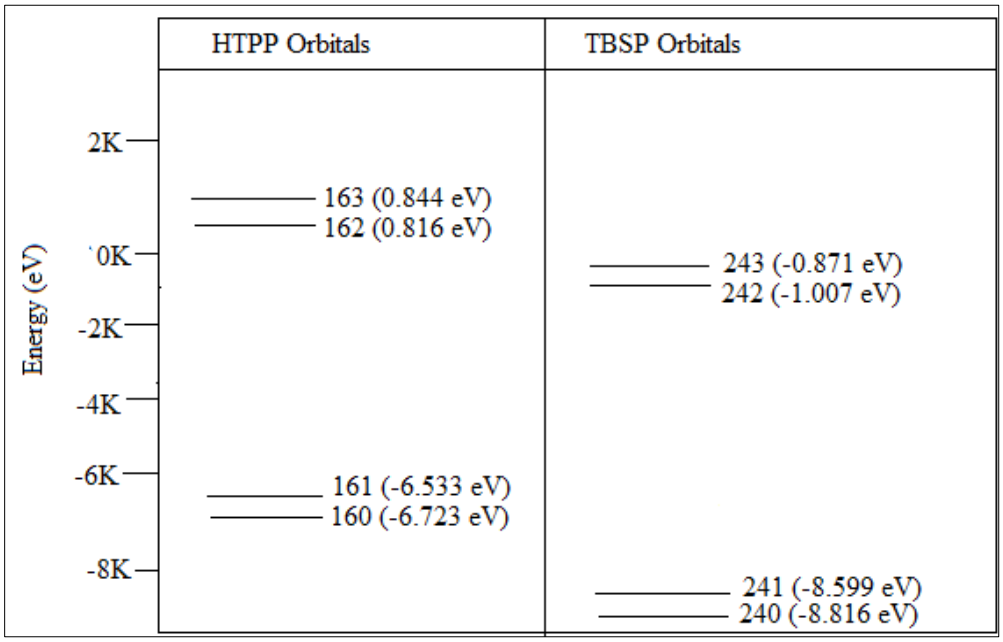

Figure Porphyrin Gaussian energy calculations.

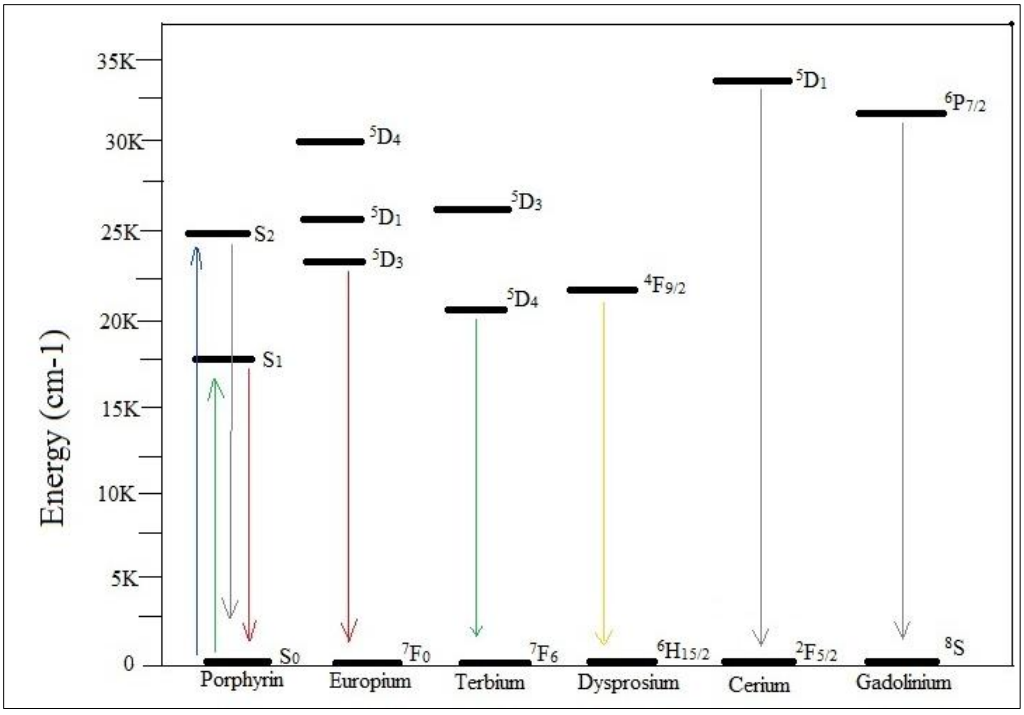

Figure Porphyrin and lanthanide energy diagram, Gaussian and Dieke calculations.

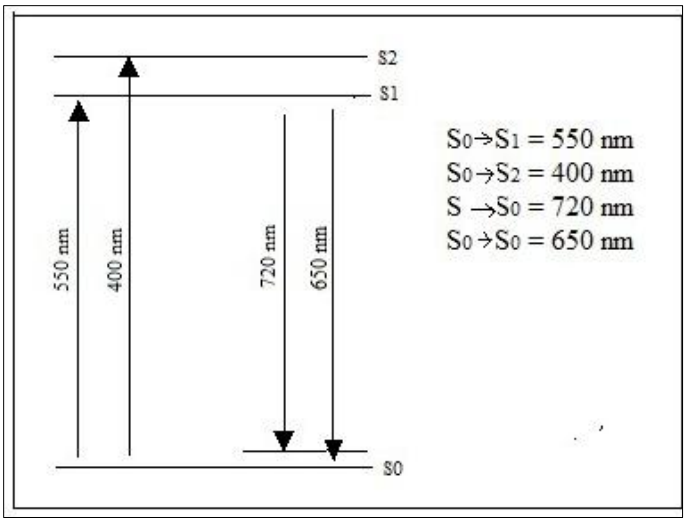

Figure Porphyrin energy transitions.

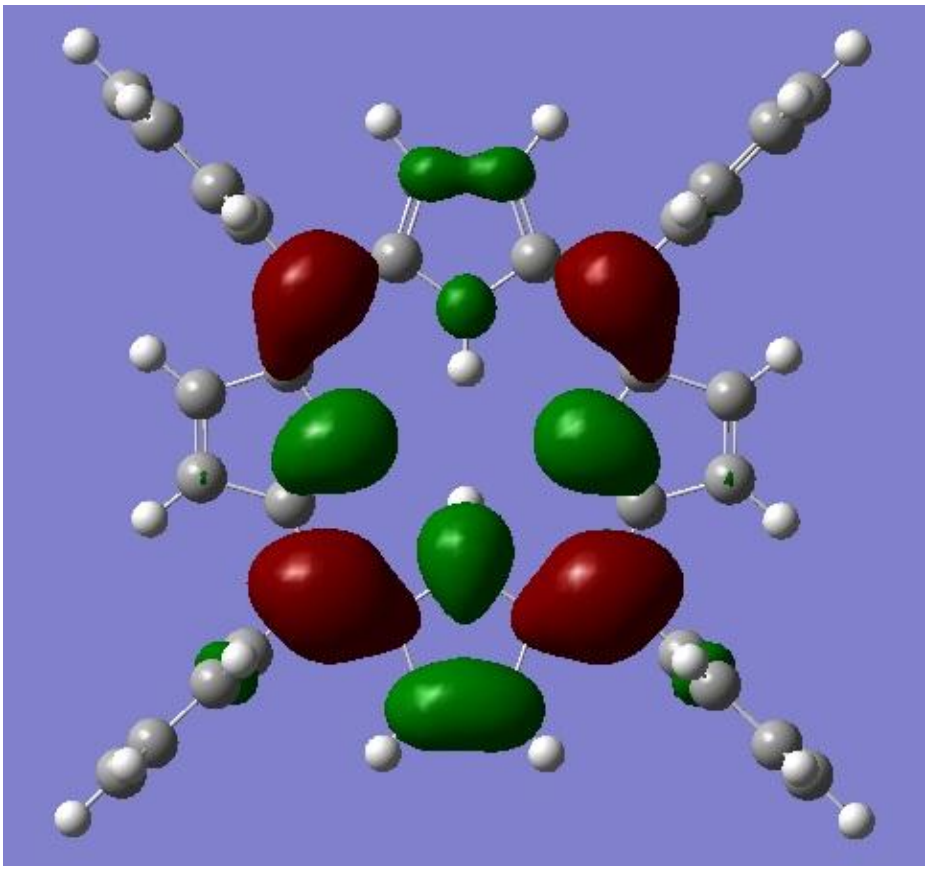

Figure Gaussian data HTPP second HOMO 160.

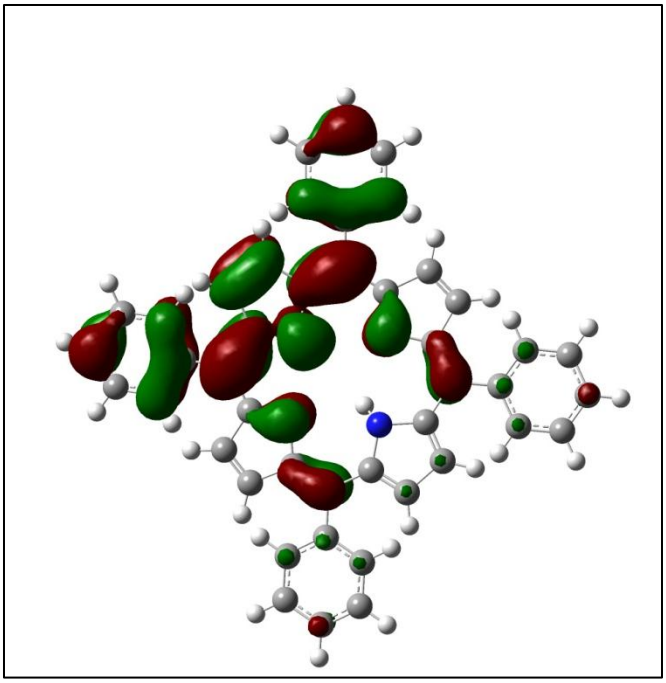

Figure Gaussian data HTPP HOMO 161.

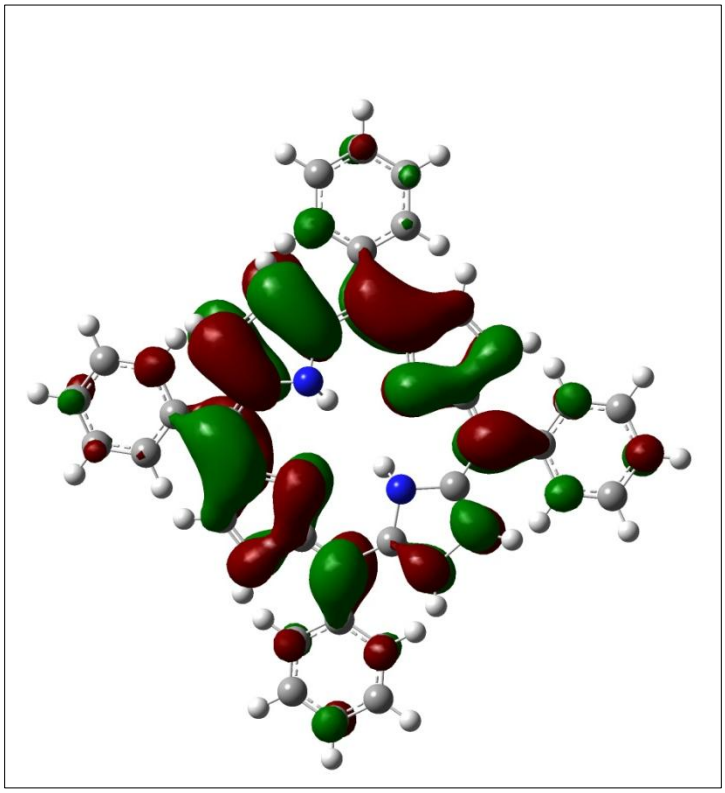

Figure Gaussian data HTPP LUMO 162.

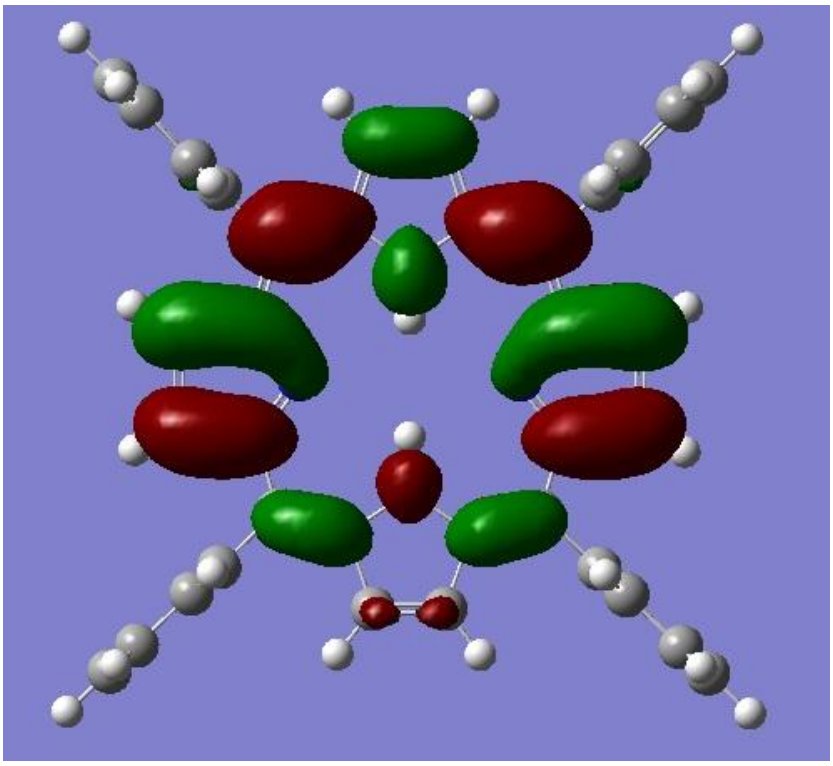

Figure Gaussian data HTPP second LUMO 163.

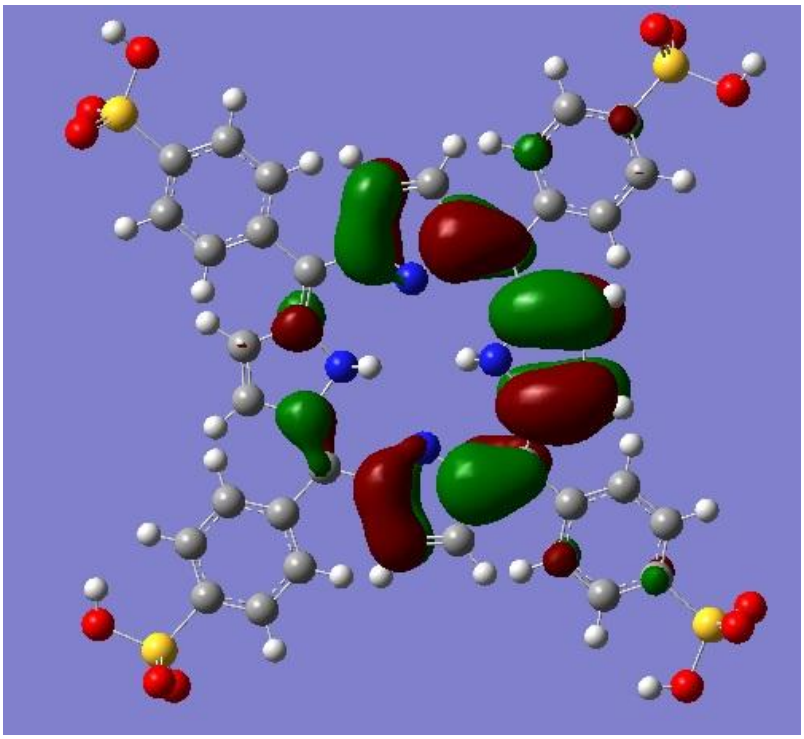

Figure Gaussian data TBSP second HOMO 240.

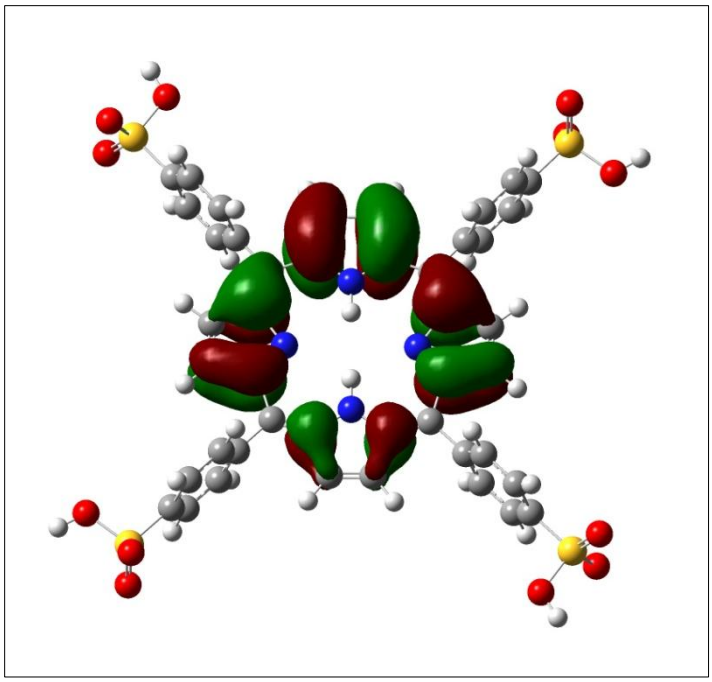

Figure Gaussian data TBSP HOMO 241.

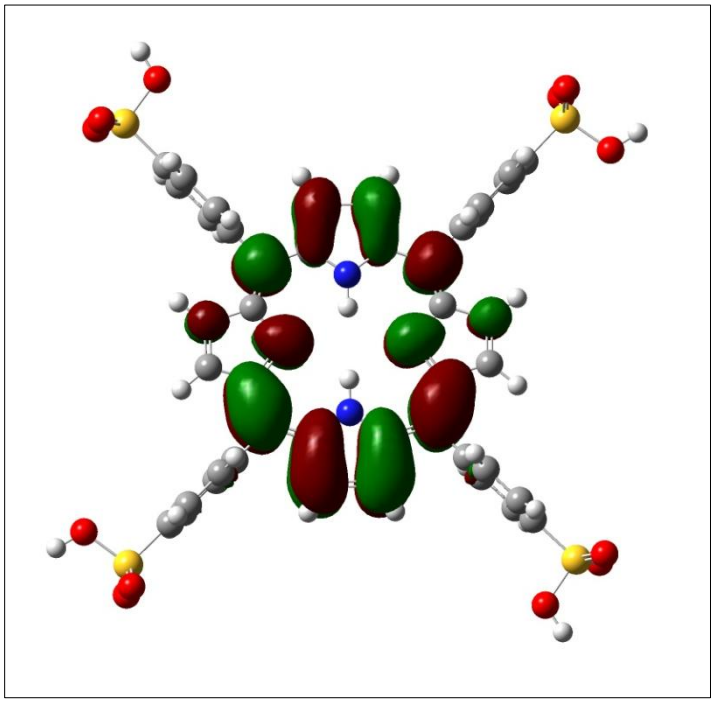

Figure Gaussian data TBSP LUMO 242.

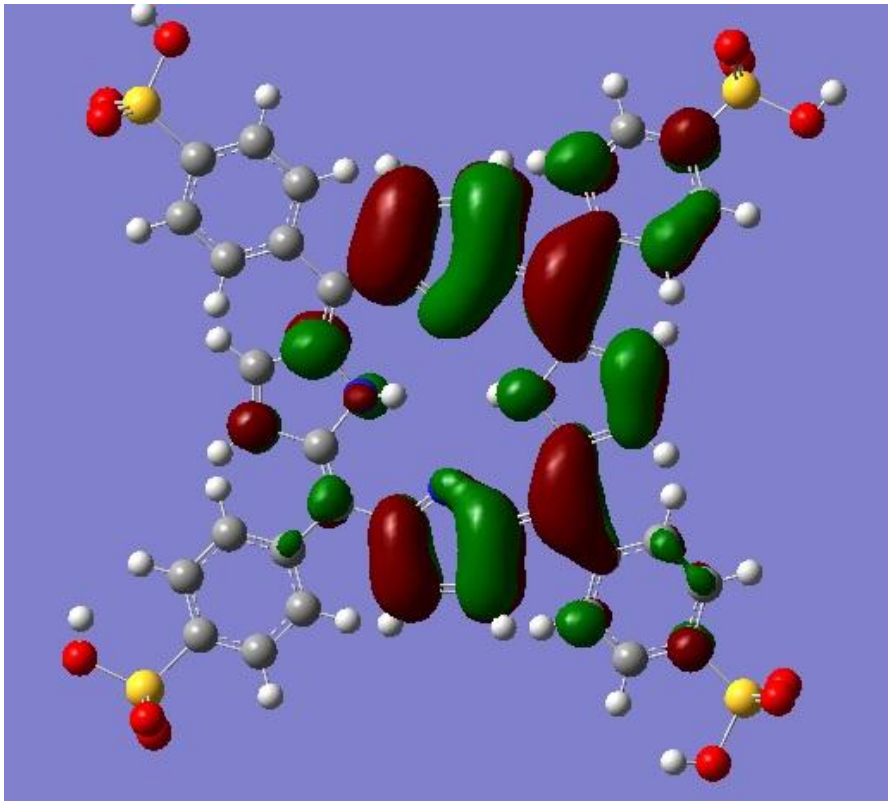

Figure Gaussian data TBSP second LUMO 243.